Ocean Optics & Biogeochemistry Protocols for Satellite Ocean Colour Sensor Validation

Volume 1: Inherent Optical Property Measurements and Protocols: Absorption Coefficient (v1.0)

Editors
Aimee R. Neeley and Antonio Mannino

Authors
Emmanuel Boss, Eurico J. D'Sa, Scott Freeman, Ed Fry, James L. Mueller, Scott Pegau,
Rick A. Reynolds, Collin Roesler, Rüdiger Röttgers, Dariusz Stramski,
Michael Twardowski and J. Ronald V. Zaneveld

IOCCG Ocean Optics and Biogeochemistry Protocols for Satellite Ocean Colour Sensor Validation

IOCCG Protocol Series Volume 1.0, 2018

Inherent Optical Property Measurements and Protocols: Absorption Coefficient

Edited by:

Aimee R. Neeley and Antonio Mannino

Report of a NASA-sponsored workshop chaired by Aimee R. Neeley with contributions from (in alphabetical order):

Emmanuel Boss	University of Maine, Orono, ME, USA
Eurico J. D'Sa	Louisiana State University, Baton Rouge, LA, USA
Scott Freeman	Goddard Space Flight Center, Greenbelt, MD, USA
Ed Fry	Texas A&M University, College Station, TX, USA
James L. Mueller	San Diego State University, CA, USA
Scott Pegau	Prince William Sound Science Center, AK, USA
Rick A. Reynolds	Scripps Institution of Oceanography, La Jolla, CA, USA
Collin Roesler	Bowdoin College, Brunswick, ME, USA
Rüdiger Röttgers	Helmholtz-Zentrum Geesthacht, Germany
Dariusz Stramski	Scripps Institution of Oceanography, CA, USA
Michael Twardowski	Harbor Branch Oceanographic Institute, FL, USA
J. Ronald V. Zaneveld	Oregon State University, Corvallis, OR, USA

Correct citation for this volume:

IOCCG Protocol Series (2018). Inherent Optical Property Measurements and Protocols: Absorption Coefficient, Neeley, A. R. and Mannino, A. (eds.), IOCCG Ocean Optics and Biogeochemistry Protocols for Satellite Ocean Colour Sensor Validation, Volume 1.0, IOCCG, Dartmouth, NS, Canada.

http://www.ioccg.org

Table of Contents

Chapter 1: The Absorption Coefficient, An Overview

Michael Twardowski[1], Rüdiger Röttgers[2], and Dariusz Stramski[3]

[1]*Harbor Branch Oceanographic Institute, Florida Atlantic University, Fort Pierce, FL, USA*
[2]*Institute of Coastal Research, Helmholtz-Zentrum Geesthacht,*
Centre for Materials and Coastal Research, Germany
[3]*Scripps Institution of Oceanography, La Jolla, CA, USA*

Inherent Optical Properties (IOPs) of each discrete constituent of the water medium are additive, so that the total (or combined) absorption and scattering properties of a sample of natural water consist of the sums of the IOPs of pure water itself (with or without dissolved salts), each discrete particle and aggregate, and each dissolved substance. "Discrete" here specifically refers to particles not being too close in proximity; typically, they must be separated by at least three times their radii or there will be interference in their scattering properties (van de Hulst 1981). This condition is considered fulfilled in natural waters except for only extremely turbid environments. Note that even for a single "discrete" particle, the scattering intensity and its angular pattern will be dependent on the specific orientation of that particle relative to a frame of reference, unless it is a homogeneous sphere. Discontinuities in the refractive index of water due to fine-scale variability in temperature and salinity that may be influenced by physical processes, such as turbulence, also constitute a scattering IOP with effects at near-forward angles (Bogucki et al. 2004, 2007; Mikkelsen et al. 2008). IOPs of individual constituents are usually grouped (e.g., dissolved and particulate, with respect to particle type, etc.) based on methodological capabilities and constraints, or conceptual convenience. IOPs can be described with respect to spectral variability (typically in the Ultraviolet-visible-Near-Infrared range for underwater optics and remote-sensing applications), and scattering has an angular dependency characterized by the volume scattering function (VSF or β), also known as the differential scattering cross-section. Whereas the VSF specifically describes the angular scattering of unpolarized radiation, scattering of the polarized elements of the Stokes vector can similarly be described and may contain unique information about particle characteristics.

Different combinations of individual biogeochemical constituents of natural water collectively determine the IOPs (including magnitude, spectral shape, and angular dependence), which in turn strongly influence remote sensing reflectance (Gordon et al. 1988; Morel 1988; Morel et al. 2002; Werdell et al. 2013). The physical basis for determining constituent concentrations of natural waters from ocean color measurements lies in methods and algorithms that effectively invert these relationships.

1.1 Absorption by Pure Water

It is challenging to experimentally determine the absorption of pure water, a_w (m^{-1}), in the laboratory due, principally, to the difficulty of making and maintaining pure water, a powerful solvent, during the course of an experiment. The UV range is particularly sensitive to dissolved organic and inorganic absorbing contaminants, and absorption by water is generally low relative to measurement signal-to-noise at wavelengths shorter than about 500 nm. Methods used to determine pure water absorption include conventional transmission, an integrating cavity absorption meter (ICAM; see Chapter 3 of this volume), and photothermal techniques such as laser calorimetry, photoacoustics, photothermal deflection, and the thermal lens (Grundinkina 1956; Ghormley and Hochanadel 1971; Tam and Patel 1979; Quickenden and Irvin 1980; Boivin et al. 1986; Sogandres and Fry 1997; Pope and Fry 1997; Cruz et al. 2011; Kröckel and Schmidt 2014). Note that some studies employing transmission-based methods report their values as absorption even though attenuation is actually measured, so that the contribution from molecular scattering must be removed (Section 2.5.2). This is particularly important in the UV portion of the spectrum where molecular scattering from water is similar in magnitude to its absorption. Other studies using the ICAM and photothermal techniques do not have contributions from molecular scattering in their measurements. Because of the difficulty in making water with sufficient purity, others have also taken the approach of trying to infer pure water absorption from passive radiometric measurements in the world's clearest waters (Smith and Baker 1981; Morel et al. 2007; Lee et al. 2014). There is value in this approach, as water in some locations, such as the central South Pacific gyre, is maintained naturally at very high levels of clarity, which at least can be used to stipulate upper bounds for pure water absorption. However, background absorbing constituents in these waters are nonetheless still present and require assumptions in accounting for their effects.

For detailed discussions on the physical basis of absorption by water, see Jonasz and Fournier (2007) and Wozniak and Dera (2007).

1.1.1 Visible, Near-Infrared, and Infrared domains

It is accepted that the work of Pope and Fry (1997) represents the state-of-the-art for pure water absorption from about 420 to 725 nm due to the fidelity of the ICAM technique, including its long effective pathlength (~10 m) and insensitivity to scattering, and the level of water purity achieved in the study. Portions of their data in the visible have been verified by other studies using completely different techniques (e.g., Sogandares and Fry 1997; Cruz et al. 2011). The resolution of these data is fine enough to show expected inflections from overtone modes of water absorption, allowing precise modeling with combination Gaussian fitting informed by physical theory (Jonasz and Fournier 2007). For the spectral range 420–725 nm the values of Pope and Fry (1997) are listed in Table 1.1. For the near-infrared (NIR) and infrared (IR) domains (from 730 to 1230 nm), the values of Kou et al. (1993) are accepted as state-of-the-art and listed in Table 1.1. Note that the reported values in Pope and Fry and Kou et al. overlap in the range ~667 to 727.5 nm and are offset ~0.04 m^{-1} higher for Kou et al. at 670 nm and ~0.07 m^{-1} higher for Kou et al. at 725 nm. This offset is not taken into account in the Table 1.1 data (other than to choose the carefully collected Pope and Fry data for the spectral range of overlap), as we have no basis for doing so at this time. On an absolute basis, this discrepancy is significant.

1.1.2 Ultraviolet domain

Water purity is absolutely essential for pure water absorption measurements in the UV, as a wide range of both organic and inorganic dissolved substances absorb, often quite strongly, in this region, whereas absorption by water is comparatively low. As a result, state-of-the-art studies for water absorption in the UV have used sophisticated and exhaustive measures to purify water, including oxidative steps, extreme deionization quantified with conductivity readings, UV oxidation, and removal of dissolved oxygen gas. The highest quality data in the UV are thus accepted to be Ghormley and Hachanadel (1971; range between 180 and 215 nm), Quickenden and Irvin (1980; range between 196 and 320 nm), and Kröckel and Schmidt (2014; range between 181 and 340 nm), hereafter referred to as GH-QI-KS. All of these data agree within experimental error in the regions of overlap, providing continuous, high-quality measurements from 180 to 340 nm. Note that the "absorptivity" values of Quickenden and Irvin (1980) are base 10 logarithms of the inverse of transmission divided by pathlength, so the values must be multiplied by 2.303 to convert to the absorption coefficient. Molecular scattering of water was subtracted from all of these data to derive pure water absorption. Other notable high-quality absorption data in (or near) the UV were collected by Boivin (1986) at 254, 313, 366, and 406 nm, and by Grundinkina (1956; as cited by Jonasz and Fournier 2007) from 200 to 350 nm. Neither of these studies accounted for possible absorption from dissolved oxygen and the purification steps overall were not as rigorous as the previously mentioned studies. The values of Sogandares and Fry (1997) and Pope and Fry (1997) in the UV are significantly higher than these other careful works, indicating possible contamination in their purified water for this spectral range.

Jonasz and Fournier (2007) provide physical equations, based on theory, for pure water absorption in the UV that produce an excellent fit to the GH-QI-KS measurements:

$$a_w = 7.067 \times 10^{-40} \exp\left(\frac{\lambda_r}{\lambda - \Delta\lambda}\right) + 5 \times 10^6 \, \nu^{-5/4} \exp\left(-0.076 \, Z_c\right) \exp\left(\frac{\lambda_r}{\lambda - \Delta\lambda}\right), \tag{1.1}$$

$$\text{where} \qquad Z_c = \left(\frac{\nu^{11/12}}{\sqrt{T}}\right)^{2/3}, \qquad \nu = 10^7 \left(\frac{1}{\lambda_r} - \frac{1}{\lambda}\right),$$

$\Delta\lambda = 0.0465(T - 298)$, λ_r is a reference wavelength arbitrarily chosen as 150 nm, and T is temperature in degrees Kelvin. These equations allow for the explicit treatment of the effects of temperature on pure water absorption in the UV. Values between 180 and 340 nm in Table 1.1 were derived from this analytical model solved at 22 °C. Conveniently, at 340 nm the analytical model agrees with the extrapolated values recommended by Morel et al. (2007; see a_{w2} values in their Table 2, based on an extrapolation between the data of Quickenden and Irvin (1980) and Pope and Fry 1997). The values of Morel et al. (2007) are used between 340 and 415 nm in Table 1.1. While providing satisfying continuity in the values for pure water absorption, it should be emphasized that the values between 340 and 420 nm (a relatively wide and ecologically important spectral range) are merely extrapolated; there is a clear need for high-quality water

absorption measurements in this spectral range. <u>Addendum</u>: A recent study by Mason et al. (2016) includes measurements of absorption in this spectral range.

Recent work by Cruz et al. (2009, 2011) using a thermal lens technique presents three values for pure water absorption in (and near) the UV at 351, 364, and 406 nm that are significantly lower than the extrapolation of data from GH-QI-KS in the region between 340 and 420 nm. The Cruz et al. values at longer wavelengths are consistent with Pope and Fry (1997) within measurement errors. The smallest absorption value, measured at 364 nm, is more than a factor of 3 less than the extrapolation in this region, effectively creating a much more significant transmission window in that part of the UV than currently thought. The Cruz et al. data would shift the minimum in pure water absorption from the 400–420 nm range to somewhere likely between 360 and 380 nm. Such a "hole" in pure water absorption in this region is not consistent with expectations of a monotonic exponential function through this region from physical theory (Jonasz and Fournier 2007). Their absorption data between 351 and 406 nm have an entirely new shape relative to other high-quality measurements from the literature in this region (particularly Grundinkina 1956 and Boivin 1986). In this spectral range, possible errors in other studies due to organic contaminants in their purified water and/or scattering-reflection effects would be spectrally broad and monotonic, inconsistent with a ~20-nm full-width-half-maximum (FWHM) error spectrum peaking in the 360–380-nm range. The Cruz et al. measurements also, paradoxically, were made with water purified with a typical Millipore MilliQ® Plus ultrafiltration system of 18 MΩ•cm purity, without any additional purification or any removal of dissolved gases, contrasting markedly with exhaustive purification measures taken in the most comprehensive works (e.g., GH-QI-KS). These data, therefore, cannot be considered at this time without further verification.

Recent work by Lee et al. (2015) found values offset about 0.002 m^{-1} lower from 350 to 500 nm than the values recommended here based on semi-analytic inversion of *in situ* radiometric data and models that accounted for the absorbing components besides pure seawater in the water column. These data were collected alongside the radiometric measurements of Morel et al. (2007) that guided the conclusions on recommended pure water values in that work (see above; these are essentially the values recommended in Table 1.1 for this spectral region). Considering associated uncertainties and assumptions in the radiometric inversion method, the Lee et al. (2015) values are not deemed inconsistent with the recommended values.

Jonasz and Fournier (2007) suggest that the effect of dissolved oxygen alone may explain the differences between the oxygen-free water data of GH-QI-KS and the data collected with water saturated in oxygen from Boivin (1986) and Grundinkina (1956). Jonasz and Fournier (2007) additionally provide physical relationships based on data from Heidt and Johnson (1956) to represent both the effects of oxygen being present on pure water absorption and the direct absorption by oxygen dissolved in water in the spectral range 200–215 nm. This approach was supported by good agreement with the direct measurements of Grundinkina (1956) in that spectral range. Since the physical data collected by Heidt and Johnson (1956) did not extend longer than 215 nm, Jonasz and Fournier (2007) fit the data of Grundinkina (1956) and Boivin (1986) using the same physical relationship used to fit the oxygen-free pure water absorption data of GH-QI. Assuming this fit only accounts for the presence of oxygen in water, significant absorption effects from dissolved oxygen are apparent out to at least ~370 nm, where the GH-QI and Boivin (1986) values converge (also see Morel et al. 2007, their Fig. 10). Detectable absorption from dissolved oxygen at wavelengths longer than about 280 nm appears inconsistent with the findings of previous studies (e.g., Copin-Montegut 1971 as cited in Shifrin 1988), although we are not aware of any careful measurements to potentially resolve very low (but still perhaps significant) absorption from oxygen in the long UV range. Regarding the differences between GH-QI-KS and the data of Grundinkina (1956) and Boivin (1986), Fig. 2 from Quickenden and Irvin (1980), which shows the decrease in absorption following sequential purification steps, may be instructive, as water of "purity 2" (only deionized and distilled) is a close approximation to the higher values and spectral shape of absorption presented by these other authors. The final "purity 4" water from Quickenden and Irvin (1980) had several additional distillation and oxidation steps. All levels of purity had oxygen removed through bubbling with nitrogen gas, so that the "purity 2" water (and perhaps the water of Grundinkina 1956 and Boivin 1986) presumably contained organic contaminants.

Importantly, dissolved inorganic molecules besides oxygen, such as NO$_3$, Br$^-$, and other salt ions comprising sea salts all have significant absorption in the UV (Armstrong and Boalch 1961; Ogura and Hanya 1966; Johnson and Coletti 2002; as cited in Shifrin 1988: Lenoble 1956; Copin-Montegut 1971).

Note these effects have received scarce attention in recent literature. At 230 nm, these constituents all have more than an order of magnitude higher absorption than the values of GH-QI-KS, with steeply increasing absorption at shorter UV wavelengths. An unresolved question is how much these constituents may absorb at wavelengths longer than 300 nm, as the tail absorption effects have typically not been studied with the required accuracy. Again, even relatively small contributions could be significant since pure water absorption is very low, particularly in the 320 to 420-nm range ($<= 0.01$ m^{-1}). Armstrong and Boalch (1961) found significant effects of sea salt absorption out to 400 nm, but rigorous purification steps were not taken, so it is unclear if their additions of artificial sea salts introduced organic contaminants.

In summary, it is worth emphasizing that UV absorption for seawater devoid of particles and dissolved organic substances will be substantially influenced by the typical assortment of dissolved inorganic constituents, so that the absorption values in the UV presented in Table 1.1 will require supplementation based on high-quality molar absorptivity data for these constituents (which are currently not available to our knowledge) and ancillary measurements of their respective concentrations. This is a critical area of needed research in the future study of radiative transfer in the UV.

1.1.3 Temperature and salinity dependence

The absorption by pure water exhibits linear dependencies on temperature and salinity, which have been quantified empirically by Pegau et al. (1997), Twardowski et al. (1999), and Sullivan et al. (2006) for reflective tube absorption devices with individual spectral bandwidths of approximately 10–18 nm FWHM. Sullivan et al. (2006) further provided estimated values for the linear slopes of temperature and salinity dependencies with the effect of spectral smearing from bandwidth limitations removed, which should be closer to what may be considered physical constants describing the effect. Recently, Röttgers et al. (2014) determined these coefficients with an integrating cavity absorption meter and a spectrophotometer with a spectral range spanning 400 to ~2700 nm. The Röttgers et al. data agree within the experimental error of the Sullivan et al. coefficients but exhibit finer detail due to improved signal-to-noise and narrower bandwidths (3 nm for 400–700 nm, 2 nm for 700–850 nm, and 2–4 nm for > 850 nm). We recommend the Röttgers et al. coefficients for describing the physical phenomenon, which are reproduced in Table 1.1.

For applying pure water absorption values to measurements, the spectral bandwidth characteristics of the sensor and the temperature and salinity of the water should be accounted for, which, when optimal accuracy is desirable, becomes rapidly quite complex. For the linear dependency with respect to temperature, the Röttgers et al. values may be convolved with the spectral bandwidth of the measurement device to derive a coefficient specific for that device at that centroid wavelength. With a concurrent measurement of ambient temperature, the effect of the temperature dependence can then be removed by choosing a reference temperature for all data (Section 2.5.1). Alternatively, empirically derived coefficients specific for that sensor may be used, if available. For salinity, the effect is more challenging since the physical effect of pure water dependence on salt content (e.g., as reported by Röttgers et al., 2014) is always convolved with some instrument specific transmission effect resulting from the interaction of optical interfaces with solutions of varying refractive index (Sullivan et al. 2006). In this case, using empirically derived coefficients for a specific sensing device would be advisable. For this reason, the Sullivan et al. (2006) coefficients for temperature and salinity dependencies of pure seawater absorption specific for the Sea-Bird Scientific (formerly WET Labs) ac-s are also provided in Table 1.1. Note also that the pure seawater absorption values discussed above have been measured at specific ambient temperature, and spectral bandwidth, e.g., the Pope and Fry (1997) values were measured at 22 °C with a nominal bandwidth of 1.9 nm, which, for optimal accuracy, should be accounted for in some applications. Moreover, when working in the NIR spectral range, caution should be exercised due to strong spectral gradients and significant absolute peak values in temperature and salinity dependencies in pure water absorption.

1.2 Absorption by Colored Dissolved Matter

Material in the dissolved fraction of natural water that absorbs light is known as colored dissolved matter (CDM). Since CDM absorption in the visible range is dominated by refractory organic humic substances, material in the dissolved fraction is commonly referred to as colored dissolved organic matter (CDOM), or *gelbstoff* (i.e., "yellow substances," after Kalle 1966). The associated absorption coefficient is $a_g(\lambda)$ with units of m^{-1}. A primary source of CDOM in natural waters is terrestrial runoff, with riverine

inputs in the coastal ocean being a substantial driver of observed distributions. A key sink for CDOM is photodegradation in surface waters. Normally, absorption by a dissolved substance will vary linearly with its concentration, as described by the Lambert-Beer Law. However, since CDOM is a broad pool of many dissolved compounds collectively known as humic substances and since the composition of this pool varies, absorption (or fluorescence) by CDOM cannot generally be used to quantifiably derive CDOM concentrations (Blough and Blough 1994). Spectra of a_g monotonically decrease with increasing wavelength (Fig. 1.1) and are typically modeled reasonably well with an exponential or power-law model (Bricaud et al. 1981; Twardowski et al. 2004). Either model fit, however, is only an approximation of the spectral shape of absorption from a complex mixture of compounds, so the spectral range over which a slope is derived is an essential piece of information that should be additionally reported (Twardowski et al. 2004; Loiselle et al. 2009). Note that much of the literature quantifies CDOM concentration by the associated magnitude of the absorption coefficient at a specific wavelength.
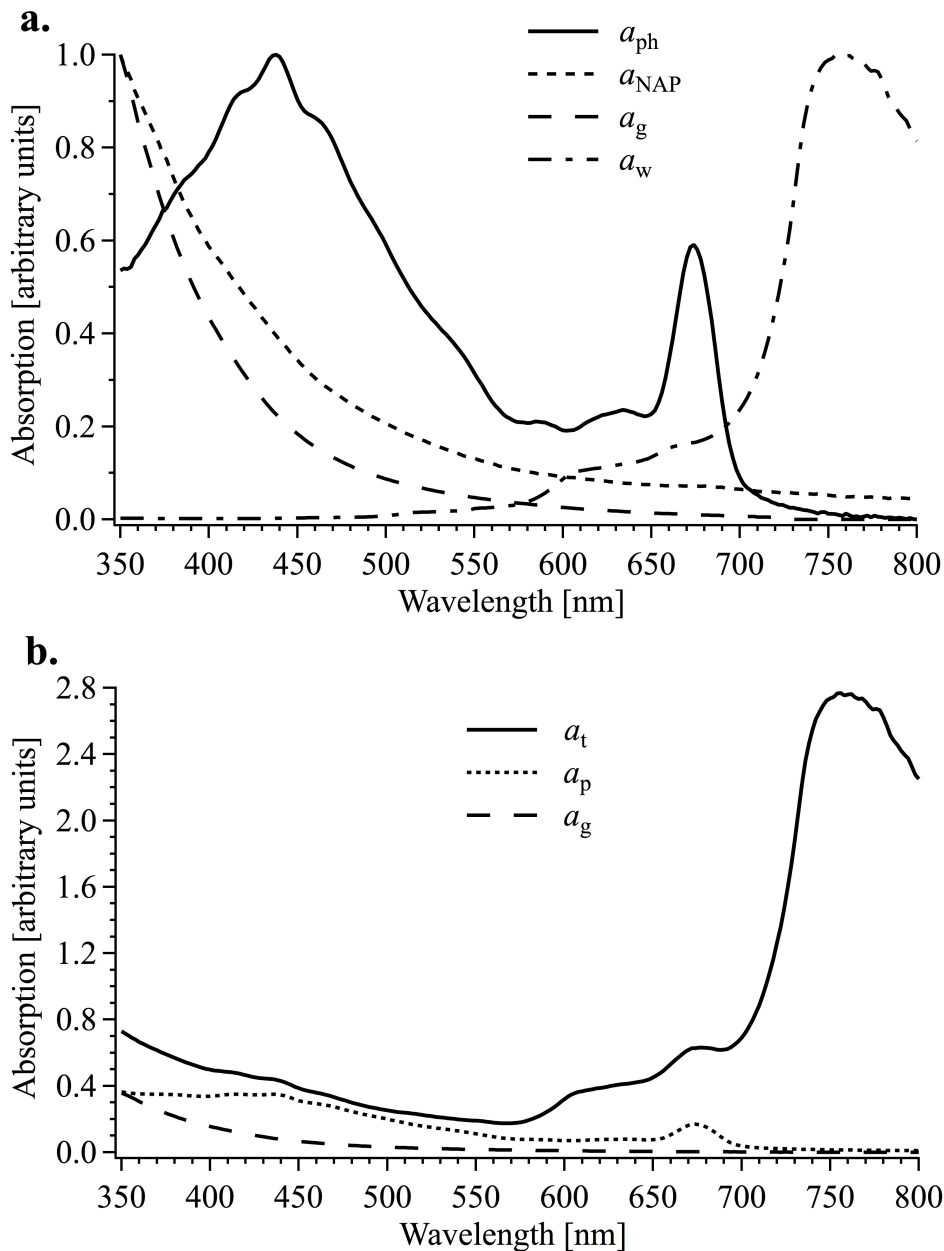
Figure 1.1. **a)** Typical spectral shapes of absorption by different components in seawater. A qualitative comparison of the shapes of absorption spectra of pure water (a_w), phytoplankton (a_{ph}), non-algal particulate (also detrital) matter (a_{NAP}), and CDOM (a_g); **b)** The absolute spectral absorption coefficients of total absorption (a_t), total particulate absorption ($a_p = a_{ph} + a_{NAP}$), and a_g. Absorption spectra were analyzed on a sample collected from the German Bight (R. Röttgers, *unpubl. data*).

Preparing a sample for measurement involves removing particles via filtration, but the filter type and pore size are important considerations. For processing samples in the lab, glass fiber disk filters (GF/F) are sometimes used, but care should be taken to pre-rinse these filters, as glass fibers may leach into the filtrate. The nominal pore size of GF/Fs is 0.7 μm, but can be <0.5 μm, according to Chavez et al. (1995). A better option is polycarbonate disk filters that do not contaminate the filtrate and have a more restrictive pore size of 0.2 μm, although sample flow rates through these filters are slower than for GF/Fs. Another option is hydrophilic nylon, pleated capsule filters that can accommodate substantial flow rates with a relatively small pore size of 0.2 μm. These are preferred for *in situ*, continuous flow methods for determining absorption. The outer capsule of these filters may be carefully removed to additionally enhance flow rates. Note that time is important, as the material passing through filters can recombine into particles following filtration (Verdugo 2012).

Possible effects of contamination of absorption measurements from any colloidal particles remaining in the filtrate depend on the pore size of the filter that was used, turbidity characteristics of the original sample, and the method for determining absorption. Such particles may have non-negligible absorption and may cause a scattering error for certain measurement devices (e.g., reflective tube absorption meters and conventional benchtop spectrophotometers). Possible scattering errors for reflective tube absorption meters have been found to be negligible for a wide range of natural waters passing through a 0.2-μm pleated capsule filter by confirming agreement with concurrent measurements of attenuation (i.e., absorption plus scattering) (Twardowski et al. 1999, 2004). It may be assumed that if there is negligible scattering in these filtered samples, that any particulate absorption cross-section should also be negligible. However, scattering errors have been found previously for samples with high sediment loads dominated by clays, analyzed with a benchtop spectrophotometer. Röttgers and Doerffer (2007) also noted a scattering error for benchtop spectrophotometric measurements of North Sea samples passed through 0.22-μm filters. The effect may have resulted from microbubbles induced by vacuum filtration, making the impact sporadic.

Once a sample is 0.2 μm filtered, it may be stored at 4 °C for at least several weeks before analysis without biasing laboratory absorption measurements (Green and Blough 1994). It is advisable to refilter samples after storage, as any particles forming from coagulation during storage should be removed. Care should be taken to ensure water blanks and samples are at the same ambient temperature (Section 1.1). Caution should also be exercised in handling samples to avoid contamination.

1.3 Absorption by Particles in Suspension

Spectral absorption determined in a whole sample, i.e., containing both particulate and dissolved fractions, is typically represented as $a_{pg}(\lambda)$. Since many techniques use pure water blanks, this is a commonly measured IOP. Total spectral absorption $a_t(\lambda)$, important for remote-sensing algorithm work, would then be derived by adding water absorption $a_w(\lambda)$ to $a_{pg}(\lambda)$ (accounting for specific temperature and salinity characteristics of the water). If $a_{pg}(\lambda)$ is obtained from measurements then the determination of the particulate absorption coefficient, $a_p(\lambda)$, requires subtraction of $a_g(\lambda)$ from $a_{pg}(\lambda)$, which indicates that $a_g(\lambda)$ must also be measured or known. There also exist techniques for measuring the particulate absorption coefficient more directly, for example the so-called filter pad technique, further described in Section 5 of this volume (e.g., Mitchell 1990; Tassan and Ferrari 1995; Stramski et al. 2015).

It is usually convenient to partition the spectral absorption coefficient associated with particles, $a_p(\lambda)$ with units m^{-1}, into the spectral absorption coefficient of pigment-containing phytoplankton, $a_{ph}(\lambda)$, and the spectral absorption coefficient of non-algal particles, $a_{NAP}(\lambda)$ (note that historically a term detrital absorption coefficient denoted as a_d has been used to refer essentially to non-algal absorption). This two-component description of particulate absorption is useful because the pigments in phytoplankton produce unique spectral structure whereas most NAP absorption spectra monotonically decrease with increasing wavelength (with notable exceptions for mineral particles containing iron; see Babin and Stramski 2004, Estapa et al. 2012). The convenience of this grouping extends to benchtop absorption measurement techniques that allow individual quantification of phytoplankton and NAP through the use of pigment extracting solvents such as methanol (Kishino et al. 1985). Note that, as a result of this experimental method, $a_{ph}(\lambda)$ specifically represents the absorption by extractable pigments only, primarily associated with phytoplankton. The absorbing fraction of NAP, $a_{NAP}(\lambda)$, obtained from this method is generally

assumed to be composed of organic detrital material and minerogenic particles, although other absorbing compounds such as non-extractable components of phytoplankton cells (for example, phycobilins) and heterotrophic microorganisms may also contribute to NAP absorption. Nevertheless, the difference between the measured total particulate absorption, $a_p(\lambda)$, and $a_{NAP}(\lambda)$ is commonly assumed to represent phytoplankton absorption coefficient, $a_{ph}(\lambda)$. This extraction-based method as applied to a filter pad technique has long been in routine use in the analysis of particulate absorption and its components in natural seawater samples, (e.g., Bricaud and Stramski 1990). Example spectra of a_{ph}, a_{NAP}, and a_g are shown in Fig 1.1.

Other approaches to experimentally separate the absorption contributions of phytoplankton pigments and non-algal particles or organic and inorganic particles have been also proposed in the past such as exposure of sample to UV radiation (Konovalov and Bekasova 1969), bleaching of sample with a strong oxidizing agent sodium hypochlorite (Ferrari and Tassan 1999), and combustion of sample at high temperature (Bowers et al. 1996). To our knowledge, the UV treatment was used only in early work of Russian investigators. Bleaching with sodium hypochlorite is generally considered to oxidize phytoplankton pigments faster than other particulate organic matter, so this method has been commonly assumed to separate the absorption signals associated with these two components. The use of the strong bleaching agent can, however, introduce unwanted effects and artifacts, especially in the short-wavelength portion of the visible spectrum and in the UV, which is a significant limitation of its applicability. The method based on high-temperature combustion involves the removal of organic material from the particulate sample at 500 °C. The absorption measurement of the combusted particles is assumed to represent the inorganic (mineral) particles. Thus the difference between the measured total particulate absorption coefficient, $a_p(\lambda)$, and the mineral absorption coefficient, $a_m(\lambda)$, provides an estimate of the absorption coefficient of organic particles. Note that in this method the organic particles comprise phytoplankton pigments and other combustible organic material including detrital matter. The combustion method may affect the optical properties of the inorganic particles remaining in the sample after the high-temperature treatment, which is a significant limitation. The bleaching and combustion methods have not been in routine use, and the methanol extraction has remained as the most widely used method for experimental partitioning of $a_p(\lambda)$ into $a_{NAP}(\lambda)$ and $a_{ph}(\lambda)$ components.

The particulate absorption coefficient or its components can be represented as a product of mass-specific absorption coefficient of a specific constituent and the mass concentration of that constituent in water. For example, the phytoplankton absorption coefficient, $a_{ph}(\lambda)$, can be expressed as a product of chlorophyll-*a*–specific absorption coefficient of phytoplankton, $a^*_{ph}(\lambda)$ with units m^2 mg^{-1}, and concentration of chlorophyll *a*, Chl, with units mg m^{-3} (e.g., Prieur and Sathyendranath 1981) Therefore, $a_{ph}(\lambda)$ can be derived if $a^*_{ph}(\lambda)$ and Chl are known or assumed. There is a large body of literature on Chl-specific phytoplankton absorption based on both field measurements of natural phytoplankton populations and lab measurements of phytoplankton cultures; for example, empirical relationships between $a^*_{ph}(\lambda)$ and Chl have been established on the basis of large field data sets which enable estimations of a^*_p, and also $a_{ph}(\lambda)$, from measurements of Chl (Bricaud et al. 1995). Similar relationships were established for chlorophyll-specific absorption coefficient of total particulate matter, $a^*_p(\lambda)$ (Bricaud et al. 1998). The determinations of mass-specific absorption coefficients for non-algal particles, notably for mineral fraction of particulate matter or mixed particulate assemblages dominated by mineral fraction have been also addressed in numerous studies in the past (e.g., Bowers et al. 1996; Binding et al. 2003; Babin and Stramski 2004; Stramski et al. 2004; Bowers and Binding 2006; Stramski et al. 2007; Estapa et al. 2012). In these studies, the mass-specific absorption coefficients were expressed on the basis of determinations of mass concentrations of mineral particles, total suspended particulate matter, or iron content of particulate matter.

1.4 General Comment on Measuring Absorption Components

Some IOPs can be resolved directly, whereas others must be derived or even inferred from other measurements. Some sensors and methods are designed for *in situ* data collection, whereas others are intended for laboratory use. Laboratory-based methods have the advantages of a stable environment and power supply, and the ability to process samples before measurement if desired. Disadvantages include the requirement of sample collection and transfer, which may alter constituents of the water in some ways and logistically restricts the number of possible discrete samples and associated temporal and/or spatial resolving capability. Laboratory methods capable of accommodating continuously flowing samples from a ship can allow greater lateral spatial resolution in IOPs. The next several chapters detail the current state-of-the-art for in-water and lab-based methods of determining the absorption coefficient and its components.

Table 1.1 lists the current state-of-the-art in pure water absorption coefficients and uncertainties between 180 and 1230 nm and coefficients for the dependency of pure water absorption on temperature and salinity for available spectral ranges. The listed $a_w(\lambda)$ values are based on Jonasz and Fournier (2007) for the spectral range 180–340 nm (see Eq. 1.1), Morel et al. (2007) for 340–415 nm, Pope and Fry (1997) for 420–725 nm, and Kou et al for 730–1230 nm (see text for details). Röttgers et al. (2014) temperature and salinity dependencies represent best estimates of the physical constants whereas the Sullivan et al. (2006) values are specific to Sea-Bird Scientific (formerly WET Labs) ac-s devices. Addendum: Table has not been updated with recent values in the 250–550 nm range from Mason et al. (2016).

The following labels apply to each column of Table 1.1 on the corresponding pages, below:

A: Wavelength (nm)
B: a_w (1/m)
C: σ (1/m)
D: $\Delta a_w / \Delta T$ (m^{-1} C^{-1}) $*10^{-4}$
E: $\sigma: \Delta_{aw} / \Delta_T$ (m^{-1} C^{-1}) $*10^{-4}$
F: Δ_{aw} / Δ_S (m^{-1} psu^{-1}) $*10^{-4}$
G: $\sigma: \Delta_{aw} / \Delta_S$ (m^{-1} psu^{-1}) $*10^{-4}$
H: Δ_{aw} / Δ_{T}_ac-s (m^{-1} C^{-1}) $*10^{-4}$
I: $\sigma: \Delta_{aw} / \Delta_{T}$_ac-s (m^{-1} C^{-1}) $*10^{-4}$
J: Δ_{aw} / Δ_{S}_ac-s: a (m^{-1} psu^{-1}) $*10^{-4}$
K: $\sigma: [\Delta_{aw} / \Delta_{S}$_ac-s: a (m^{-1} psu^{-1}) $*10^{-4}$
L: Δ_{aw} / Δ_{S}_ac-s: c (m^{-1} psu^{-1}) $*10^{-4}$
M: $\sigma: \Delta_{aw} / \Delta_{S}$_ac-s: c (m^{-1} psu^{-1}) $*10^{-4}$

			Table 1.1: Absorption Coefficients and Uncertainties									
			JF2007 (180 – 295 nm) Röttgers et al. (2014) (300 – 1230 nm)		Röttgers et al. (2014)		Sullivan et al. (2006)		Sullivan et al. (2006)		Sullivan et al. (2006)	
Wavelength (nm)	a_w (1/m)	σ (1/m)	$\Delta a_w /\Delta T$ (m^{-1} C^{-1}) *10^{-4}	$\sigma : \Delta_{aw} /\Delta_T$ (m^{-1} C^{-1}) *10^{-4}	Δ_{aw} /Δ_S (m^{-1} psu^{-1}) *10^{-4}	$\sigma : \Delta_{aw} /\Delta_S$ (m^{-1} psu^{-1}) *10^{-4}	Δ_{aw} /Δ_T_ac-s (m^{-1} C^{-1}) *10^{-4}	$\sigma : \Delta_{aw} /\Delta_T$_ac-s (m^{-1} C^{-1}) *10^{-4}	Δ_{aw} /Δ_S_ac-s: a (m^{-1} psu^{-1}) *10^{-4}	$\sigma : [\Delta_{aw} /\Delta_S$_ac-s: a (m^{-1} psu^{-1}) *10^{-4}	Δ_{aw} /Δ_S_ac-s: c (m^{-1} psu^{-1}) *10^{-4}	$\sigma : \Delta_{aw} /\Delta_S$_ac-s: c (m^{-1} psu^{-1}) *10^{-4}
A	B	C	D	E	F	G	H	I	J	K	L	M
180	7647	765	1634433									
185	527	53	107540									
190	42.4	4.2	8175									
195	4.23	0.42	725									
200	0.727	0.073	85									
205	0.304	0.030	21									
210	0.207	0.021	12									
215	0.160	0.016	9									
220	0.128	0.013	7									
225	0.104	0.010	6									
230	0.086	0.009	5									
235	0.072	0.007	4									
240	0.061	0.006	4									
245	0.052	0.005	3									
250	0.045	0.005	3									
255	0.0392	0.0039	3									
260	0.0344	0.0034	2									
265	0.0303	0.0030	2									
270	0.0269	0.0027	2									
275	0.0240	0.0024	2									
280	0.0216	0.0022	2									
285	0.0194	0.0019	1									
290	0.0176	0.0018	1									
295	0.0160	0.0016	1									
300	0.0147	0.0015	1	5								

A	B	C	D	E	F	G	H	I	J	K	L	M

A	B	C	D	E	F	G	H	I	J	K	L	M
305	0.0134	0.0013	1	4								
310	0.0124	0.0012	1	3								
315	0.0114	0.0011	1	2								
320	0.0106	0.0011	1	2								
325	0.0098	0.0010	0	2								
330	0.0092	0.0009	0	1								
335	0.0085	0.0009	0	2								
340	0.0080	0.0008	1	2								
345	0.0075	0.0007	0	1								
350	0.0071	0.0007	-1	2								
355	0.0068	0.0007	-1	1								
360	0.0066	0.0007	0	1								
365	0.0063	0.0007	0	1								
370	0.0060	0.0007	-0.7	0.6								
375	0.0056	0.0007	-1	1								
380	0.0052	0.0007	0	2								
385	0.0050	0.0007	0	1								
390	0.0048	0.0007	0	1								
395	0.0047	0.0007	-0.2	1								
400	0.0046	0.0007	0.1	0.4	0.43	0.10	1	2	-0.1	0.4	0.3	0.3
405	0.0046	0.0007	0.1	0.4	0.37	0.08	1	1	-0.2	0.4	0.4	0.3
410	0.0046	0.0007	0.0	0.5	0.36	0.08	0.2	0.8	-0.2	0.4	0.4	0.3
415	0.0046	0.0006	0.2	0.3	0.34	0.09	0.5	1.2	-0.2	0.3	0.4	0.3
420	0.00454	0.0006	0.0	0.4	0.32	0.08	0.1	0.9	-0.3	0.3	0.4	0.3
425	0.00478	0.0006	-0.1	0.4	0.28	0.08	-0.1	0.8	-0.3	0.3	0.3	0.3
430	0.00495	0.0006	-0.1	0.3	0.26	0.07	-0.1	0.7	-0.3	0.3	0.3	0.3
435	0.00530	0.0005	0.0	0.3	0.25	0.06	-0.3	0.4	-0.3	0.3	0.3	0.3
440	0.00635	0.0005	0.0	0.3	0.22	0.06	-0.2	0.4	-0.4	0.3	0.2	0.2
445	0.00751	0.0006	0.1	0.3	0.19	0.06	-0.1	0.6	-0.4	0.3	0.2	0.2
450	0.00922	0.0005	0.2	0.3	0.17	0.06	-0.2	0.4	-0.4	0.3	0.2	0.2
455	0.00962	0.0004	0.1	0.3	0.16	0.05	-0.3	0.3	-0.4	0.3	0.2	0.2
460	0.00979	0.0005	0.1	0.3	0.14	0.05	-0.1	0.4	-0.4	0.3	0.2	0.2
465	0.01011	0.0006	0.0	0.3	0.13	0.04	-0.1	0.4	-0.4	0.2	0.2	0.2
470	0.0106	0.0005	-0.1	0.3	0.11	0.05	0.0	0.2	-0.4	0.2	0.1	0.2
475	0.0114	0.0007	-0.1	0.3	0.09	0.05	-0.1	0.2	-0.4	0.2	0.1	0.2
480	0.0127	0.0008	0.0	0.3	0.08	0.05	0.0	0.3	-0.4	0.2	0.1	0.2
485	0.0136	0.0007	-0.1	0.3	0.06	0.04	0.1	0.4	-0.4	0.2	0.1	0.2
490	0.0150	0.0007	-0.1	0.3	0.06	0.04	0.0	0.1	-0.4	0.2	0.1	0.2
495	0.0173	0.001	0.0	0.3	0.05	0.04	0.1	0.3	-0.4	0.2	0.1	0.2
500	0.0204	0.0011	0.1	0.3	0.05	0.04	0.3	0.3	-0.4	0.2	0.1	0.2

Table 1.1: Absorption Coefficients and Uncertainties (cont'd)

A	B	C	D	E	F	G	H	I	J	K	L	M
Table 1.1: Absorption Coefficients and Uncertainties (cont'd)												
505	0.0256	0.0013	0.3	0.3	0.04	0.04	0.3	0.5	-0.4	0.2	0.1	0.2
510	0.0325	0.0011	0.8	0.3	0.02	0.04	1	1	-0.4	0.2	0.1	0.1
515	0.0396	0.0012	1.2	0.3	0.08	0.04	1	1	-0.4	0.2	0.1	0.1
520	0.0409	0.0009	1.1	0.3	0.13	0.04	1	1	-0.4	0.2	0.1	0.1
525	0.0417	0.001	0.7	0.3	0.14	0.04	1	1	-0.4	0.2	0.1	0.1
530	0.0434	0.0011	0.4	0.3	0.15	0.04	0.3	0.6	-0.4	0.2	0.1	0.1
535	0.0452	0.0012	0.1	0.4	0.15	0.04	0.3	0.5	-0.4	0.2	0.1	0.1
540	0.0474	0.001	0.0	0.3	0.15	0.04	0.2	0.4	-0.4	0.2	0.1	0.1
545	0.0511	0.0011	-0.1	0.3	0.13	0.04	0.2	0.5	-0.4	0.2	0.1	0.1
550	0.0565	0.0011	0.0	0.3	0.13	0.04	0.2	0.4	-0.4	0.1	0.1	0.1
555	0.0596	0.0012	-0.2	0.3	0.16	0.05	0.1	0.4	-0.4	0.1	0.0	0.1
560	0.0619	0.001	-0.4	0.3	0.16	0.05	0.0	0.4	-0.4	0.1	0.0	0.1
565	0.0642	0.0009	-0.6	0.3	0.15	0.05	0.0	0.4	-0.4	0.1	0.0	0.1
570	0.0695	0.0011	-0.7	0.3	0.13	0.04	0.2	0.5	-0.4	0.1	-0.1	0.1
575	0.0772	0.0011	-0.6	0.4	0.10	0.05	1	1	-0.5	0.1	-0.1	0.1
580	0.0896	0.0012	0.0	0.4	0.04	0.05	2	1	-0.5	0.1	-0.1	0.1
585	0.1100	0.0012	1.2	0.4	0.01	0.05	4	1	-0.5	0.1	-0.1	0.1
590	0.1351	0.0012	2.5	0.4	0.03	0.05	6	1	-0.5	0.1	-0.1	0.1
595	0.1672	0.0014	4.5	0.4	-0.02	0.05	8	1	-0.5	0.1	-0.1	0.1
600	0.2224	0.0017	7.9	0.8	-0.16	0.05	10	1	-0.3	0.1	0.0	0.1
605	0.2577	0.0019	10.3	0.8	0.43	0.07	10	1	-0.1	0.1	0.2	0.1
610	0.2644	0.0019	9.5	0.7	0.75	0.07	9	1	0.1	0.1	0.4	0.1
615	0.2678	0.0019	7.2	0.4	0.83	0.07	7	1	0.2	0.1	0.5	0.1
620	0.2755	0.0025	5.4	0.6	0.84	0.08	6	1	0.2	0.1	0.6	0.1
625	0.2834	0.0028	3	1	0.80	0.07	4	1	0.2	0.1	0.6	0.1
630	0.2916	0.0027	0.9	0.7	0.77	0.08	2	1	0.2	0.1	0.5	0.1
635	0.3012	0.0028	-0.5	0.6	0.73	0.08	1	1	0.1	0.1	0.5	0.1
640	0.3108	0.0028	-2	1	0.70	0.08	-0.2	1.1	0.1	0.1	0.4	0.1
645	0.325	0.003	-3	1	0.66	0.07	-0.4	0.9	0.0	0.1	0.3	0.1
650	0.340	0.003	-3.0	0.6	0.60	0.08	0.1	0.8	-0.1	0.1	0.3	0.1
655	0.371	0.003	-2.2	0.7	0.34	0.08	1	1	-0.1	0.1	0.2	0.1
660	0.410	0.004	0.8	0.7	0.41	0.08	2	1	-0.2	0.1	0.2	0.1
665	0.429	0.004	0.9	0.4	0.63	0.09	1	1	-0.2	0.1	0.2	0.1
670	0.439	0.004	-0.4	0.9	0.62	0.07	1	1	-0.2	0.1	0.1	0.1
675	0.448	0.004	-2.1	0.8	0.46	0.08	-0.3	1.2	-0.3	0.1	0.0	0.1
680	0.465	0.004	-4	1	0.25	0.10	-1	1	-0.6	0.1	-0.2	0.1
685	0.486	0.004	-4	1	-0.02	0.09	-1	1	-0.8	0.1	-0.5	0.1
690	0.516	0.004	-4.3	0.7	-0.34	0.09	0.2	0.7	-1.1	0.1	-0.8	0.1
695	0.559	0.005	-4.1	0.7	-0.70	0.07	3	1	-1.5	0.1	-1.2	0.1
700	0.624	0.006	-2.0	1.4	-1.16	0.10	7	2	-1.8	0.1	-1.5	0.1

A	B	C	D	E	F	G	H	I	J	K	L	M
705	0.704	0.006	1.7	0.8	-1.4	0.1	15	3	-2.1	0.1	-1.8	0.1
710	0.827	0.007	11	1	-1.8	0.1	26	4	-2.2	0.1	-2.0	0.1
715	1.007	0.009	27.3	0.8	-1.9	0.1	41	5	-2.3	0.1	-2.1	0.1
720	1.231	0.011	46.3	0.8	-1.8	0.2	63	6	-2.4	0.1	-2.1	0.1
725	1.489	0.006	65.8	0.8	-2.1	0.3	89	7	-2.3	0.1	-2.0	0.1
730	1.97	0.05	98.3	0.5	-4.4	0.4	113	6	-1.7	0.1	-1.3	0.1
735	2.51	0.04	148.5	0.7	-3.7	0.4	131	3	-0.2	0.1	0.2	0.1
740	2.78	0.04	161	1	1.8	0.3	136	4	2.2	0.2	2.6	0.1
745	2.83	0.04	137.2	0.9	4.7	0.8	127	7	4.5	0.3	5.0	0.2
750	2.85	0.04	105.0	0.5	6.5	0.8	107	9	6.2	0.3	6.7	0.3
755	2.88	0.04	74.4	0.7	6.8	0.7						
760	2.86	0.04	44.7	0.3	6.6	0.6						
765	2.86	0.04	18.6	0.9	6.0	0.7						
770	2.82	0.04	-4.4	0.6	5.3	0.6						
775	2.76	0.04	-24.5	0.8	4.5	0.8						
780	2.69	0.04	-40.4	0.7	3.6	0.7						
785	2.59	0.04	-52.1	0.5	2.3	0.7						
790	2.47	0.04	-59.4	0.9	1.1	0.9						
795	2.36	0.04	-62	1	-0.1	0.7						
800	2.25	0.04	-60.0	1.2	-1.3	0.7						
805	2.20	0.04	-52	1	-2.8	0.8						
810	2.19	0.04	-38.4	0.6	-4.4	0.9						
815	2.23	0.04	-20	1.7	-5.2	0.9						
820	2.34	0.04	0	1	-6.2	0.9						
825	2.61	0.05	33	1	-9	1						
830	3.22	0.05	101.0	0.7	-13	1						
835	3.72	0.04	153	1	-8	1						
840	3.94	0.04	145.0	0.5	-2	1						
845	4.09	0.04	115	2	0	1						
850	4.20	0.04	83	2	0	1						
855	4.32	0.04	49	2	0	1						
860	4.60	0.05	27	1	-2	1						
865	4.60	0.05	-0.8	1	-6	2						
870	4.77	0.05	-46	6	-8	2						
875	5.01	0.05	-63	7	-12	1						
880	5.28	0.05	-78	7	-16	2						
885	5.57	0.06	-87	8	-20	1						
890	5.85	0.06	-90	7	-22	2						
895	6.13	0.06	-85	6	-23	1						
900	6.40	0.06	-70	11	-25	2						

Table 1.1: Absorption Coefficients and Uncertainties (cont'd)

A	B	C	D	E	F	G	H	I	J	K	L	M
											Table 1.1: Absorption Coefficients and Uncertainties (cont'd)	
905	6.72	0.06	-47	9	-28	1						
910	7.12	0.06	-10	10	-29	1						
915	7.68	0.06	60	10	-31	1						
920	8.61	0.07	150	10	-34	1						
925	10.1	0.1	284	9	-42	2						
930	12.2	0.1	463	9	-47	1						
935	14.9	0.3	680	17	-56	2						
940	18.3	0.4	920	22	-61	1						
945	22.7	0.5	1180	13	-81	2						
950	28.8	0.7	1520	18	-124	3						
955	37.7	0.4	1950	78	-158	2						
960	44.2	0.5	2400	120	-117	3						
965	46.9	0.4	2550	80	-40	3						
970	48.0	0.4	2440	33	-1	1						
975	48.6	0.4	2060	20	14	1						
980	48.3	0.4	1570	14	21	1						
985	47.2	0.4	1050	8	20	1						
990	45.4	0.4	560	15	3	1						
995	43.1	0.3	130	16	-16	1						
1000	40.7	0.3	-220	19	-35	2						
1005	38.1	0.2	-480	20	-54	1						
1010	35.3	0.2	-670	20	-72	2						
1015	32.6	0.2	-800	17	-85	1						
1020	29.8	0.7	-870	14	-96	2						
1025	27.0	0.6	-890	16	-101	1						
1030	24.4	0.5	-880	13	-99	1						
1035	22.1	0.5	-840	10	-94	2						
1040	20.0	0.4	-790	11	-89	2						
1045	18.2	0.4	-726	8	-81	2						
1050	16.7	0.4	-660	8	-72	2						
1055	15.6	0.3	-590	11	-61	17						
1060	14.8	0.3	-534	7	-53	17						
1065	14.3	0.3	-478	7	-48	17						
1070	14.1	0.3	-428	9	-43	17						
1075	14.1	0.3	-382	9	-43	17						
1080	14.4	0.3	-337	9	-43	17						
1085	15.3	0.4	-287	7	-47	18						
1090	16.2	0.4	-229	9	-46	17						
1095	17.3	0.4	-165	7	-57	17						
1100	18.9	0.5	-82	9	-62	18						

A	B	C	D	E	F	G	H	I	J	K	L	M
1105	20.4	0.6	10	22	-64	17						
1110	22.1	0.7	140	23	-64	17						
1115	23.5	0.7	290	26	-66	18						
1120	25.2	0.8	500	25	-72	18						
1125	28.1	0.7	810	30	-99	16						
1130	33.4	0.8	1310	40	-152	16						
1135	43.2	0.9	2110	90	-258	16						
1140	59.3	0.9	3300	200	-376	17						
1145	78.6	1.4	4700	420	-388	18						
1150	97.0	1.3	5900	560	-275	18						
1155	110	2	6300	410	-92	19						
1160	117	2	5700	140	36	18						
1165	120	2	4690	50	94	18						
1170	121	2	3600	130	103	17						
1175	123	2	2500	150	85	17						
1180	124	2	1600	150	56	17						
1185	125	2	800	120	12	17						
1190	127	2	80	80	-34	17						
1195	128	2	-570	90	-69	17						
1200	127	2	-1200	120	-96	17						
1205	127	2	-1700	130	-128	17						
1210	126	2	-2200	140	-161	17						
1215	124	2	-2500	120	-207	16						
1220	122	2	-2800	110	-255	17						
1225	120	2	-3100	100	-309	16						
1230	119	2	-3210	90	-362	15						

REFERENCES

Armstrong, F. A. J., and G. T. Boalch, 1961: The ultra-violet absorption of sea water. *J. Mar. Biol. Assoc. UK*, **41(03)**: 591–597.

Babin, M. and D. Stramski, 2004: Variations in the mass-specific absorption coefficient of mineral particles suspended in water. *Limnol. Oceanogr.* **49:** 756–767.

Binding, C.E., D.G. Bowers, and E.G. Mitchelson-Jacob, 2003: An algorithm for the retrieval of suspended sediment concentrations in the Irish Sea from SeaWiFS ocean colour satellite imagery. *Int. J. Remote Sens*., **24:** 3791–3806.

Bogucki, D.J., J.A. Domaradzki, R.E. Ecke, and R. Truman, 2004: Light scattering on oceanic turbulence. *Appl. Opt.*, **43(30):** 5662–5668.

Bogucki, D.J., J. Piskozub, M.-E. Carr and G.D. Spiers, 2007: Monte Carlo simulation of propagation of a short light beam through turbulent oceanic flow. *Opt. Exp.*, **15(21)**: 13988–13996.

Boivin L.P., W.F. Davidson, R.S. Storey, D. Sinclair, and E.D. Earle, 1986: Determination of the attenuation coefficients of visible and ultraviolet radiation in heavy water. *Appl. Opt*., **25**: 877–882.

Bowers, D.G. and C.E. Binding, 2006: The optical properties of mineral suspended particles: A review and synthesis. *Estuar. Coast. Shelf Sci.*, **67**: 219–230.

Bowers, D.G., G.E.L. Harker, and B. Stephan, 1996: Absorption spectra of inorganic particles in the Irish Sea and their relevance to remote sensing of chlorophyll. *Int. J. Remote Sens*., **17:** 2449–2460.

Bricaud, A., A. Morel, and L. Prieur, 1981: Absorption by dissolved organic matter of the sea (yellow substance) in the UV and visible domains. *Limnol Oceanogr,* **26(1):** 43–53.

Bricaud, A. and D. Stramski, 1990: Spectral absorption coefficients of living phytoplankton and nonalgal biogenous matter: A comparison between the Peru upwelling area and the Sargasso Sea. *Limnol. Oceanogr.*, **35(3)**: 562–582.

Bricaud, A., M. Babin, A. Morel, and H. Claustre, 1995: Variability in the chlorophyll-specific absorption coefficients of natural phytoplankton: Analysis and parameterization. *J. Geophys. Res.*, **100(C7)**: 13321–13332.

Bricaud, A., A. Morel, M. Babin, K. Allali, and H. Claustre, 1998: Variations of light absorption by suspended particles with chlorophyll a concentration in oceanic (Case 1) waters: Analysis and implications for bio-optical models. *J. Geophys. Res., C, Oceans,* **103(C13):** 98JC02712.

Chavez, F.P., K.R. Buck, R.R. Bidigare, D.M. Karl, D. Hebel, M. Latasa, L. Campbell, and J. Newton, 1995: On the chlorophyll a retention properties of glass-fiber GF/F filters. *Limnol. Oceanogr*., **40:** 428–433.

Copin-Montegut, G., A. Ivanoff, and A. Saliot, 1971: Coefficient d'atténuation des eaux de mer dans l'ultra-violet. *CR Acad. Sci. Paris,* **272:** 1453–1456.

Cruz, R. A., A. Marcano, C. Jacinto, and T. Catunda, 2009: Ultrasensitive thermal lens spectroscopy of water. *Opt. Lett*., **34(12)**: 1882–1884.

Cruz, R. A., M.C. Filadelpho, M. P. P. Castro, A. A. Andrade, C. M. M. Souza, and T. Catunda, 2011: Very low optical absorptions and analyte concentrations in water measured by Optimized Thermal Lens Spectrometry. *Talanta*, **85(2)**: 850–858.

Estapa, M. L., E. Boss, L.M. Mayer, and C.S. Roesler, 2012: Role of iron and organic carbon in mass specific light absorption by particulate matter from Louisiana coastal waters. *Limnol. Oceanogr.*, **57(1):** 97–112.

Ghormley, J.A. and C.J. Hochanadel, 1971: Production of H, OH, H_2O_2 in the flash photolysis of ice. *J. Phys. Chem.*, **75(1)**: 40–44.

Gordon, H.R., O. B. Brown, R. H. Evans, J. W. Brown, R. C. Smith, K. S. Baker, and D. K. Clark, 1988: A semianalytic radiance model of ocean color. *J. Geophys. Res., Atmospheres*, **93(D9)**: 10909–10924.

Green, S. A., & Blough, N. V., 1994: Optical absorption and fluorescence properties of chromophoric dissolved organic matter in natural waters. *Limnol. Oceanogr.*, **39(8)**: 1903–1916.

Grundinkina N.P., 1956: Absorption of ultraviolet radiation by water. *Opt. Spektrosk.*, **1**: 658–662.

Johnson, K. S. and L.J. Coletti, 2002: In situ ultraviolet spectrophotometry for high resolution and long–term monitoring of nitrate, bromide and bisulfide in the ocean. *Deep-Sea Res. Pt. I*, **49(7)**: 1291–1305.

Jonasz, M., and G. R. Fournier. *Theoretical and Experimental Foundations Light Scattering by Particles in Water*, Elsevier, 2007.

Kalle, K., 1966: The problem of the gelbstoff in the sea. *Oceanogr. Mar. Biol. Annu. Rev.*, **4(9):** l–104.

Kishino, M., M. Takahashi, N. Okami, and S. Ichimura, 1985: Estimation of the spectral absorption coefficient of phytoplankton in the sea. *Bull. Mar. Sci.*, **37:** 634–642.

Konovalov, B.V. and O.D. Bekasova, 1969: Method of determining the pigment content of marine phytoplankton without extraction [in Russian]. *Oceanology* **9**: 883–892.

Kou, L., D. Labrie, and P. Chylek, 1993: Refractive indices of water and ice in the 0.65 to 2.5 μm spectral range. *Appl. Opt.*, **32:** 3531–3540.

Kröckel, L. and M.A. Schmidt, 2014: Extinction properties of ultrapure water down to deep ultraviolet wavelengths. *Opt. Mater. Exp.*, **4(9):** 1932–1942.

Lee, Z., J. Wei, K. Voss, M. Lewis, A. Bricaud, and Y. Huot, 2015: Hyperspectral absorption coefficient of "pure" seawater in the range of 350–550 nm inverted from remote sensing reflectance. *Appl. Opt.*, **54(3)**: 546–558.

Lenoble, J, 1956: Etude de la penetration de l'ultraviolet dans la mer. *Annales de Geophysique*. Vol. 12.

Loiselle, S. A., L. Bracchini, A. M. Dattilo, M. Ricci, and A. Tognazzi, 2009: Optical characterization of chromophoric dissolved organic matter using wavelength distribution of absorption spectral slopes. *Limnol. Oceanogr.*, **54(2)**: 590–597.

Mason, J. D., M. T. Cone, and E. S. Fry, 2016: Ultraviolet (250–550 nm) absorption spectrum of pure water. *Appl. Opt.*, **55**: 7163–7172.

Mikkelsen O.A., T.G. Milligan, P.S. Hill, R.J. Chant, C.F. Jago, S.E. Jones, V. Krivtsov, and G. Mitchelson-Jacob, 2008: The influence of schlieren on in situ optical measurements used for particle characterization. *Limnol. Oceanogr.: Methods*, **6**:133–143.

Mitchell, B.G., 1990: Algorithms for determining the absorption coefficient for aquatic particulate using the quantitative filter technique. In *Ocean Optics* X, Proceedings of SPIE 1302, The International Society for Optical Engineering, Bellingham, WA, pp. 137–148.

Morel, A., 1988: Optical modeling of the upper ocean in relation to its biogenous matter content (Case I waters). *J. Geophys. Res.*, **93(10)**: 749–10.

Morel, A. and S. Maritorena, 2001: Bio-optical properties of oceanic waters: A reappraisal. *J. Geophys. Res.*, **106(C4):** 7163–7180.

Morel, A., D. Antoine and B. Gentili, 2002: Bidirectional reflectance of oceanic waters: accounting for Raman emission and varying particle scattering phase function. *Appl. Opt.*, **41(30)**: 6289–6306.

Morel, A., Y. Huot, B. Gentili, P. J. Werdell, S. B. Hooker, and B. A. Franz 2007: Examining the consistency of products derived from various ocean color sensors in open ocean (Case 1) waters in the perspective of a multi-sensor approach. *Remote Sens. Env.*, **111(1)**: 69–88.

Ogura, N., and T. Hanya, 1966: Nature of ultra-violet absorption of seawater. *Nature*, **212.5063**: 758–758.

Pegau, W.S., D. Gray, and J.R.V. Zaneveld, 1997: Absorption and attenuation of visible and near-infrared light in water: dependence on temperature and salinity. *Appl. Opt.*, **36(24)**: 6035–6046.

Pope, R.M. and E.S. Fry, 1997: Absorption spectrum (380–700 nm) of pure water. II. Integrating cavity measurements. *Appl. Opt.*, **36**: 8710–8723.

Prieur, L. and S. Sathyendranath, 1981: An optical classification of coastal and oceanic waters based on the specific spectral absorption curves of phytoplankton pigments, dissolved organic matter, and other particulate materials. *Limnol. Oceanogr.*, **26(4)**: 671–689.

Quickenden, T.I. and J.A. Irvin, 1980: The ultraviolet absorption spectrum of liquid water. *J. Chem. Phys.*, **72:** 4416–4428.

Röttgers, R., and R. Doerffer, 2007: Measurements of optical absorption by chromophoric dissolved organic matter using a point-source integrating-cavity absorption meter. *Limnol. Oceanogr. Methods*, **5(5):** 126–135.

Röttgers, R., D. McKee, and C. Utschig, 2014: Temperature and salinity correction coefficients for light absorption by water in the visible to infrared spectral region. *Opt. Express*, **22(21)**: 25093–25108.

Shifrin, K. S. *Physical optics of ocean water*. Springer Science & Business Media, 1988.

Smith, R.C. and K.S. Baker, 1981: Optical properties of the clearest natural waters (200–800 nm). *Appl Opt.*, **20(2)**: 177–184.

Sogandares, F.M. and E.S. Fry, 1997: Absorption spectrum (340–640 nm) of pure water. I. Photothermal measurements. *Appl. Opt.*, **36(33)**: 8699–8709.

Stramski, D., M. Babin, and S.B. Woźniak, 2007: Variations in the optical properties of terrigeneous mineral-rich particulate matter suspended in seawater. *Limnol. Oceanogr.*, **52**: 2418−2433.

Stramski, D., R.A. Reynolds, S. Kaczmarek, J. Uitz, and G. Zheng, 2015: Correction of pathlength amplification in the filter-pad technique for measurements of particulate absorption coefficient in the visible spectral region. *Appl. Opt.*, **54**: 6763−6782.

Stramski, D., S. B. Woźniak, S. B., and P. J. Flatau, 2004: Optical properties of Asian mineral dust suspended in seawater. *Limnol. Oceanogr.*, **49**: 749−755.

Sullivan J. M., M. S. Twardowski , J. R. Zaneveld, C. Moore, A. Barnard, P. L. Donaghay, and B. Rhoades, 2006: The hyper-spectral temperature and salinity dependent absorption of pure water, salt water and heavy salt water in the visible and near-IR wavelengths (400–750 nm). *Appl. Opt.*, **45**: 5294–5309.

Tam, C.K.N. and A.C. Patel, 1979. Optoacoustic spectroscopy of liquids. *Appl. Phys. Lett.*, **34**: 467–470.

Tassan, S. and G.M. Ferrari, 1995: An alternative approach to absorption measurements of aquatic particles retained on filters. *Limnol. Oceanogr.*, **40:** 1358–1368.

Twardowski, M.S., J.M. Sullivan, P.L. Donaghay, and J.R.V. Zaneveld. 1999: Microscale quantification of the absorption by dissolved and particulate material in coastal waters with an ac-9. *J. Atmos. Oceanic Tech.*, **16:** 691–707.

Twardowski, M. S., E. Boss, J. M. Sullivan, and P. L. Donaghay, 2004: Modeling the spectral shape of absorption by chromophoric dissolved organic matter. *Mar. Chem.*, **89(1)**: 69–88.

van de Hulst, H. C. 1981. *Light Scattering by Small Particles*, Dover, New York

Verdugo, P., 2012: Marine microgels. *Annu. Rev. Mar. Sci.*, **4**: 375–400.

Werdell, P. J., B. A. Franz, S. W. Bailey, G. C. Feldman, E. Boss, V. E. Brando, M. Dowell, T. Hirata, S. J. Lavender, Z. Lee and H. Loisel, 2013: Generalized ocean color inversion model for retrieving marine inherent optical properties. *Appl. Opt.*, **52(10)**: 2019–2037.

Wozniak, B. and J. Dera. *Light absorption in seawater*. Vol. 33. New York: Springer, 2007.

Chapter 2: Reflective Tube Absorption Meters

Michael Twardowski[1], Scott Freeman[2], Scott Pegau[3], J. Ronald V. Zaneveld[4], James L. Mueller[5] and Emmanuel Boss[6]

[1]*Harbor Branch Oceanographic Institute, Florida Atlantic University, Fort Pierce, FL, USA*
[2]*Goddard Space Flight Center, 8800 Greenbelt Rd, Greenbelt, MD, USA*
[3]*Prince William Sound Science Center, Cordova, AK, USA*
[4]*College of Oceanographic and Atmospheric Sciences, Oregon State University, Corvallis, OR, USA*
[5]*Center for Hydro-Optics and Remote Sensing, San Diego State University, CA, USA*
[6]*University of Maine, Orono, ME, USA*

The present chapter focuses on absorption measurements from commercial devices known as the ac-9 and ac-s (Sea-Bird Scientific, Bellevue, WA, USA, formerly WET Labs Inc.), which concurrently measure spectral absorption and attenuation (Zaneveld et al. 1992). These sensors and associated methods have defined the conventional in-water approach for measuring absorption in natural waters over the last 25 years. These sensors have been deployed in support of ocean color algorithm development and validation activities from ships in vertical profiling and underway flow-through systems, moored platforms, towed platforms, autonomous underwater vehicles, autonomous profilers, and helicopters (e.g., Twardowski et al. 2005).

2.1 The Reflective Tube Approach

2.1.1 Background: measuring volume absorption coefficients for medium with particles in suspension

To determine the spectral volume absorption coefficient $a(\lambda)$ with a source and detector pair arranged on a common axis of length Δr, the flux reaching the detector window Φ_K from the incident source flux Φ_i must include the sum of directly transmitted and scattered fluxes, *i.e.* $\Phi_K = \Phi_T + \Phi_B$. If the source and collector are equal in area and the water path between them enclosed in a perfectly reflecting tube, then all forward-scattered photons would be redirected into the beam and reach the detector. For the present, we will postpone consideration of the flux loss due to backscattered photons and treat it as being negligible. Under this construct and assumption, the Eq. 2.1 may be written as:

$$\lim_{\Delta r \to 0}\left\{\frac{\Phi_T(\lambda)+\Phi_B(\lambda)-\Phi_i(\lambda)}{\Phi_i(\lambda)\Delta r}\right\} = -\lim_{\Delta r \to 0}\left\{\frac{A(\lambda)}{\Delta r}\right\} = a(\lambda) \qquad (2.1)$$

where A is absorptance and represents the ratio of absorbed flux to incident flux.

Eq. 2.1 may be expressed in differential form (Eq. 2.2):

$$\frac{d\Phi_K(\lambda,r)}{\Phi(\lambda,r)} = -a(\lambda)dr . \qquad (2.2)$$

Eq. 2.2 can be integrated over discrete path 0 to r_T to obtain Eq. 2.3:

$$a(\lambda) = \frac{\ln\Phi_o(\lambda,0,0,\bullet)-\ln\Phi_K(\lambda,r_T,0,\bullet)}{r_T} = \frac{-\ln T_K(\lambda,r_T)}{r_T} \text{ m}^{-1} . \qquad (2.3)$$

Therefore, knowing pathlength r_T, a can be derived from measurements of incident and transmitted fluxes. In practice, relative intensities for these fluxes are measured and absolute absorption coefficients are derived using a reference material as a blank (Section 2.3). The typical reference material for ocean optics applications has been purified water, discussed later in this chapter.

Absorption measurement accuracy da/a is approximately equivalent to $dS(e^{ar}/ar)$, where S is the electronic noise in the measured signals (Højerslev 1975). Accuracy is thus optimized when $ar = 1$. Theoretically, this relationship can be used to choose an optimal pathlength r for a water type of interest with specific a. The optimal pathlength achieves a balance between progressive loss of transmitted signal with longer pathlengths (i.e., signal-to-noise limitation for the transmission detector) and progressive loss of ability to resolve smaller changes in transmitted versus incident power with smaller pathlengths (coupled

A/D bit noise limitation). Increasing the pathlength, therefore, provides a large change in transmitted power relative to incident power, which is a desirable characteristic for resolving the amount of absorbed flux, but signal-to-noise continually decreases for the transmission detector. The opposite is true for decreasing pathlengths. In practice, very long pathlengths (i.e., several meters would be ideal for the open ocean) are not possible with the practical embodiment of a sensor, so increases in accuracy have been primarily achieved through minimizing dS by optimizing electronics.

Technology intended for *in situ* measurements has a myriad of design challenges associated with working in a medium that is chemically active and conductive, often exposed to high ambient light, under significant pressure, laden with living and non-living particles that may foul optical windows and mechanical components, highly variable in temperature, and relatively viscous with associated drag and boundary layer effects. The most significant advantages are measurement in the ambient medium with as little sample disruption as possible (particularly when the measurement can be made in a remote volume) and high spatial resolution. Sampling rate for *in situ* sensors directly influences spatial resolving capability. Various forms of autonomous deployment have the potential to dramatically increase the temporal- and/or spatial-resolving capabilities for absorption relative to conventional static ship profiling, although possible errors from calibration drift and biofouling must be effectively managed. Considering these challenges, impressive levels of accuracy have nonetheless been achieved using in-water reflective tube sensing capabilities when the proper protocols are followed.

2.1.2 Reflective tube absorption meter concept

The reflecting tube method has been used to measure spectral absorption in the laboratory for many decades (James and Birge 1938). The basic method involves retention of most of the forward scattered light in the detected signal when passing a collimated light beam through a particle suspension, enabled by using a highly reflective cuvette that redirects scattered light toward a diffuser in front of a detector. A highly reflecting cuvette may be simply achieved from a quartz tube surrounded by air (Zaneveld et al. 1992, 1994; Kirk 1992, 1995). It is thus readily apparent that a typical cylindrical cuvette used with benchtop spectrophotometers is a suitable reflecting tube; such an apparatus may be made an effective reflective tube absorption meter by placing a diffuser such as opal glass or a dampened filter pad at the end of the cuvette (Shibata 1957; Yentsch 1962). The method is therefore relatively straightforward to carry out with typical commercially available benchtop equipment.

As mentioned, a reflective tube absorption meter has also been the primary method for carrying out *in situ* absorption measurements in the field for the last 25 years (Zaneveld et al. 1992). The primary disadvantage in the general method is that a significant amount of scattered light in the cuvette is not directed toward the diffuser, resulting in a scattering error that requires some sort of correction scheme (Zaneveld et al. 1994). Additionally, as natural particle composition varies, the fraction of scattered light that is not considered in the measurement also varies.

In Section 2.1 it was observed that to determine the absorption coefficient associated with transmission over an optical pathlength r_T, it would be necessary to measure the sum of transmitted and scattered flux at the detector, $\Phi_K(r_T) = \Phi_T(r_T) + \Phi_B(r_T)$. Neglecting backscattering (typically no more than 2–3% of total scattering), it was suggested that perhaps one might redirect all forward scattered flux to the detector using an *ideal reflective tube*, and determine the absorption coefficient as

$$a = \frac{-1}{r_T} \ln\left(\frac{\Phi_T(r_T) + \Phi_B(r_T)}{\Phi_o(0)} \right). \tag{2.4}$$

Of course, a perfectly reflecting tube cannot be realized in a practical embodiment of an instrument. Nevertheless, because the scattering phase function of suspended particles in natural waters is strongly peaked in the forward direction (e.g., Jonasz and Fournier 2007), it is generally possible to retain about 75 - 85% of scattered photons in the beam reaching the diffuse detector apparatus of such an instrument for natural waters. Note that the exact fraction is a function of the phase function of a particular natural hydrosol and the properties of the specific reflecting tube. James and Birge (1938) built a laboratory version of such an instrument to measure absorption spectra of lake waters, and Zaneveld et al. (1992) introduced an instrument of this type for *in situ* absorption measurements. In some sense, such an instrument is merely a poor transmissometer, failing to exclude all of the singly scattered photons from its beam transmittance

measurement, and therefore, in its ideal realization would measure only losses due by absorption as per Eqs. 2.1 and 2.2.

The transmittance, absorption, scattering and reflection interaction processes that occur in a real reflective tube absorption meter are illustrated schematically in Fig. 2.1. A source emits collimated flux with a cross-sectional area slightly less than that of the reflective tube, and flux reaching the other end of the tube is measured by a detector behind a diffuser that covers its entire cross-sectional area. The diffuser is necessary to ensure the detected signal does not have any bias toward the directionality of the rays received at the end of the cuvette. Ray paths extending directly from the source to the diffuse detector indicate direct transmittance of flux. Ray paths that terminate within the water volume enclosed by the tube indicate absorbed flux. In natural waters, a large fraction of scattered photons is only slightly deflected in the near forward direction (Fig. 2.1) and proceeds directly to the large-area detector without encountering the tube walls. Ray paths with larger scattering angles may encounter the water-quartz interface, where refraction and reflection take place; the refracted portion is transmitted to the outer quartz-air interface, where another refraction and reflection interaction occurs. For simplicity in this conceptual discussion, we do not consider multiple reflection and refractive transmittance interactions within the thin quartz layer. Ray paths containing a scattering angle less than the critical angle ψ_c associated with total internal reflection (TIR) at the outer quartz-air interface, are totally reflected on each encounter with the tube wall and are transmitted to the detector over a slightly elongated path; for a quartz reflective tube, $\psi_c \cong 42°$, and thus the total internal reflectance represents a large fraction of all flux scattered by particles.

Flux transmitted along ray paths with a scattering angle in the range $\psi_c < \psi < \dfrac{\pi}{2}$ undergoes partial transmittance losses $[1 - \rho_g(\psi)]$ at each encounter with the reflectance tube, with the reflected portion continuing over a zig-zag path until either reaching the detector or disappearing due to attenuation by absorption and transmission losses in multiple encounters with the tube wall. Flux along ray paths containing a scattering angle $\psi \geq \dfrac{\pi}{2}$, $i.e.$ backscattered flux, is generally lost from the forward transmittance altogether.
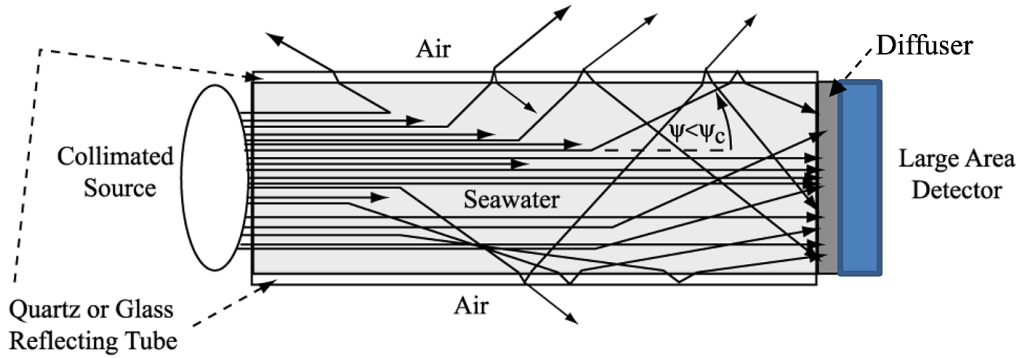
Figure 2.1. Schematic illustration of light interactions and transmission in a reflective tube absorption meter. Ray paths ending in the water represent absorption, and those extending directly from the source to diffuse detector represent beam transmittance. Other ray paths indicate scattering interactions: 1) backward scattered paths do not reach the detector, 2) paths with forward scattering at an angle less than the critical angle, $i.e.$ $\psi \leq \psi_c$, experience total internal reflection by the tube and reach the detector over an elongated optical path, and 3) forward scattered ray paths at angles in the range $\psi_c < \psi < \dfrac{\pi}{2}$ experience partial losses from the tube at the quartz-air interface, and may or may not reach the detector depending on whether the internally reflected path survives the absorption process. Light paths reflecting off windows at the end of the tube are not shown for clarity.

Given the above, in the single scattering approximation, the flux measured by the detector of a reflective tube absorption meter may thus be written as:

$$\Phi_m\left(r_T\right) = \Phi_T\left(r_T\right) + 2\pi\Phi_o\left(0\right)\int_0^{r_T}\int_0^{\psi_c}\beta\left(\psi\right)e^{-cr}e^{-a\frac{r_T-r}{\cos\psi}}\sin\psi\,d\psi\,dr +$$
$$2\pi\Phi_o\left(0\right)\int_0^{r_T}\int_0^{\psi_c}\beta\left(\psi\right)e^{-cr}e^{-a\frac{r_T-r}{\cos\psi}}\left[\rho_g\left(\psi\right)\right]^{N\left(r_T-r\right)}\sin\psi\,d\psi\,dr$$

, (2.5)

where $\rho_g\left(\psi\right)$ is net reflectance of the quartz tube beyond the critical angle, and the exponent $N(r_T - r;\psi)$ is the average number of wall reflections required for a ray path to reach the detector following a scattering event at distance r and angle ψ. The first integral on the right-hand-side of Eq. 2.5 represents flux scattered at angles less than the critical angle over the optical path, and the second integral represents flux reaching the detector following scattering by angles greater than the critical angle. In either case, the pathlength to the detector from a scattering interaction at distance r is $\frac{r_T - r}{\cos\psi}$, and both types of scattered-reflected paths are attenuated by absorption over this elongated path. The second term also is reduced by incomplete reflectance in $N(r_T - r;\psi) \geq 1$ interactions with the reflective tube. This is not a complete description, as some light scattered close to the diffuser at angles larger than Ψ_c will still impinge on the diffuse-detector assembly and some light will be reflected off both source and detector windows back into the tube.

The measured absorption coefficient is therefore greater than the true absorption coefficient since

$$a_m = \frac{-1}{r_T}\ln\left(\frac{\Phi_m\left(r_T\right)}{\Phi_o\left(0\right)}\right) > a = \frac{-1}{r_T}\ln\left(\frac{\Phi_T\left(r_T\right) + \Phi_B\left(r_T\right)}{\Phi_o\left(0\right)}\right),$$

and the two may be related as

$$a_m = a + 2\pi\int_0^\pi W\left(\psi\right)\beta\left(\psi\right)\sin\psi\,d\psi, \qquad (2.6)$$

where the weighting coefficient $W\left(\psi\right)$ accounts for the absorption and wall reflection losses in the two integral terms of Eq. 2.5 and for the exclusion of backscattering in the measured flux. In other words, the weighting coefficient $W\left(\psi\right)$ may be interpreted as the fraction of light that is scattered at angle ψ that does not reach the absorption detector; it may take values from 0, indicating all light scattered at that angle reaches the detector, to 1, indicating that none of the light reaches the detector. Note this error term, often denoted as ε, is a function of the angular shape of the VSF (β) and thus will vary with associated natural variability in particle composition.

McKee et al. (2013; and also mentioned in Leymarie et al. 2010) numerically modeled the weighting function for the scattering error of Sea-Bird Scientific ac devices with Monte Carlo simulations. They computed a presumably more accurate weighting function for a theoretical 100% TIR cuvette, accounting for all possible reflections (Fig. 2.2). They additionally tested the effect of varying the reflectivity efficiency (95–100%) of the flow tube wall, since it may be reasonably assumed that, either through imperfections in the manufacturing of the tube and/or wear through use, ideal or even consistent reflectivity may not be achieved in practice. All modeled weighting functions (including the ideal 100% reflectivity case) exhibited non-negligible weightings at angles smaller than the angle of TIR, i.e., the error included significant scattering at angles smaller than the angle of TIR (Fig. 2.2). Because the VSF is steeply forward peaked, these weighting functions are expected to appreciably increase the relative error, from about 5–15% of total scattering (Zaneveld et al. 1994), to an estimated 15–25% (McKee et al. 2013; Röttgers et al. 2013). The amount of scattering in the angular range $\Psi < TIR$ that is included increases dramatically with small decreases in the reflectivity of the flow tube surface from the ideal value of 100%.

Beyond typical random electronic noise, the uncertainty of absorption coefficients determined from measurements with a reflective tube instrument is largely determined by the uncertainty of the methods

used to correct for the integrated scattering error (Zaneveld et al. 1994), which will be discussed in Section 2.5. The remaining sections of this chapter summarize protocols related to characterization, measurement, and data analysis for the commercially available Sea-Bird Scientific reflective tube absorption meters, known as the ac-9 and ac-s.
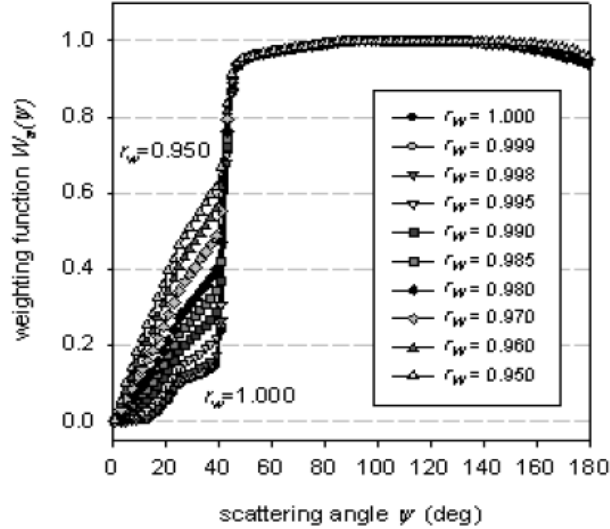
Figure 2.2. Modeled angular weighting functions for the scattering error of the reflective flow tube used in Sea-Bird Scientific ac devices, assuming different initial reflectivities of the inner surface of the tube (from McKee et al. 2013). Angle of total internal reflection (TIR) for a quartz tube surrounded by an air gap is ~42 degrees.

2.2 Description of a Reflective Tube Spectral Absorption Meter

The following sections pertain to the commercially available ac-9 and ac-s devices currently manufactured by Sea-Bird Scientific. As of 2014 the ac-9 is not commercially sold but is still serviceable by Sea-Bird Scientific. These sensors concurrently measure absorption and attenuation through two separate optical systems sharing a rotating wheel with embedded interference filters, integrated into a single device (Fig. 2.3). For each optical path, the quasi-collimated beam from a dedicated tungsten lamp source is sampled by a reference detector using a beam splitter, with the remaining beam passing through the interference filter and subsequently entering the sample volume through an optical glass window. The absorption measurement uses a reflecting quartz tube surrounded by an air gap as a flow cell, with a diffuse collector at the end of the tube, in front of a large area detector. For spectral discrimination, the ac-s uses a linear variable filter (LVF) spliced into two segments, individually mounted on the rotating wheel, with each segment imaged in typically 42 discrete spectral locations to provide 84 wavelengths in typically the 398–730-nm spectral range. The spectral split typically occurs around 574 to 578 nm. Individual spectral increments are therefore about 4 nm and have full-width–half-maximum (FWHM) bandwidths ranging between about 10 nm for centroid wavelengths near the center of each filter, to about 18 nm for centroid wavelengths near the edges of each filter. With the ~4 nm spectral resolution of the ac-s, there are methods of analytically approximating removal of the smoothing or damping effect of the bandwidths on spectra (Sullivan et al. 2006; Chase et al. 2013, with code provided to implement). The ac-9 uses nine individual interference filters, each with a typical bandwidth of 10 nm. Because of the bandwidths used for both ac-9 and ac-s, absorption measurements near the peak for *in vivo* chlorophyll absorption (~675 nm) include some fraction of chlorophyll fluorescence (centered at ~683 nm), although the fluoresced light is only a few percent at most relative to the absorbed light and fluorescence overlaps the tail of the 10 nm FWHM bandwidth of the absorption measurement centered at 675 nm. Because of the inherent similarities between the ac-s and the ac-9, all procedures described in this document generally pertain to both instruments, except where noted.

Sea-Bird Scientific employs either a 10-cm or 25-cm pathlength for the sample volume. As the optimal pathlength in measuring absorption for a given environment is normally equivalent to the inverse of the

absorption coefficient of the natural water medium (hydrosol) of interest (Section 2.1), the two pathlength choices for ac devices are theoretically optimal for water with 10-m^{-1} and 4-m^{-1} absorption, respectively. The vast majority of coastal and open ocean waters exhibit absorption coefficients far lower than these values; in fact, open ocean absorption values in the green part of the visible are typically one to two orders of magnitude lower than the 4-m^{-1} value. However, 20-m pathlengths are impractical for routine *in situ* measurements. Adequate signal-to-noise is nonetheless achievable using a 25-cm pathlength due to advances in A/D conversion and stable, quiet electronics over the past several decades. Acceptable accuracies are even achievable for the clearest waters on Earth with a 25-cm path (Twardowski et al. 2007; Claustre et al. 2007). Accuracy can be further increased by averaging over large number of measurements, e.g., when deploying ac-meters on moorings or in-line systems or on profiling systems with slow rates of descent/ascent (Slade et al. 2010).

The ac-9 and ac-s were introduced in 1993 and 2002, respectively. Sea-Bird Scientific provides detailed protocols for calibrating and using this instrument, and for analyzing its data, both in the ac-9 and ac-s user manuals, and in a detailed protocols manual (Van Zee et al. 2002), all of which are available online at www.seabird.com. Additional detailed background information related to characterization, calibration and data analysis methods for this instrument may be found in Zaneveld et al. (1992) and Twardowski et al. (1999). Here, we will briefly highlight critical aspects of the protocols that must be carefully followed to obtain accurate $a(\lambda)$ measurements using this, or a similar, instrument in the field.
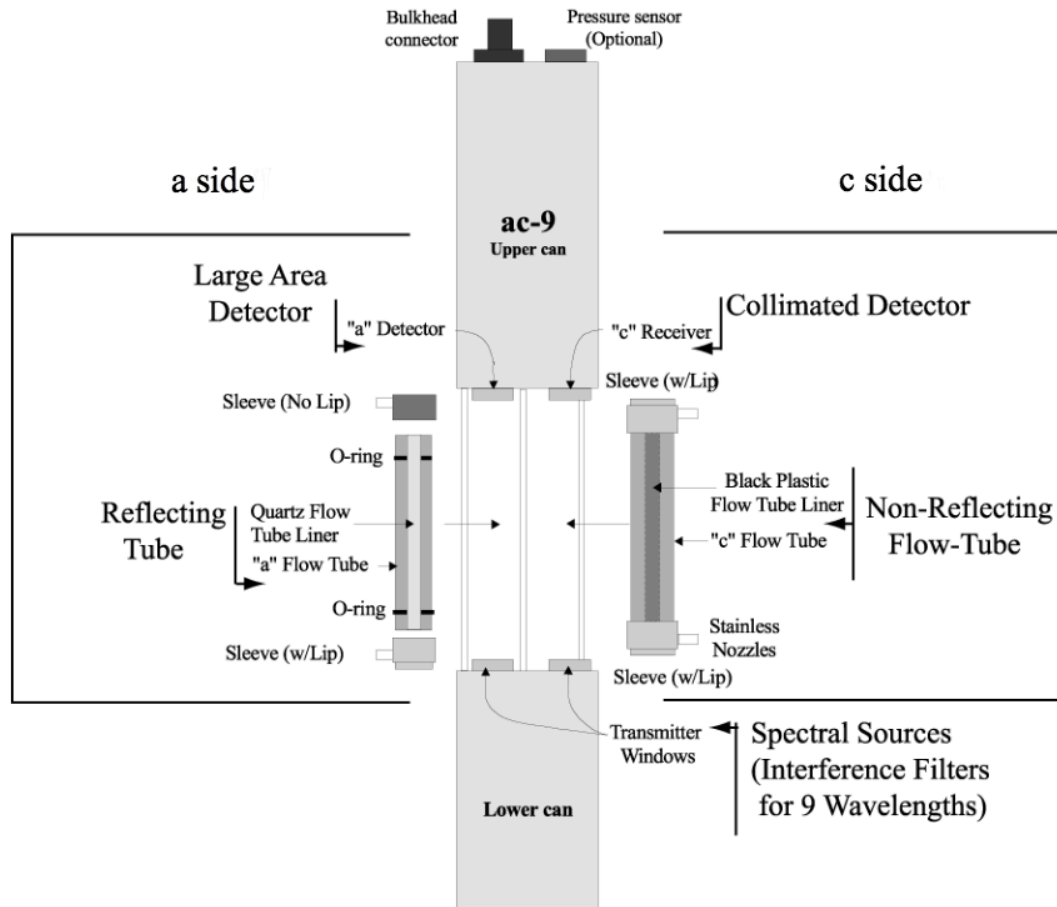
Figure 2.3. Schematic illustration of the ac-9 beam attenuation and absorption meter (courtesy of Sea-Bird Scientific).

2.3 Calibration of a Reflective Tube Spectral Absorption Meter

2.3.1 Pure water calibration

Reflective tube absorption measurements require calibration to some reference medium because gains for the Φ_m and Φ_i detectors are relative and not absolute measures of power. Even if these detectors were calibrated to absolute power using the best techniques available, one would also have to account for the transmission and reflection characteristics of every interface in the optical path to avoid using a reference. Detector responses and the component interface characteristics also change over time with use, so that a complete reassessment would continually be required. It is far simpler to calibrate by passing a reference solution with rigorously characterized optical properties through the sample volume in the exact configuration the sensor will be used for actual measurements. This process can be repeated over time to track calibration drift. An acceptable substance for such calibrations at this time is purified water produced by commercially available water polishing systems with resin cartridges for the removal of organic impurities and a UV oxidizing lamp to remove CDOM. If the interest is only in particulate measurements, periodic measurements of dissolved materials (e.g., water passing through a 0.2-μm filter) can serve as the appropriate reference, effectively canceling any purified water calibration (e.g., Boss and Zaneveld, 2003).

The calibration equation for measured absorption a_m blanked to purified water, is:

$$a_m = \frac{1}{r} ln \left[\frac{(V_{samp})(V_{rfac})}{(V_{fcal})(V_{rsamp})} \right] \tag{2.7}$$

$$a_{wcal} = \frac{1}{r} ln \left[\frac{(V_{wcal})(V_{rfac})}{(V_{fcal})(V_{rcal})} \right] \tag{2.8}$$

$$a_{corr} = a_m - a_{wcal} = \frac{1}{r} ln \left[\frac{(V_{samp})(V_{rcal})}{(V_{wcal})(V_{rsamp})} \right] \tag{2.9}$$

where a_{corr} is calibration corrected absorption, a_m is absorption measured in water sample, a_{wcal} is water calibration absorption, r is pathlength, V_{samp} is detector reading (voltage or digital counts) for water sample, V_{rcal} is reference reading during water calibration, V_{wcal} is detector reading during water calibration, and V_{rsamp} is reference reading for water sample. Values V_{fcal} (detector reading) and V_{rfac} (reference reading) are from a factory water calibration supplied in a sensor-specific device file that should be used for all measurements, i.e., the factory calibration is effectively a baseline blank. Results from a_{wcal} measurements can be used to track instrument drift over time. When a_{wcal} is subtracted from a_m, the factory calibration cancels.

All resultant measurements for natural waters thus represent the absorption from all constituents in the water sample minus the absorption from purified water itself. Note the temperature of the calibration water must be recorded to correct for the temperature dependency of pure water absorption (see Chapter 1 and Section 2.5), which is typically carried out by choosing a reference temperature for all data (calibration water and field data).

2.3.2 Preparation of purified water suitable for calibration

The concept behind the water calibrations is simple. The idea is to provide the instruments with a source of bubble-free water purified of optically significant contaminants that can be used as a reference blank. As was mentioned in Chapter 1, making "pure water" is extraordinarily difficult and certainly is not possible for routine sensor calibrations. The challenge then is obtaining water of sufficient optical purity on a routine basis that may approximate the pure water ideal for reflective tube absorption measurement calibrations. High-end water polishing stations from commercial manufacturers such as Barnstead and Millipore that include resin cartridges for removal of organic impurities and filtration for particle removal produce water of sufficient purity for this purpose.

Water calibrations are performed by the manufacturer, but also should be performed periodically by the user to track short-term drift. Instrument drift is particularly of concern when working in clear waters, where water calibrations should be carried out daily to ensure high-quality data. Significant drift can also occur during instrument shipping.

Sea-Bird Scientific prepares purified water for instrument calibrations using a commercial deionization system and filtration system. After primary deionization, the water is processed using an Elga Medica Pro-30 polishing system and stored in a large holding tank. To maintain purity, water in the holding tank is recirculated through a UV chamber and additional particle filters. Water for calibrations is drawn through a 0.01-μm filter at the point of delivery. The circulating holding tank allows the highly reactive deionized water to equilibrate with ambient conditions and the UV chamber primarily prevents any biological growth from contaminating the reservoir.

During the manufacturer's calibration for an ac device, the internal temperature response of the instrument electronics is also determined along with a correction matrix that is implemented during data processing. Since this correction matrix may also drift, it is recommended that an ac device undergoes a full manufacturer's calibration if consistent departures in absorption are observed over specific internal temperature ranges. The correction matrix produced by Sea-Bird Scientific is typically for instrument temperature varying from about 10 to 35 °C and the correction becomes more significant (increasing potential bias errors in resulting absorption) at internal temperatures greater than about 30 °C. Because of differences in placement of the internal thermister, in water less than 5 °C the internal temperature of an ac-9 will equilibrate near 10 °C, while an acs will equilibrate closer to that of the surrounding water. For field measurements in extremely cold or warm waters, a calibration over an extended internal temperature range can be requested.

For field calibrations by the user, purified water can be produced in the lab and transported to the ship, especially for short cruises. Some research vessels permanently install a water deionization and purification system to support the scientific party. If so, care must be taken to ensure that the system is adequately maintained to produce high-quality purified water. Alternatively, a portable water purification system may be transported and set up temporarily on the ship. Input water should be pre-filtered and preferably passed through a deionization or reverse osmosis system to increase the lifetime of the cartridges in the purification system. Purified water should be produced in advance of calibrations, stored in a clean acid- and base-rinsed polycarbonate carboy, and allowed to stand for several hours to equilibrate with ambient temperature and remove small bubbles.

To calibrate an ac-9, the carboy may be equipped with a cap having barb fittings to connect tubing to a pressurization unit that pushes water to the instrument (Fig. 2.4). The carboy is pressurized to a few psi using an oil-free air pump, a tank of dry nitrogen gas, or a hand pump. The air supply tube inside the carboy should be kept above the water level to prevent the creation of bubbles when pressurizing the carboy, and the outlet tube should extend to the bottom of the carboy. Tubing connecting the carboy to the ac-9 must be opaque to avoid ambient light leaks; the absorption channel is very sensitive in this regard. Standard Tygon® tubing can be wrapped in black tape or certain types of tubing are available with an opaque black sheath. Various types of plastic tubing have chemicals that can leach into the water, possibly affecting the optical properties, although typically the water must sit in the tube for a prolonged period of time to observe this. Thus, most tubing types are fine for calibrations as long as the tubing is kept very clean. Tubing with water flowing from the carboy is connected to the bottom nozzle of the ac-9 flow tube. Tubing connected to the top nozzle (outflow) of the flow tube should have an attached valve, both to control the rate of water flow through the system and to provide backpressure, which helps to keep gases in solution and prevent the formation of small bubbles. After flow appears bubble-free, this valve can be restricting to flow rates as slow as a drip. After practice, a calibration can be achieved with as little as 500 ml of purified water. It is recommended that personnel carrying out calibration are trained initially by people who routinely collect high-quality ac meter data.
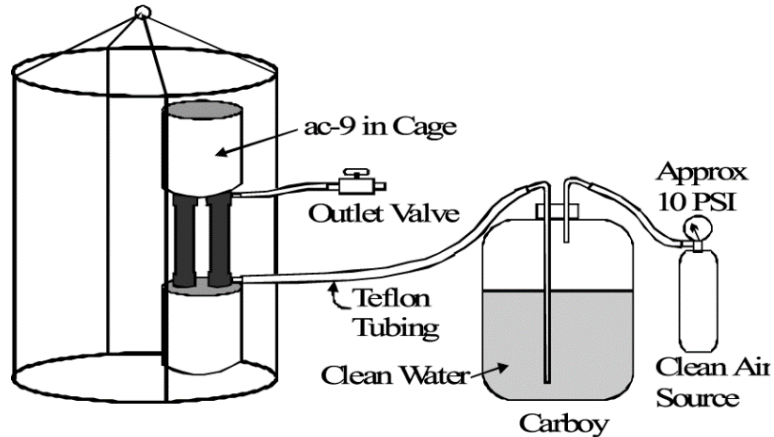
Figure 2.4. Schematic illustration of a pure-water supply system for field calibrations of an ac-9.

Water calibration using a gravity feed with funnel has been carried out previously with success (Sullivan et al. 2006) but is more challenging to execute. With any method, replication is the key to ensuring that a good calibration has been achieved. The ac device cannot be calibrated in the horizontal orientation; it must be oriented vertically.

Whatever the mode of deployment, it is always optimal to calibrate the Sea-Bird Scientific ac device while mounted in the deployment platform or cage in the same orientation as it will be deployed.

2.3.3 Air calibrations

Instructions for air calibrations are provided by the manufacturer, but these cannot be used as an accurate proxy for water calibration drift and thus have limited applicability (Twardowski et al. 1999).

2.4 Measuring Spectral Absorption Coefficients with Reflective Tube Meters

The ac device should be mounted for deployment following directions provided by the manufacturer (Van Zee et al. 2002). Twardowski et al. (1999) also provides additional detail for vertical profiling deployments. Opaque tubing must be attached to the inflow and outflow nozzles of the flow tubes for the absorption and attenuation measurements to avoid ambient light contamination. Sample water must be pumped through the tubes, typically with a submersible pump. A SeaBird Electronics SBE 5 is typically used. The pump is plumbed after the outflow, so the sample is effectively sucked through the sample tubes. A "Y" fitting is typically used to join the flows from the absorption and attenuation paths before reaching the pump. A degassing "Y" fitting (an inverted "Y" with an inserted Teflon™ plug containing a pinhole in the center) should be used after the "Y" flow fitting and before the pump to allow the entire plumbed volume to degas when the sensor is submersed (to avoid air-locking the pump). The intake tubing should be positioned at the desired sampling location on the platform. A separate intake tube should be used for each flow cell, i.e., a single intake split with a "Y" to each measurement tube should be avoided to prevent any possible particle sorting (Twardowski et al. 1999). If the ac device is vertical, the intake will be attached to the lower nozzle on the flow tubes. The device should be plumbed to enable all air to escape when the sensor is submerged. This is typically much easier to achieve when the ac device is positioned vertically. Flow tubes and optical windows should be kept clean using soft tissues such as lens paper or another low-lint wiper (e.g., Kimwipes®) and a 50% ethanol solution.

Coincident measurements of water temperature and salinity data are required for corrections described below in Section 2.5.1. This is typically achieved with an ancillary CTD. Depth positioning of the CTD relative to the ac device, as well as differences in flow rates during profiling and differences in time lag for data collection, should be accounted for in processing (Twardowski et al. 1999; Sullivan et al. 2006).

Power for the ac device and pump can be provided with onboard batteries or via a sea cable. The ac meter and pump should not be powered on until the sensor is fully submerged and degassed or the pump will not function. Degassing can be promoted by lowering the package several meters. After the ac device and pump are powered on, the package can be raised to surface and allowed to equilibrate before profiling. It is highly recommended to use a sea cable with ac meters so that data can be visualized in real time to make sure bubbles are appropriately flushed and, if CDOM absorption is being measured, particle contamination is not present (see below).

When the instrument package is stored on deck for a prolonged period between casts, cover it with a tarpaulin to protect the absorption meter from direct exposure to the sun. Excessive solar heating of the instrument may exceed the practical limits (5 $^{\circ}$C to 30 $^{\circ}$C) of internal temperature corrections for an ac-9, and thus invalidate its measurements until it has cooled sufficiently to restore normal operations.

2.4.1 Filtering the water intake port of an ac-9 for measurements of absorption by CDOM

The absorption coefficient of dissolved material may be measured by attaching a 0.2 μm pore-size filter to the intake(s) of an ac device. Measurements in the filtered intake configuration are also very useful for testing the operational performance of ac-9; quality control procedures using dissolved measurements are discussed in Section 2.6. Note that after particle removal, both the absorption and attenuation measurement should be nominally equivalent. This is a case where the flow may be split to each flow cell using a "Y" connected to a single intake with attached prefilter.

Examples of suitable filters are the Pall Gelman Suporcap 100 and Pall Gelman Maxi-cap (0.2 μm) filters. Generally, these are pleated, hydrophilic filters with large surface areas. These filters have high flow rates at low differential pressure and do not adsorb or leach materials. The outer housings of these commercial filter cartridges may be cut off to expose the pleated filter and increase the flow-rate. Before use, a filter should soak for several hours in clean water to remove air pockets in the filter membrane.

Replace the filter when it becomes visibly discolored. With prolonged measurement in productive coastal waters, this can be daily. Soaking the filter in clean water between measurements can prolong the life of the filter. Flow rates through a filter decrease with use, requiring techniques to independently estimate lag time for each cast (Twardowski et al. 1999). Slow flow rates smear fine structure in absorption measurements. An indirect technique for estimating flow-rate related lag times is to match depths of changes in the a (715) channel with depths of strong changes in water temperature; these changes are linked because absorption by water is temperature dependent in the near infrared (Section 2.5.1), and the time lag between matched changes can be derived from the depth separation and the profiler rate of descent. Another technique is to profile consecutively at different descent rates. Once the correct flow lag-time is chosen, then inflections in the vertical structure of absorption become aligned.

A combination of unfiltered and filtered ac measurements can be used to derive particle absorption. There are several combinations that can be used:

- From measurements using a single ac device with the c side filtered and the a side unfiltered, particulate absorption can be obtained as $a_{\mathrm{p}}(\lambda) = a(\lambda) - a_{\mathrm{w}}(\lambda) - \left[c_{\mathrm{g}}(\lambda) - c_{\mathrm{w}}(\lambda) \right]$, where the measurements have been corrected using the methods described in Section 2.5 below. The subscript "g" is associated with CDOM, based on historical use of the term "*Gelbstoff*", or yellow-matter, as a pseudonym of CDOM.

- From measurements with two ac devices—one filtered and one unfiltered—$a_{\mathrm{g}}(\lambda)$ is derived directly from the filtered measurements, after the corrections of Section 2.5, and $a_{\mathrm{p}}(\lambda) = a(\lambda) - a_{\mathrm{g}}(\lambda)$, where $a(\lambda)$ is derived from the unfiltered instrument.

- Another alternative approach is to make successive casts (if profiling) with one instrument, filtering the a intake on one cast, and the c intake on the other. The filtered and unfiltered measurements from the two casts can be combined as above.

The approach yielding the lowest instrumental uncertainty of the particulate absorption is to derive it from filtered and unfiltered measurements with the same instrument on consecutive casts. Calibration

offsets, whether known or not, are identical in the filtered and unfiltered measurements on each side, and therefore, the offsets cancel when particle absorption is determined as the difference between the two measurements. On the other hand, potentially larger uncertainty may result from possible changes in the IOP profiles between casts, due to horizontal advection and/or vertical displacement of IOP features by internal waves. For consecutive casts, it is optimal to align optical properties with respect to density. There is currently no method for direct *in situ* measurement of particulate absorption subcomponents, e.g., from phytoplankton and detrital material. Partitioning of particulate absorption into these components must be carried out with spectral decomposition modeling (Zheng and Stramski 2013; Zheng et al. 2015).

2.5 Data Analysis Methods

A purified-water blank, corrected to a chosen reference temperature (see below), is first subtracted from the raw collected data. Two additional analysis steps are necessary to obtain accurate absorption coefficients from an ac device or similar instrument: 1) corrections for *in situ* water temperature and salinity, and 2) corrections for scattering errors.

2.5.1 Temperature and salinity corrections

The absorption by pure water exhibits linear dependencies on temperature and salinity described in Chapter 1 and Table 1.1. Pegau et al. (1997) and Twardowski et al. (1999) have empirically determined values for the linear slopes for these dependencies for the ac-9, and Sullivan et al. (2006) has values for the ac-s (Table 1.1). It should be noted that the Sullivan et al. (2006) values were for a specific ac-s (one of the first produced). Changes have since been made by Sea-Bird Scientific in wavelength registrations, so these coefficients may not ideally suit other ac-s devices.

Temperature and salinity corrections are applied to measured absorption according to:

$$a_{\mathrm{m}}^{TS}(\lambda) = a_{\mathrm{m}}(\lambda) - \frac{\partial a_{\mathrm{w}}(\lambda)}{\partial T}(T - T_{\mathrm{r}}) - \frac{\partial a(\lambda)}{\partial S} S. \tag{2.10}$$

The salinity term is left out when applying to water calibrations. Temperature and salinity must be measured concurrently to apply these corrections. Note any temperature can be chosen for T_r since the purified water blank that is corrected to the same T_r must be subtracted in a previous processing step, i.e., the temperature effect is ultimately being completely removed.

Corrections for temperature and salinity dependences only become significant at red and near-infrared wavelengths (see Table 1.1). However, it should be noted that some scattering correction methods *for all wavelengths* discussed in the next section depend on accurate values of $a_{\mathrm{m}}^{TS}(\lambda_{\mathrm{NIR}})$ and $c_{\mathrm{m}}^{TS}(\lambda_{\mathrm{NIR}})$ at a NIR reference wavelength, normally $\lambda_{\mathrm{NIR}} \approx 715\,\mathrm{nm}$ for an ac device. Since naturally occurring absorption is typically low in the NIR, especially for oceanic waters, accurately correcting for temperature and salinity becomes critically important in optimizing accuracy in final absorption spectra with these methods.

2.5.2 Scattering correction methods

Systematic scattering offsets between true absorption and absorption measured with a reflective tube instrument, as described in Eq. 2.6 and related text in Section 2.2, were evaluated by Zaneveld et al. (1994). They recommended three possible methods for correcting the scattering offsets to the measured absorption $a_{\mathrm{m}}^{TS}(\lambda)$ after water blank, temperature, and salinity corrections.

I. Baseline correction. Subtract the measured absorption at a near-infrared reference wavelength, e.g., $\lambda_{NIR} = 715$ nm, from the entire absorption spectrum. This method assumes negligible absorption at λ_{NIR} so that the entire measured signal at the reference wavelength is due to wavelength independent scattering errors. The value of $a_{\mathrm{m}}^{TS}(\lambda_{\mathrm{NIR}})$ should be reported with the corrected absorption values when using this method. Importantly, if measurements of absorption in the dissolved fraction (CDOM) are also available, any absorption from CDOM observed at the reference wavelength should be removed before applying this method.

II. Constant percentage error. Assuming a wavelength-independent scattering phase function appropriate for the type of particles in a given water mass, and a weighting function $W(\psi)$ based on

instrument characteristics, estimate $F = \varepsilon/b$, i.e., the scattering error relative to total scattering, multiply this F by estimated scattering at each wavelength, and subtract from the measured absorption at each wavelength:

$$a(\lambda) = a_m^{TS}(\lambda) - F\,[c_m^{TS}(\lambda) - a_m^{TS}(\lambda)\,]. \tag{2.11}$$

Note that the b derived from $[c_m^{TS}(\lambda) - a_m^{TS}(\lambda)]$ is not precisely equivalent to the b in the F estimate since the $a_m^{TS}(\lambda)$ includes the scattering error. Measured $c_m^{TS}(\lambda)$ also has an acceptance angle error (Voss and Austin 1993; Boss et al. 2009). Since using *a priori* assumptions of particle composition and subsequent phase functions may be speculative for most measurements in natural waters, this method is not typically applied. The method may be useful, however, if a) measurements in the NIR were not made, b) the assumption of negligible absorption in the NIR is thought to be unreasonable (e.g. Tassan and Ferrari 2003; Röttgers et al. 2013), and c) some ancillary information about the particle field may be available that could be used to independently approximate a reasonable proportionality value. Another advantage is uncertainties about temperature and salinity corrections in the NIR do not affect the rest of the spectrum. Several recent publications (Twardowski et al. 2001; Berthon et al. 2007; Whitmire et al. 2010; Sullivan et al. 2013) have shown using theory and experimentation that backscattering ratios (b_b/b) in a broad range of natural waters are approximately spectrally independent, at least within our measurement capabilities at this time. Thus, it may be reasonably assumed that b_b/b also will approximately exhibit spectral independence as well. The fraction F may reasonably vary from about 0.1 to 0.3 for natural particle fields.

III. Proportional correction. This method is a combination of the first two, accounting for the spectral variation in ε as a constant proportion of total scattering b, based on the assumption of a wavelength-independent scattering phase function. The assumption of negligible absorption by dissolved and/or particulate material in the NIR in natural waters is made, so that the measured absorption, a_m(NIR), is then equivalent to ε. The method also relies on concurrent measurements of attenuation $c_m(\lambda)$ so that $b(\lambda)$ may be estimated. The method derives corrected absorption values $a_{corr}^{TS}(\lambda)$ as follows:

$$a_{corr}^{TS}(\lambda) = a_m^{TS}(\lambda) - \frac{a_m^{TS}(\lambda_r)}{c_m^{TS}(\lambda_r) - a_m^{TS}(\lambda_r)}[c_m^{TS}(\lambda) - a_m^{TS}(\lambda)] \tag{2.12}$$

where $\varepsilon(\lambda)$ is the complete term to the right of subtraction, $a_m^{TS}(\lambda_r)$ is assumed to be $\varepsilon(\lambda_r)$ at a suitable wavelength in the NIR (typically 715 nm; note that when evaluated at λ_r the term to the right reduces to $a_m^{TS}(\lambda_r) = \varepsilon(\lambda_r)$, and the spectrally independent proportion of b that comprises ε is represented by the fraction highlighted in gray in the term on the right. Note this method does take into account that $a_m^{TS}(\lambda)$ in the term to the right of subtraction includes $\varepsilon(\lambda)$. Additionally, acceptance angle errors in the c measurement may be expected to approximately cancel.

Considering the primary assumptions for the Zaneveld proportional correction of 1) negligible absorption from dissolved and particulate material in natural waters in the NIR, and 2) a constant proportionality between the correction ε and total scattering spectrally (i.e., a wavelength-independent scattering phase function), the first of these is generally the most concerning (Stockley et al. 2017). The assumption of negligible NIR absorption has been shown to be particularly problematic in turbid coastal waters (e.g. Tassan and Ferrari 2003; Röttgers et al. 2013; see discussion above on assumed spectral independence in ε/b). In data from the North Sea, Röttgers et al. (2013) found an average of 21% of the measured absorption at 715 nm with an ac-9 resulted from real, natural absorption from the dissolved and particulate fractions. Whenever any non-negligible absorption is present in the NIR, the proportional correction will tend to overcorrect. If this fraction F_a of "true" absorption at 715 nm is known or may be reasonably assumed, then a $(1 - F_a)$ term can be added to the numerator of the right hand ε term in Eq. 2.12 to improve the accuracy of the correction. While in most cases the wavelength-independence of the scattering phase function may be a reasonable assumption, there are cases of very high turbidity and strong bloom conditions where this assumption may break down (McKee et al. 2009; Chami et al. 2006; Werdell et al. 2018). Two new scattering correction approaches (see IV and V below) attempt to address one or both of these issues.

There are some considerations in optimizing accuracy in applying the proportional correction to ac device data, especially in coastal waters. First, if CDOM absorption measurements have been made, non-negligible absorption by dissolved materials in the NIR can be subtracted out before applying the correction. Note there is typically no scattering error in absorption collected in the dissolved fraction (Section 1.2). Care must also be taken in the choice of a reference wavelength, with the standard 715 nm

currently serving as the convention. Since dissolved and particulate material show decreases in magnitude entering the NIR from the visible, it would seem reasonable to choose a longer wavelength than 715 nm for the reference in the ac devices. However, uncertainties in pure water absorption due to temperature and salinity dependencies in the NIR increase dramatically for longer wavelengths, making 715 nm a reasonable compromise.

Since the Zaneveld et al. publication in 1994, the proportional correction has generally been regarded as the most accurate method, although the necessity of assuming negligible absorption in the NIR is a significant drawback. Another drawback (also suffered by method II) is the requirement of ancillary data. Even though attenuation data are recorded by the same instrument in an ac device, the measurement is made in a different sample volume. With sampling intakes for the a and c measurements positioned in close proximity, averaging of data is still usually recommended before applying this correction method to smooth out spiking from large particles that may be present in one channel or the other at any given time. Moreover, recent comparisons between the baseline correction (method I) and the proportional correction (method III) have shown similar results, so that the simple baseline correction may be applied in most cases without compromising accuracy relative to method III, and without injecting additional uncertainty from ancillary measurements.

IV. Semi-empirical scattering correction. Röttgers et al. (2013) presented an updated version of the proportional correction method that incorporates two significant new features. The first is to include an empirical relationship between the absorption measured by ac devices in the NIR and values obtained from corresponding PSICAM measurements, which are assumed to be more accurate. The second is to include a correction for the scattering collection error of the attenuation sensor based on observations presented by Boss et al. (2009). The resulting scattering correction is expressed as

$$a_{ac9}(\lambda) = a_m(\lambda) - (a_{m715} - a_{715})\frac{[(1/e_c)c_m(\lambda) - a_c(\lambda)]}{[(1/e_c)c_{m715} - a_{715}]} \tag{2.13}$$

where a_{715} is an estimate of true absorption at 715 nm derived from the empirical relationship mentioned above which had the form

$$a_{715} = 0.212a_{m715}^{1.135} \tag{2.14}$$

This scattering correction approach was found to produce significantly reduced variation with associated PSICAM observations (Rottgers et al. 2013) and has the distinct advantage of being no more difficult to apply than the original proportional correction (Zaneveld et al. 1994). On the other hand, it retains the assumption of a wavelength-independent scattering phase function that may not always pertain. It also was found by Stockley et al. (2017) to be applicable to only relatively turbid conditions.

V. Iterative scattering correction. 3D Monte Carlo simulation of the reflective tube employed in the ac devices was used to produce angular weighting functions for the scattering error shown in Figure 2.2 (McKee et al. 2013). Variability in the reflectivity of the cuvette walls was shown to significantly affect these angular distributions. Together with similar weighting functions for the attenuation sensor geometry (Piskozub et al. 2004) and using additional backscattering measurements to support estimation of scattering phase functions, McKee et al. (2013) presented an iterative scattering error correction that was able to provide close agreement with associated PSICAM observations. The major limiting factor for implementing this correction was the unknown variability in the cuvette wall reflectance. This can be determined empirically if associated PSICAM (or equivalent) data are available. Stockley et al. (2017) and Tonizzo et al. (2017) determined a 98% reflectivity was most applicable to the reflective tubes of ac devices. Another simple option might be to use the empirical relationship described in method IV above to give an estimate of a_{715} that could be used to find the necessary wall reflectance value. While making its own assumptions, an advantage of this approach is that it makes no assumptions about spectral independence of the scattering phase function or negligible absorption in the NIR.

Another method currently under investigation is measuring the volume scattering function independently and deriving ε using Eq. 2.6, independently from the ac device measurements (Stockley et al. 2017; Tonizzo et al. 2017). As mentioned, the angular weighting function for the scattering error (see Fig. 2.2) that was most suitable for an ac device reflective tube had 98% reflectivity. A suitable volume scattering function measurement device is required for implementing this correction, however; currently, such sensors only exist as custom builds by a few laboratories globally.

2.6 Quality Control Procedures

Several quality assurance tests can be used to check how well an ac device is operating. For instance, at the most basic level, attenuation physically must be greater than absorption. One of the most important ways to help ensure accurate measurements is replicating water calibrations with better than 0.005 m^{-1} agreement for all wavelengths, with about 0.002 m^{-1} agreement achievable for most sensors. If this is not achieved, then there is a problem, such as bubbles in the purified water or inside the flow tubes. Older ac-s devices may not be able to achieve this precision in the blue, however.

Filtering both *a* and *c* measurements for an ac device is accomplished by splitting flow from a single filter with a "Y" to both flow tubes, is a useful check, as these two spectra should be equivalent within operational errors, i.e., all convolved random and bias errors, in the absence of particles. The uncertainty from random fluctuations (i.e., standard deviation) should also be < 0.001 m^{-1} (when the data are binned) for most wavelengths after particles have been removed with a prefilter, although uncertainty in the blue region with the ac-s can be higher. If multiple ac devices are used, periodic intercomparisons by attaching prefilters to all devices and deploying in the same water is recommended.

Operational uncertainties for an ac-9 that has been calibrated and corrected with optimal accuracy can be as low as 0.004 m^{-1}. This may be the expected level of agreement between fully corrected data from two ac-9s deployed in close proximity. Different ac-9s can exhibit different performance. Operational uncertainties for optimally corrected ac-s devices are slightly worse than the ac-9, typically about 0.005 m^{-1} and 0.01 m^{-1} at wavelengths above and below 450 nm, respectively. Note that there is nothing wrong with data exhibiting negative values within the uncertainty associated with random fluctuations. Averaging will remove these negative data and improve the effective signal-to-noise ratio. Averaging also enables a larger effective sample volume, so that relatively rare spiking from large particles may be better statistically represented in the absorption values. This is particularly appropriate for remote-sensing applications where IOP data collected in relatively small sample volumes is applied to remote-sensing image pixels as large as 1 km^2. For an ac-s, spectra should be relatively flat in the NIR after correcting for temperature and salinity dependencies.

If concurrent profiles of downwelling irradiance E_d were measured, diffuse attenuation coefficient (K_d) values may be derived from the exponential decrease with depth. Since K_d is typically a reasonable approximation of attenuation of vector irradiance $\vec{K}$, one may use Gershun's equation as an additional check on the accuracy of the absorption measurement, $a \approx \overline{\mu_d} K_d$, where $\overline{\mu_d}$ is the average cosine of the downwelling light field, which can be approximated near the surface from sun elevation and typical sky radiance characteristics (Morel and Prieur 1975).

2.7 Deployment Strategies of Reflective Tube Absorption Meters

Ac-meters have been deployed on a variety of platforms. General consideration: if possible, calibrate the instrument on the package in the same orientation that it will be deployed. Sample waters that have not interacted with the package (that is, on a profiling package, with the intake at the bottom as you profile downward). It is best if the operator can see the data in real-time to assess if bubbles are an issue. The collection of data with and without a prefilter on the intake of the same sensor and along the same path provides very high-quality particulate IOPs (Boss and Zaneveld 2003).

2.7.1 Platform types

1) Winched package

This category includes CTD rosettes (e.g. Bricaud et al. 1995; Sosik et al. 2001), and other winched packages that use a rectangular or round frame. The package is winched down with the package being significantly negatively buoyant (to avoid towing the package). The operator must release the wire fast enough for the package to descend even when the boat is rocking back and forth (e.g., at 0.5–1 m/s). The package should include a CTD for temperature and salinity corrections. Only data collected during the down-cast are considered for particulate measurements.

Advantage: The package can profile to several hundreds of meters rapidly.

Disadvantages: The package accelerates in rough seas, which may cause noise in data due to changes in flow and instrument angle. IOPs exhibit relatively low vertical resolution. Measurements can be

affected by ship shadow (if radiometers are included). To obtain dissolved and particulate spectra often two ac meters are used in parallel (Gardner et al. 2001), or the same one is used with and without a filter on the intake (Boss et al. 2007) (see section 2.4.1).

2) Slow Decent Rate Optical Package (SlowDROP, Barnard et al. 1998)

The SlowDROP package includes a CTD for temperature and salinity corrections and uses a rectangular or round frame with buoyancy balls attached at the top. The package descends due to the influence of gravity. An operator releases the cable as the package descends, being careful not to have tension on wire. Only down-cast data are considered good for particulate measurements. The calibration of instruments should take place on the package.

Advantages: The package does not accelerate rapidly because it is not tied to the vessel with a tight wire and, therefore, does not generate spurious peaks; nor does it change the angle of sensor as it profiles. This method provides a high vertical resolution IOPs (descent rate ~0.1–0.2 m/s) and can be released such that it is removed from the ship's shadow (if radiometers are included).

Disadvantage: This method requires hard work for profiling to depths below 100 m, often requiring manual power to bring it back to the surface.

3) Diver's package (Zaneveld et al. 2001)

The Diver's package uses sensors mounted on the SCUBA bottle on the diver's back. It is necessary to create sufficient buoyancy to offset optical package's weight. The intake is positioned by the diver's hand.

Advantage: This method may be used to obtain data very close to bottom features.

Disadvantage: Achieving a good position is challenging. Moreover, it is necessary to make sure the intake's depth is well represented by the CTD, which is also located on the diver's back.

4) Bottom tripods

Ac-9s have been deployed for months at a time on bottom tripods (Downing et al. 2009; Slade et al. 2010). The system is equipped with a switching mechanism (about 10 min/hour) for calibration-independent particulate properties and/or cleaned periodically for dissolved measurements. The ability to profile (e.g., with an arm, Sherwood et al. 2012) provides vertical dimension to data. The filters are changed by the divers on a weekly basis.

Advantage: High temporal data can be collected.

Disadvantage: Rapid fouling can occur, requiring weekly cleaning and filter changes by divers.

5) Moorings and profiling moorings

Ac meters have been attached on moorings since about 1996 (Change and Dickey 1999, 2001; Roesler and Boss 2008). Measurements are limited to total absorption.

Advantage: High temporal resolution measurements spanning from minutes to seasons.

Disadvantage: Sensor drift and fouling requires use of bio-fouling measures (Manov et al. 2004) and careful post-processing.

6) In-line

Ac-9 and ac-s instruments have been continuously measuring water flowing to research vessel for quite a long time (Balch et al. 2004; Dall'Olmo et al. 2009; Slade et al. 2010). The systems are equipped with a vortex debubbler to remove bubbles before the waters passes to the instruments. In some cases, instruments are kept in a water bath to minimize large instrument temperature changes (NB: if notified, Sea-Bird Scientific provides an extended instrument temperature compensation table for work in high or low latitudes, where instrument temperature can be beyond standard tables). When equipped with an automated switching system, if sufficiently frequent, the particulate measurement can be obtained in a manner that is calibration independent. For dissolved measurements, near-daily cleaning and calibration with deionized water are needed.

Advantage: High spatial resolution measurements and calibration independent particulate properties may be collected. This method is suited for work in very clear water.

Disadvantage: Only surface waters are sampled. Any sampling effects that may occur due to the water passing through the pumping system and long tubes have not been fully characterized (particularly issues associated with disaggregating particles). Such systems should not use an impeller pump that is known to damage particles (peristaltic and diaphragm pumps have been used successfully).

7) Towed systems

Ac meters have been deployed on towed vehicles (SeaSoar, Triaxus and Acrobat; e.g., Ashjian et al. 2006; Jones et al. 2011). The intake is placed near the front of the vehicle to sample clean water.

Advantage: These systems cover a large swath of ocean both horizontally (typically a few kilometers between repeated surface measurements) and vertically (typically a few hundred meters), resolving upper-ocean synoptic variability.

Disadvantage: It is very important to account for lags between the ac instrument and CTD for temperature and salinity corrections. Two sensors are required to obtain dissolved and total (dissolved plus particulate) measurements.

8) Autonomous underwater vehicle (AUV)

Wijesekera et al. (2005) reports on data collected on the Blue Fin AUV with an ac-9 pumped with water coming in from the nose cone with a 1.8-m-long tube. Data were used to assess spatial variability of IOPs and radiometric quantities at different depths.

Advantage: The AUV can obtain data very close to the surface to assess sub-pixel variability.

Disadvantage: Some mixing occurs from the long hose to the front cone.

REFERENCES

Antoine D., A. Morel, E. Leymarie, A. Houyou, B. Gentili, S. Victori, J.-P. Buis, N. Buis, S. Meunier, M. Canini, D. Crozel, B. Fougnie, and P. Henry, 2013: Underwater radiance distributions measured with miniaturized multispectral radiance cameras. *J. Atmos. Oceanic Technol.*, **30(1)**:74–95.

Ashjian, C.J., R. Arnone, C.S. Davis, B. Jones, M. Kahru, C.M. Lee, and B.G. Mitchell, 2006: Biological structure and seasonality in the Japan/East Sea. *Oceanogr.*, **19:** 122–133.

Balch, W., D. Drapeau, B. Bowler, E. Booth, J. Goes, A. Ashe, and J. Frye, 2004: A multi-year record of hydrographic and bio-optical properties in the Gulf of Maine: I. Spatial and temporal variability. *Prog. Oceanogr.,* **63:** 57–9833

Barnard, A. H., W. S. Pegau, and J. R. V. Zaneveld, 1998: Global relationships of the inherent optical properties of the oceans. *J. Geophys. Res.*, **103:** 24,955–24,968.

Boss, E., and J.R.V. Zaneveld, 2003: The effect of bottom substrate on inherent optical properties; evidence of biogeochemical processes. *Limnol. Oceanogr.*, **48:** 346–354.

Boss, E., R. Collier, G. Larson, K. Fennel, and W.S. Pegau, 2007: Measurements of spectral optical properties and their relation to biogeochemical variables and processes in Crater Lake National Park, OR. *Hydrobiologia*, **574:**149–159.

Boss, E., and J.R.V. Zaneveld, 2003: The effect of bottom substrate on inherent optical properties; evidence of biogeochemical processes. *Limnol. Oceanogr.*, **48:** 346–354.

Boss, E., W. H. Slade, M. Behrenfeld, and G. Dall'Olmo, 2009: Acceptance angle effects on the beam attenuation in the ocean. *Opt. Exp.*, **17**: 1535–1550.

Bricaud, A., Roesler, C., and J.R.V. Zaneveld, 1995: In situ methods for measuring the inherent optical properties of ocean waters. *Limnol. Oceanogr,,* **40**: 393–410, 1995.

Chami, M., E. B. Shybanov, G. A. Khomenko, M. E.-G. Lee, O. V. Martynov, and G. K. Korotaev, 2006: Spectral variation of the volume scattering function measured over the full range of scattering angles in a coastal environment. *Appl. Opt.* **45**: 3605–3619.

Chang, G.C. and T.D. Dickey, 1999: Partitioning in situ total spectral absorption b use of moored spectral absorption-attenuation meters. *Appl. Opt.*, **38:** 3876–3887.

Chang, G.C., and T.D. Dickey, 2001: Optical and physical variability on time-scales from minutes to the seasonal cycle on the New England shelf: July 1996–June 1997. *J. Geophys. Res.*, **106:** 9435–9453.

Chase, A., E. Boss, R. Zaneveld, A. Bricaud, H. Claustre, J. Ras, G. Dall'Ollmo, and T. K. Westberry, 2013: Decomposition of in situ particulate absorption spectra. *Methods in Oceanogr.*, **7:** 110–124.

Claustre, H., Y. Huot, I. Obernosterer, B. Gentill, D. Talliez, and M. Lewis, 2007: Gross community production and metabolic balance in the South Pacific Gyre, using a non intrusive bio-optical method. *Biogeosciences Discuss*. **4**: 3089–3121.

Dall'Olmo, G., T.K. Westberry, M.J. Behrenfeld, E. Boss, and W.H. Slade, 2009: Significant contribution of large particles to optical backscattering in the open ocean. *Biogeosciences,* **6:** 947–967.

Downing, Bryan D., E. Boss, B.A. Bergamaschi, J.A. Fleck, M.A. Lionberger, N.K. Ganju, D.H. Schoellhamer, and R. Fujii, 2009: Quantifying fluxes and characterizing compositional changes of dissolved organic matter in aquatic systems in situ using combined acoustic and optical measurements. *Limnol. Oceanogr. Methods*, **7:** 119–131.

Gardner, W.D., J. C. Blakey, I.D. Walsh, M.J. Richardson, S. Pegau, J.R.V. Zaneveld, C. Roesler, M.C. Gregg, J.A. MacKinnon, H.M. Sosik, and A.J. Williams, III, 2001: Optics, particles, stratification and storms on the New England continental shelf. *J. Geophys. Res.*, **106:** 9473–9497.

Gershun, A., 1939: The light field. *J. Math. Phys.*, **18**: 51–151.

Højerslev, N.K., 1975: A spectral light absorption meter for measurements in the sea. *Limnol. Oceanogr.*, **20**: 1024–1034.

James, H.R., and E.A. Birge, 1938: A laboratory study of the absorption of light by lake waters. *Trans. Wis. Acad. Sci.*, **31**: 1–154.

Jones, B.H., C.M. Lee, G. Toro-Farmer, E. Boss, M.C. Gregg, and C.L. Villanoy, 2011: Tidally driven exchange in an archipelago strait, biological and optical responses. *Oceanogr.*, **24(1)**: 143–155.

Kirk, J.T.O., 1992: Monte Carlo modeling of the performance of a reflective tube absorption meter. *Appl. Opt.*, **31(30)**: 6463–6468.

Kirk, J. T. O., 1995: Modeling the performance of an integrating-cavity absorption meter. Theory and calculations for a spherical cavity. *Appl. Opt.*, **34**: 4397–4408.

Leymarie, E., D. Doxaran, and M. Babin, 2010: Uncertainties associated to measurements of inherent optical properties in natural waters. *Appl. Opt.*, **49**: 5415–5436.

Manov, D., G. Chang, and T. Dickey, 2004: Methods for reducing biofouling on moored optical sensors. *J. Atmos. Ocean. Tech.,* **21:** 957–967.

McKee D., M. Chami, I. Brown, V. Sanjuan Calzado, D. Doxaran and A. Cunningham, 2009: The role of measurement uncertainties in observed variability in the spectral backscattering ratio: a case study in mineral-rich coastal waters. Appl. Opt. **48(24)**: 4663 – 4675.

McKee, D., J. Piskozub, R. Röttgers, and R.A. Reynolds, 2013: Evaluation and improvement of an iterative scattering correction scheme for in situ absorption and attenuation measurements. *J. Atmos. Ocean Tech.*, **30(7)**: 1527–1541.

Morel, A. and L. Prieur, 1975: Analyse spectrale des coefficients d'attenuation diffuse, de retrodiffusion pour diverses regions marines. *Rapport No. 17, Centre Rech. Oceanogr. De Villefrance-sur-mer, Final Report Contract No. M01-A01-78-00-4092.*

Pegau, W. S., et al. 1995: A comparison of methods for the measurement of the absorption coefficient in natural waters. *J. Geophys. Res.*, **100(C7)**, 13201–13220, doi:10.1029/95JC00456.

Pegau, W.S., D. Gray, and J.R.V. Zaneveld, 1997: Absorption and attenuation of visible and near-infrared light in water: dependence on temperature and salinity. *Appl. Opt.,* **36(24)**: 6035–6046.

Piskozub, J., D. Stramski, E. Terrill, and W. K. Melville, 2004: Influence of forward and multiple light scatter on the measurement of beam attenuation in highly scattering marine environments. Appl. Opt. **43**: 4723–4731.

Roesler, C.S. and E. Boss, 2008: In situ measurement of the inherent optical properties (IOPs) and potential for harmful algal bloom detection and coastal ecosystem observations. In: Real-Time Coastal Observing Systems for Ecosystem Dynamics and Harmful Algal Bloom, M. Babin, C.S. Roesler and J.J. Cullen, eds., UNESCO Publishing, Paris, France.

Röttgers,R., D. McKee, and S. B. Woźniak, 2013: Evaluation of scatter corrections for ac-9 absorption measurements in coastal water. *Methods in Oceanogr.,* **7**: 21–39.

Sherwood, C.R., P.J., Dickhudt, M.A. Martini, E.T. Montgomery, and E.S. Boss, 2012: Profile measurements and data from the 2011 Optics, Acoustics, and Stress In Situ (OASIS) project at the Martha's Vineyard Coastal Observatory: U.S. Geological Survey Open-File Report 2012–1178, at http://pubs.usgs.gov/of/2012/1178/.

Slade, W.H., E. Boss, G. Dall'Olmo, M.R. Langner, J. Loftin, M.J. Behrenfeld, C. Roesler, and T.K. Westberry, 2010: Underway and moored methods for improving accuracy in measurement of spectral particulate absorption and attenuation. *J. Atmos. Ocean. Tech.,* **27:** 1733–1746.

Sosik, H. M., R.E. Green, W.S. Pegau, and C.S. Roesler, 2001: Temporal and vertical variability in optical properties of New England shelf waters during late summer and spring. *J. Geophys. Res.,* **106:** 9455–9472.

Stockley, N., R. Röttgers, D. McKee, I. Lefering, J. Sullivan, and M. Twardowski, 2017: Assessing uncertainties in scattering correction algorithms for reflective tube absorption measurements made with a WET Labs ac-9. *Opt. Expr.* **25**: A1139–A1153.

Zheng, G. and D. Stramski, 2013: A model for partitioning the light absorption coefficient of suspended marine particles into phytoplankton and non-algal components. *J. Geophys. Res. Oceans*, **118**, 2977–2991, doi:10.1002/ jgrc.20206.

Sullivan J. M., M. S. Twardowski , J. R. Zaneveld, C. Moore, A. Barnard, P. L. Donaghay, and B. Rhoades, 2006: The hyper-spectral temperature and salinity dependent absorption of pure water, salt water and heavy salt water in the visible and near-IR wavelengths (400–750 nm). *Appl. Opt.*, **45**, 5294–5309.

Tonizzo, A., Twardowski, M., McLean, S., Voss, K., Lewis, M. and Trees, C., 2017: Closure and uncertainty assessment for ocean color reflectance using measured volume scattering functions and reflective tube absorption coefficients with novel correction for scattering. *Appl. Opt.*, **56**(1), 130–146.

Twardowski, M.S., J.M. Sullivan, P.L. Donaghay, and J.R.V. Zaneveld, 1999: Microscale quantification of the absorption by dissolved and particulate material in coastal waters with an ac-9. *J. Atmos. Oceanic Tech.*, **16**: 691–707.

Twardowski, M. S., H. Claustre, S. A. Freeman, D. Stramski, and Y. Huot, 2007: Optical backscattering properties of the "clearest" natural waters. *Biogeosciences Discuss.*, **4(4)**: 2441–2491.

Van Zee, H., D. Hankins, and C. deLespinasse, 2002: *ac-9 Protocol Document (Revision F)*. WET Labs Inc., Philomath, OR, 41pp.

Voss, K. J. and A. Morel, 2005: Bidirectional reflectance function for oceanic waters with varying chlorophyll concentration Measurements versus predictions. *Limnol. Oceanogr.*, **50**, 698–705.

Zaneveld, J.R.V., J.C. Kitchen, A. Bricaud, and C. Moore, 1992: Analysis of *in situ* spectral absorption meter data. *Ocean Optics XI,* G.D. Gilbert, Ed., SPIE, **1750**: 187–200.

Zaneveld, J.R.V., J.C. Kitchen, and C. Moore, 1994: The scattering error correction of reflecting-tube absorption meters. *Ocean Optics XII, Proc. SPIE*, **2258**: 44–55.

van de Hulst, H. C. 1981. *Light Scattering by Small Particles*, Dover, New York.

Voss, K. J. and R.W. Austin, 1993: Beam-attenuation measurements error due to small-angle scattering acceptance. *J. Atmos. Oceanic Technol.*, **10:** 113–121.

Wijesekera, H.W., W.S. Pegau, and T.J. Boyd, 2005: Effect of surface waves on the irradiance distribution in the upper ocean. *Opt. Exp.*, **13:** 9257–9264.

Zaneveld, J.R.V., E. Boss, and C.M. Moore, 2001: A diver operated optical and physical profiling system. *J. Atmos. Oceanic. Tech.,* **18:** 1421–1427.

Zheng, G. and Stramski, D., 2013: A model for partitioning the light absorption coefficient of suspended marine particles into phytoplankton and nonalgal components. *J. Geophys. Res.: Oceans*, **118(6):** 2977–2991

Zheng, G., Stramski, D. and DiGiacomo, P.M., 2015: A model for partitioning the light absorption coefficient of natural waters into phytoplankton, nonalgal particulate, and colored dissolved organic components: A case study for the Chesapeake Bay. *J. Geophys. Res.: Oceans*, **120(4):** 2601–2621.

Chapter 3: Integrating Cavity Absorption Meters

Ed Fry

Texas A&M University, College Station, TX, USA

The original motivation for the development of the integrating cavity absorption meter (ICAM) was to solve the scattering problems associated with measuring the optical absorption of pure water and ocean water. The ICAM employs a closed cavity with diffuse (Lambertian) reflecting walls to achieve an isotropic, homogeneous illumination of the sample; consequently, the sample illumination is essentially independent of any scattering effects (i.e., scattering cannot change the isotropic and homogeneous character of the sample illumination). The measured optical absorption includes the absorption by scattering particulates in the sample as well as the absorption by the medium in the cavity. Absorption by the suspended particulates is measured in their naturally occurring population densities, without needing to concentrate them by filtration or centrifuge. The light intensity incident on the walls of the cavity provides the critical measurement parameter; it has an inverse dependence on the sample absorption and is not affected by scattering in the sample (elastic scattering does not remove any energy from the cavity). The ICAM takes advantage of the high reflectivity (typically >99%) of the walls of the integrating cavity to achieve a very long effective pathlength via multiple reflections through the sample; it thereby enhances the sensitivity to a very small absorption by the sample.

In 1970, Elterman introduced the concept of using an integrating cavity to measure absorption (Elterman 1970). His idea provided the basis for the development of the ICAM some 25 years later for measurements of the absorption of pure water in the visible spectral region (Pope and Fry 1997). However, the ICAM concept differs from Elterman's approach in that it uses two integrating cavities, one inside the other. The outer cavity provides an approximately isotropic, homogeneous illumination of the sample in the inner cavity. Specifically, light is introduced into the outer cavity, reflects back and forth between the two cavities, and is converted from an inherently anisotropic field into a nearly isotropic one. This isotropic light field then diffuses through the wall of the inner cavity and uniformly illuminates the sample. The signal is obtained from the ratio between the equilibrium radiant energy densities in the inner sample cavity and in the outer cavity (basically, the signal from the outer cavity provides the normalization). Another significant extension of the ICAM is the point source integrating cavity absorption meter or PSICAM (Kirk 1997; Röttgers et al. 2005). It employs a single integrating cavity that contains the sample, and a point source inside the cavity to illuminate the sample. For the same reasons, the PSICAM also has the ICAM advantages of a long effective pathlength and independence of scattering effects.

It is important to contrast the fundamental differences between the ICAM concept and innovative techniques based on integrating cavities that have been implemented by several others (e.g., Bricaud et al. 1983 or Haardt and Maske 1987). Specifically, rather than illumination of the sample from a single direction and using an integrating cavity to try to collect the scattered light, the ICAM provides isotropic illumination of the sample and thereby inherently avoids scattering effects. In addition, rather than a single pass through the sample, the ICAM provides many passes, which significantly enhances the sensitivity to a weak absorption.

The ICAM implementation actually uses two integrating cavities, where the integrating cavity containing the sample is placed inside a second cavity, see Fig. 3.1. Light is supplied to the outer cavity via a fiber optic through its wall. The wall of the cavity containing the sample has >99% reflectivity, but since it is inside another integrating cavity the light bounces back and forth and tries many times to get through the wall into the inner cavity. If there are no absorption losses, the optical energy density would be the same in both the outer cavity and the inner (sample) cavity; but, in practice, the optical energy density is always smaller in the empty sample cavity. The reason for this double cavity arrangement is to obtain an isotropic field distribution in the outer cavity, which then leaks through the inner cavity wall and provides an isotropic illumination of the sample in the inner cavity. In short, the double cavity converts an inherently anisotropic illumination field into a nearly isotropic one. With no external cavity and only the sample cavity, the input field would have unavoidable directionalities until after at least a couple reflections from the walls.
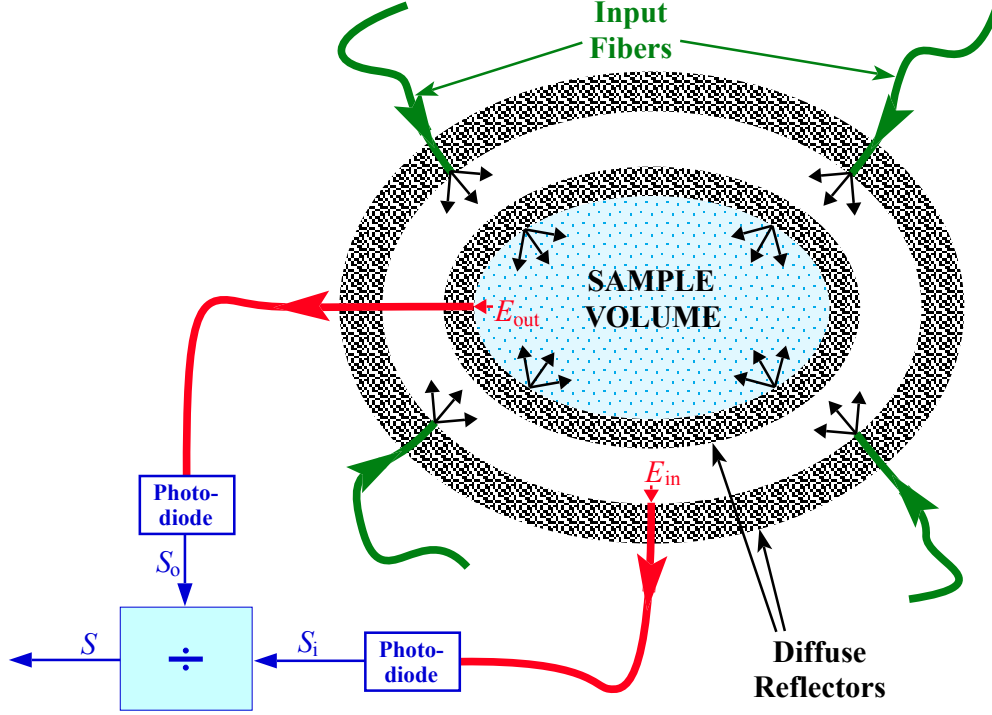
Figure 3.1. Cross-section of a generic ICAM with an inner integrating cavity containing the sample, and an outer integrating cavity to provide isotropic illumination of the sample in the inner cavity.

3.1 Theoretical Background for the ICAM

The rigorous theoretical basis for our instrument was outlined previously (Fry and Kattawar 1988; Fry et al. 1992) and is reviewed here. Let the scalar $L(\mathbf{r}, \hat{\Omega})$ denote the radiance in the direction of the unit vector $\hat{\Omega}$ at a point $\mathbf{r}$. Then, at point $\mathbf{r}$, we can define a vector irradiance $\mathbf{E}$,

$$\mathbf{E} = \int_{\Omega} L(\mathbf{r},\hat{\Omega})\,\hat{\Omega}\,d\Omega , \tag{3.1}$$

and a radiant energy density U,

$$U = \frac{n}{c}\int_{\Omega} L(\mathbf{r},\hat{\Omega})\,d\Omega, \tag{3.2}$$

where the integral is over solid angle Ω, c is the velocity of light in vacuum, and a homogeneous medium with refractive index n is assumed. Now, starting from the equation of radiative transfer, it is straightforward to show that

$$-\nabla \cdot \mathbf{E} = a\frac{c}{n}U, \tag{3.3}$$

where a is the absorption coefficient (Chandrasekhar 1960). This fundamental relation is valid at every point in a medium, irrespective of the magnitude of any scattering effects. Integrating Eq. 3.3 over a volume V of the sample and using the divergence theorem on the left-hand side gives

$$-\int_{S} \mathbf{E} \cdot d\mathbf{S} = a\frac{c}{n}\int_{V} U\,dV. \tag{3.4}$$

The left-hand side of Eq. (3.4) is, of course, the net radiant power entering the cavity containing the sample; i.e., it is the power P_{abs} that is absorbed (*i.e.* the power entering the cavity minus the power leaving the cavity). Thus, P_{abs} is given by

$$P_{abs} = a\frac{c}{n} \int_V U \, dV. \tag{3.5}$$

For a homogeneous medium, this result is exact and is, of course, rigorously independent of scattering effects. Assuming the energy density U is also homogeneous, then Eq. (3.5) becomes

$$P_{abs} = a\frac{c}{n} UV, \tag{3.6}$$

where V is the volume of the sample. This important result was also obtained by Elterman; however, he used a one-dimensional representation and assumed that the radiant energy (joules) in the cavity was attenuated with distance. A form of more practical use is obtained by relating the energy density U inside the sample to the normal component of **E** at the inside surface of the sample. This normal component is called the scalar irradiance, E_{out}, and is just the outwardly directed irradiance at the surface of the sample. If the radiance distribution $L(\mathbf{r}, \hat{\Omega})$ in the sample is both homogeneous and isotropic, then L is a constant and Eqs. (3.1) and (3.2) give, respectively,

$$E_{out} = \hat{\mathbf{n}} \cdot \int_\Omega L(\mathbf{r},\hat{\Omega}) \, \hat{\Omega} \, d\Omega = \pi L , \tag{3.7}$$

$$U = \frac{4\pi nL}{c} , \tag{3.8}$$

where $\hat{\mathbf{n}}$ is an outward unit vector normal to the surface. Combining these equations gives

$$U = \frac{4n}{c} E_{out} ; \tag{3.9}$$

and from Eq. (3.6) the final result for the absorbed power is

$$P_{abs} = 4aVE_{out} . \tag{3.10}$$

To summarize, P_{abs} is the power absorbed in the sample, a is the absorption coefficient of the sample, V is the sample volume, and E_{out} is the outward normal component of the vector irradiance from within the sample at its surface.

By conservation of energy, the power entering the sample volume must equal the power leaving the volume plus the power absorbed,

$$P_{in} = P_{out} + P_{abs}, \tag{3.11}$$

which combined with Eq. 3.10 gives

$$P_{in} = P_{out} + 4aVE_{out} , \tag{3.12}$$

The power in, P_{in}, and the power out, P_{out}, can be written in terms of the normal components of the vector irradiances E_{in} and E_{out}. Specifically, the irradiance on the walls of the outer cavity (*i.e.* the inside surface of the outer cavity wall and the outside surface of the inner cavity wall) is E_{in} and is proportional to the power P_{in} being supplied to the inner cavity. See the generic diagram of an ICAM in Figure 3.1. Similarly, the outward irradiance incident on the inside of the wall of the inner sample cavity is E_{out} and is proportional to the power exiting the sample through the sample cavity wall, as well as through exit ports, detectors, etc. Designating the proportionality constants as K_i and K_o, respectively, the energy conservation equation, Eq. (3.12), becomes

$$K_i E_{in} = K_o E_{out} + 4aVE_{out} , \tag{3.13}$$

Each irradiance, E_{in} and E_{out}, is sampled by optical fibers and detected by a single photomultiplier tube (using a chopper) to produce the two corresponding signal voltages S_i and S_o that are proportional to the irradiances E_{in} and E_{out},

$$S_i = g_i E_{in}; \qquad S_o = g_o E_{out} . \tag{3.14}$$

Although both signals are obtained from the same detector, the g's may be slightly different due to other factors such as coupling to the optical fibers. Eq. (3.13) can now be rewritten as

$$K_i \frac{S_i}{g_i} = K_o \frac{S_o}{g_o} + 4aV \frac{S_o}{g_o}. \tag{3.15}$$

Solving Eq. (3.15) for the absorption coefficient a gives

$$a = \frac{K_i}{4Vg_i} \frac{S_i}{S_o} - \frac{K_o}{4Vg_o} = \frac{1}{4V}\left(\frac{K_i}{g_i} S - \frac{K_o}{g_o} \right), \tag{3.16}$$

or equivalently,

$$a = C_i S - C_o, \tag{3.17}$$

where S is the ratio of the measured signal voltages. The simple relation, Eq. (3.17), is the working equation for the ICAM. Its implementation requires determination of two calibration constants: the signal normalization constant C_i and the offset constant C_o. From Eq. (3.16), these two parameters are constants that are combinations of the other proportionality constants and the volume V,

$$C_i = \frac{K_i}{4Vg_i} \quad ; \qquad C_o = \frac{K_o}{4Vg_o}. \tag{3.18}$$

Of course, both of these constants are functions of the wavelength.

Two partial derivatives of these relations will be useful. Eqs. (3.16) and (3.17) give respectively,

$$\left.\frac{\partial S}{\partial V}\right|_a = \frac{a}{VC_i} \quad ; \qquad \left.\frac{\partial a}{\partial S}\right|_V = C_i. \tag{3.19}$$

Solving Eqs. (3.19) for a, and eliminating C_i gives,

$$a = V \left.\frac{\partial S}{\partial V}\right|_a \left.\frac{\partial a'}{\partial S}\right|_V. \tag{3.20}$$

Eq. (3.20) gives the absorption a of an unknown sample. Specifically, the measured signal S as a function of the volume V of a sample with an unknown absorption coefficient a is linear and has the slope

$$\left.\frac{\partial S}{\partial V}\right|_a ; \tag{3.21}$$

and the known absorption coefficient a' for a variety of samples as a function of the measured signal S from a fixed sample volume is linear and has the slope

$$\left.\frac{\partial a'}{\partial S}\right|_V. \tag{3.22}$$

Depending on the design of the cavity, it may be necessary to supplement the working equation for the ICAM, Eq. (3.17). For example, in the work by Pope and Fry on the measurement of pure water absorption, the placement of the detector for S_0 at the midpoint of the cavity required some additional parameters; but, for the most recent measurements of water absorption in the UV, no additional parameters were required (Mason et al. 2016).

3.2 Flow-through ICAM

Initially, integrating cavity designs were closed systems that required discrete sampling of, for example, water; they can therefore not be used *in situ*. Consequently, an important modification of the ICAM was the development of the flow through ICAM; it is basically a long double-integrating cavity tube for which the central (sample) cavity tube is open at both ends (Gray et al. 2006; Musser et al. 2009). Water can flow through the central tube with negligible turbulence; intensity measurements are made at the midpoint of this long cavity. There is also a flow-through version of the PSICAM. A flow-through ICAM is now commercially available from Turner Designs.

The basic design of the instrument is shown in Fig. 3.2. It consists of a central cylindrical quartz tube with open ends to allow water to flow through it. The tube has an inner radius r_i, an outer radius r_o, and a length L. The inner surface of the quartz tube is polished for a smooth water flow, while the outer surface is heavily frosted to help diffuse the light field inside the sample. Surrounding this tube are two cylindrical layers of a high albedo, diffusely reflecting material. The thinner, inner layer completely surrounds and is

in contact with the outer surface of the quartz. The thicker outer layer is set back some distance from the inner one, providing for a gap between the two. The ends of these cylinders are capped, forming a closed cavity.
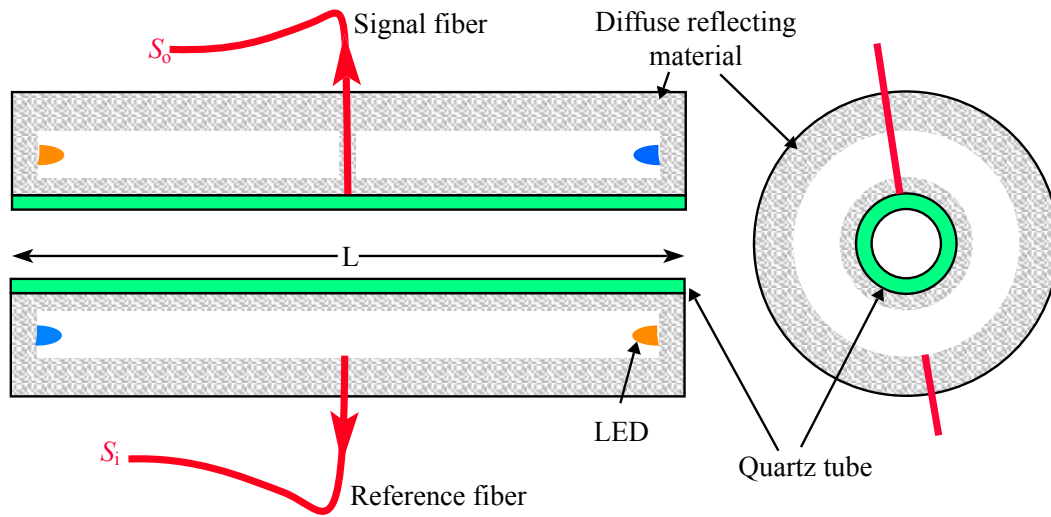
Figure 3.2. Cross-sections of a generic flow through ICAM with an inner integrating cavity surrounding a quartz tube that is open at both ends and through which the water being measured flows.

The outer cavity could be illuminated using an external light source and optical fibers; or, as in Fig. 3.2, LED's could be built directly into the outer cavity. A reference fiber inserted into the outer cavity monitors the radiant energy that is illuminating the water in the quartz tube. A signal collecting fiber passes through both the outer and inner layers of the diffuse reflecting material and is placed in contact with the outer surface of the quartz tube. The signal fiber is isolated from the light field in the outer cavity by wrapping it in aluminum foil and surrounding it with a diffuse reflecting tube in the region between the outer and inner cavity walls.

From an operational view, this design is essentially a variation of the ICAM. It is a cavity within a cavity where light is introduced into the outer cavity and then diffuses into the inner one to be absorbed by the water sample inside. However, with the flow-through design, the inner cavity is not enclosed. So, in addition to allowing water to enter and exit, the open ends of the quartz cylinder allow light to do the same. As a result, the spatial distribution of radiant energy in the water sample will be altered—the light field is neither homogenous nor isotropic. This has several important consequences, and the reader is referred to the discussions in Gray et al. (2006). But, basically, the most immediate effect is that the working equations of the original ICAM no longer apply and the instrument must be calibrated with samples of known absorption. In addition, the geometry of the instrument plays a much greater role. Radiant power will be lost out the open ends, and these losses and resulting changes in energy distribution will depend on the length L and the inner and outer radii, r_i and r_o, of the quartz tube. Finally, scattering effects could again become important due to this additional loss mechanism.

It is immediately obvious that the influence of these end effects can be minimized by making the cylinder long in comparison to its diameter, $L \gg 2r_o$. However, if the instrument is too large, it becomes prohibitively expensive and awkward to use in the field. There are also both theoretical and practical limits on how small the instrument can be made. Specifically, as the radius of the quartz cylinder decreases, the surface-area-to-volume ratio increases; the consequence is that when light reflects off one wall and travels to another, it spends less time in the intervening water sample. Hence, the effective pathlength of light in the water is decreased, and more radiant power will be absorbed or otherwise lost through the cavity walls. A smaller diameter tube will also be more likely to clog with marine debris and be more difficult to clean.

REFERENCES

Bricaud, A., A. Morel, and L. Prieur, 1983: Optical efficiency factors of some phytoplankters. *Limnol. Oceanogr.*, **28:** 816–832.

Chandrasekhar, S., 1960: *Radiative Transfer*. Dover. 393 pp.

Elterman, P., 1970: Integrating cavity spectroscopy. *Appl. Opt.*, **9:** 2141–2142

Fry, E.S. and G.W. Kattawar, 1988: Measurement of the absorption coefficient of ocean water using isotropic illumination. in *Ocean Optics IX*, **925,** M. A. Blizard, ed.: 142–148.

Fry, E.S., G.W. Kattawar and R.M. Pope, 1992: Integrating cavity absorption meter. *Appl. Opt.*, **31:** 2055–2065.

Gray, D.J., G.W. Kattawar, and E.S. Fry, 2006: Design and analysis of a flow-through integrating cavity absorption meter. *Appl. Opt.,* **45:** 8990–8998.

Haardt, H. and H. Maske, 1987: Specific in vivo absorption coefficient of chlorophyll a at 675 nm. *Limnol. Oceanogr.*, **32:** 608–619.

Kirk, J.T.O., 1997: Point-source integrating-cavity absorption meter: theoretical principles and numerical modeling. *Appl. Opt.,* **36:** 6123–6128.

Mason, J.D., M.T. Cone, and E.S. Fry, 2016: Ultraviolet (250–400) absorption spectrum of pure water. *Appl. Opt.,* **55(25):** 7163–7172.

Musser, J.A., E.S. Fry, and D.J. Gray, 2009: Flow-through integrating cavity absorption meter: experimental results. *Appl. Opt.,* **48:** 3596–3602.

Pope, R.M. and E.S., Fry, 1997: Absorption spectrum (380–700 nm) of pure water. II. Integrating cavity measurements. *Appl. Opt.,* **36:** 8710–8723.

Röttgers, R, W. Schönfeld, P. Kipp, and R. Doerffer, 2005: Practical test of a point-source integrating cavity absorption meter: the performance of different collector assemblies. *Appl. Opt.,* **44:** 5549–5560.

Turner Designs, https://www.turnerdesigns.com

Chapter 4: Point-Source Integrating Cavity Absorption Meters

Rüdiger Röttgers

Helmholtz-Zentrum Geesthacht, Centre for Materials and Coastal Research, Germany

A possibility to overcome problems with scattering and sample handling when determining a_p is to measure the original sample inside an integrating sphere. The integrating sphere approach avoids scattering interference with the optical density determination and provides sufficient sensitivity by a long optical pathlength (up to several meters). One way to reduce scattering effects to an insignificant level is to arrange an isotropic light field inside the sphere, such that any additional scattering event inside the sphere does not change the light field. A simple way to do this is to use a central isotropic light source, as proposed and theoretically described by Kirk (1995, 1997) as the point-source integrating-cavity absorption meter (PSICAM). The PSICAM concept was further investigated by Leathers et al. (2002) and Lerebourg et al. (2002) and successfully tested by Röttgers et al. (2005). Results with a simple lab instrument are shown by Röttgers et al. (2007) and Röttgers and Doerffer (2007).

Integrating cavities of the PSICAM (Fig. 4.1) can have inner diameters of between 5.0 cm and 9.0 cm (the smaller diameters are used for highly absorbing water) and are made out of a block of a diffuse, highly reflective, PTFE-based plastic material (OP.DI.MA, Gigahertz Optik, Germany; or Spectralon, Labsphere Inc., USA). The reflectivity of this material depends on the material thickness and reaches 97 - 99% for a thickness of >10 mm. The surface of these materials is water-repellent and contamination by natural substances—soluble or particulate— is much reduced. The central light source consists of a small scattering sphere made out of a diffuse quartz glass with an outer diameter of 10.0 mm. A typical, simple lab version of the PSICAM has two openings that can be closed by Teflon stoppers, one for inserting and changing the central light source and one for filling and emptying the cavity. Light is provided by an electronically stabilized 150-W halogen bulb and is detected by a photodiode array spectroradiometer. The setup allows a spectral range of 370–800 nm; however, strong water absorption at wavelengths > 700 nm typically limits the range to 370–720 nm.
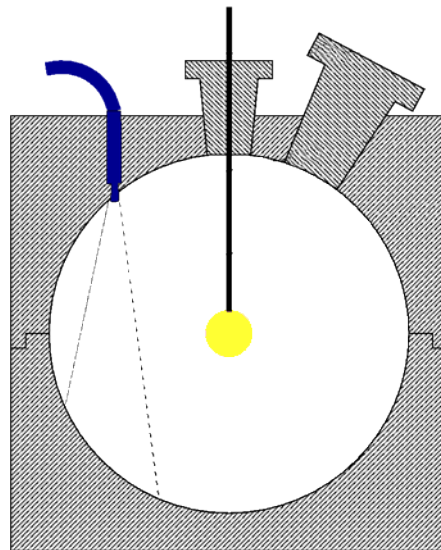
Figure 4.1. Schematic cross-section of a PSICAM showing the central light source, the light detector (top left) with its field of view indicated (dashed lines) and the inner cavity. The light detector is a tip of a fiber optic with the other end connected to a spectroradiometer. The central light source is a sphere made from a diffuse quartz glass sitting on the tip of a fiber optic connected to an external halogen light source.

4.1 Theoretical Considerations of the PSICAM

According to Kirk (1997) and Leathers et al. (2000), the "transmission" difference between two samples (A and B), T_{AB}, in a PSICAM is the ratio of the diffuse reflected irradiance F_0 at the inner wall when the cavity is filled with either the sample A or B (Eq. 4.1). (Note: for simplification, the dependency of wavelength is omitted in the following when not necessary.) Each irradiance is proportional to the number of times a photon is reflected by the wall, N_c, before it is absorbed either by the wall or by the sample fluid, hence,

$$T_{AB} = \frac{F_0^A}{F_0^B} = \frac{N_c^A}{N_c^B}. \tag{4.1}$$

N_c is the fraction of photons reaching the wall directly and indirectly by reflection on the wall for one, or more times (Eq. 4.2). It depends (1) on the probability P_0 that a photon, coming from the central light source, reaches the wall directly, (2) on the reflectivity of the wall, ρ, and (3) on the probability P_s that a photon, which is reflected, will return to the wall. In the PSICAM set-up used here the detector does not collect light that comes directly from the light source, thus, for N_c this gives

$$N_c = P_0 \rho P_s + P_0 \rho^2 P_s^2 + \cdots = P_0 \sum_{n=1}^{\infty} (\rho P_s)^n = \frac{\rho P_0 P_s}{1 - \rho P_s}. \tag{4.2}$$

Therefore,

$$T_{AB} = \frac{P_0^A P_s^A (1 - \rho P_s^B)}{P_0^B P_s^B (1 - \rho P_s^A)}. \tag{4.3}$$

P_0 and P_s are related to the radii of the PSICAM $r_0 = r - r_s$ and r, respectively, where r is the inner radius of the cavity and r_s the radius of the central light source, and to the absorption coefficient a in the following way (see Kirk 1997 for details):

$$P_0(a, r_o) = \exp(-a r_0) \tag{4.4}$$

$$P_s(a, r) = \frac{1}{2a^2 r^2} [1 - \exp(-2ar)(2ar + 1)]. \tag{4.5}$$

Finally, the "transmission" in the PSICAM is related to the absorption coefficients a_A and a_B of the two solutions as

$$T_{AB} = exp[-r_0(a_A - a_B)] \left[\frac{1 - \rho P_s(a_B, r)}{1 - \rho P_s(a_A, r)} \frac{P_s(a_A, r)}{P_s(a_B, r)} \right] \tag{4.6}$$

When using Eq. (4.5) and (4.6), T_{AB} is a function of the light absorption of the samples a_A and a_B, the radii r and r_0, and the reflectivity ρ. Solving Eq. (4.6) for the reflectivity gives

$$\rho = \frac{T_{AB} \exp(-a_B r_0) P_s(a_B, r) - \exp(-a_A r_0) P_s(a_A, r)}{T_{AB} \exp(-a_B r_0) P_s(a_A, r) P_s(a_B, r) - \exp(-a_A r_0) P_s(a_B, r) P_s(a_A, r)}. \tag{4.7}$$

4.2 Calibration of the PSICAM

The error for absorption determination in a PSICAM is related mainly to the error in determining the inner radius, r, the reflectivity, ρ, and to the "transmission" determination in the PSICAM. The "transmission" measurement is influenced by the stability of the light source and that of the spectroradiometer response. From these errors, the error related to ρ has the strongest influence: a 1% error in ρ leads to >10% error in the absorption determination. Hence, ρ has to be known with a high accuracy. It is determined using Eq. (4.7), by measuring the "transmission" by two solutions with known absorption coefficients. Determining ρ in this way has the advantage that it will eliminate errors associated with the

true ρ of the wall material, and with r_0, a_A, a_B, and the known water absorption, if the same values are later used for calculating either a_A or a_B. However, the error of the necessary determination of the absorption coefficient with a photometer, directly influences the error of the absorption determination with the PSICAM.

Practically, ρ is determined following the suggestion and description by Leathers et al. (2000). Therefore, T_{AB} is determined from a sample solution A with an absorption coefficient a_A measured against a reference solution B with an absorption coefficient a_B in the PSICAM. The reference solution B consists simply of purified water. The assumed absorption coefficient spectrum of this purified water, a_w, is taken from published pure water absorption coefficients (Pope and Fry 1997) that can be adjusted and smoothed to have a complete spectrum for the considered wavelengths range (370–720 nm). As discussed above any error in this pure water absorption is compensated by the calibration procedure described here, the exact pure water absorption is of less significance.

Solution A is prepared from the colored stain Nigrosine (Certistain, Merck, Germany), following suggestions of Kirk (1997). Compared to other dye solutions Nigrosine has the advantage of having a considerably high absorption coefficient at all required wavelengths. A Nigrosine stock solution is prepared by dissolving a few crystals of Nigrosine in 100 ml of purified water. The optical density of this solution is roughly determined photometrically in a 1-cm cuvette at 578 nm, to be able to calculate the necessary volume of this stock solution when later preparing the calibration solutions. A calibration solution with absorption coefficient (a_{578nm}) between 0.5 and 2 m^{-1} (on the log_n scale) are prepared by diluting a few milliliters of the 0.2-µm-filtered stock solution in a large enough volume of purified water to conduct several measurements. The exact spectral absorption coefficients of this Nigrosine in solution is determined spectrophotometrically in the range of 350–800 nm (using a 10 cm cuvette in a commercial dual-beam spectrophotometer, or in a liquid waveguide system with pathlengths of 50 cm to 1 m) and purified water as the reference.

The "transmission" measurements in the PSICAM are conducted in triplicate by determining the light intensity inside the cavity when the cavity is first filled with purified water, F_w, and second with the calibration solution, F_{nig}. In each case the temperature of the fluid (t_w and t_{nig}) inside the cavity is recorded for a later temperature correction of the pure water absorption. After the calibration solution has been measured, the PSICAM has to be cleaned as the stain adsorbs considerably fast on the cavity wall of the PSICAM. Therefore, the PSICAM is bleached for 15 min with a 0.1% sodium hypochlorite solution (NaOCl, Riedel de Haen, Germany). Afterward, the bleach is removed from the PSICAM by washing the cavity several times with purified water.

The reflectivity is calculated for each pair of pure water/calibration solution using the pure water absorption as a_B, and the sum of absorptions of pure water and Nigrosine as a_A. The pure water absorption is calculated beforehand for each fluid using the specific fluid temperature, the instrument-specific temperature correction coefficient (see below) and published values of the water absorption of Pope and Fry (1997). Calibration should be done repetitively and regularly with each measurement set (Fig. 4.2).

4.2.1 Calibration procedure

1. Prepare 100 ml Nigrosine stock solution ($A_{580nm}{}^{1cm}$ ca. 3 OD).
2. Prepare a sufficient volume of Nigrosine calibration solution (1 – 2L; a_{580nm} = 0.5–2 m^{-1}).
3. Determine the Nigrosine absorption, a_{nig}, of the calibration solution (10 cm cuvette in spectrophotometer, or using a LWCC system (in triplicate).
4. Determine "transmission" (nigrosine solution vs. purified water) in the PSICAM (in triplicate), cleaning and bleaching of the cavity after each nigrosine solution.
5. Calculate the reflectivity with Eqs. (4.7) and (4.5) (including temperature correction of pure water absorption), where
   $a_A = a_w(t_{nig}) + a_{nig}$,
   $a_B = a_w(t_w)$,
   $T_{AB} = F_{nig}/F_w$,
   $r_0 = 0.040$ m, (example for a 90 mm diameter cavity),
   $r = 0.045$ m (example for a 90 mm diameter cavity).
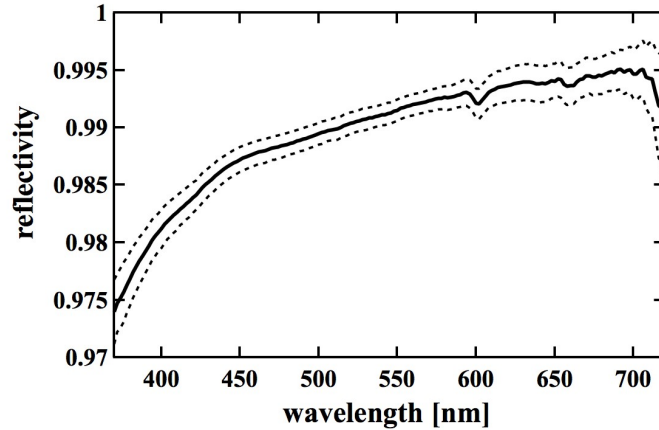
Figure 4.2. Reflectivity, ρ, for a typical PSICAM with indicated confidence limits for repetitive measurements (n=61) done during one ship cruise. Small artifacts at water absorption shoulders, i.e., at 600, 660, and >700 nm are visible due to differences in the optical resolution between PSICAM measurement and that during determination of the pure water absorption; these do not have effects on the determination of the absorption coefficients. The confidence interval represents an error in ρ that would lead to errors in the absorption coefficient of between 1 and 3% (mean: 1.4%).

4.3 Measurement and Calculation of the Absorption Coefficient with the PSICAM

Regular measurements are done by measuring the light intensity inside the cavity when it is filled with either purified water or the sample. This can be done in an alternating way until the sample is measured three times. For each measurement, the fluid temperature and the sample salinity need to be recorded for a later temperature and salinity correction of the pure water absorption. In addition, the light intensity might be measured when an additional short-pass filter is placed in front of the external light source to measure the sample's chlorophyll fluorescence, which is used to correct the absorption for the influence of this fluorescence inside the cavity in the range of the fluorescence, i.e. 670–700 nm. For each sample measurement, T_{AB} can be calculated two times using the reference measurement taken before and after the sample measurement. The real T_{AB} is the mean of these two values, this corrects for possible constant drifts in the light intensity by either a drift in the lamp output or the detector response.

There is no analytical solution for any absorption coefficient $a(\lambda)$ in Eq. (4.6). When $\rho(\lambda)$ is known, $a(\lambda)$ is determined by solving this equation numerically. This is done by minimizing the least square function $G(a(\lambda))$ for the measured transmission, $T_{meas}(\lambda)$ using a numerically calculated transmission $T_{num}(\lambda)$.

$$G\big(a_{(\lambda)}\big) = \sqrt{(T_{num}(\lambda) - T_{meas}(\lambda))^2} \qquad (4.8)$$

For the absorption coefficient of pure water, the same data have to be used as for the calibration (e.g., Pope and Fry 1997). To obtain the absorption coefficient of the water constituents (besides water), the water absorption coefficient has to be subtracted from the resulting absorption coefficient of the sample.

4.3.1 Measurement procedure

1. Fill the PSICAM with purified water, measure the fluid's temperature (t_w) and then the light intensity, F_w.
2. Fill the PSICAM with the sample, measure the fluid's temperature (t_{sample}) and then the light intensity, F_{sample}, record the sample's salinity (S_{sample}). Afterwards wash the cavity with purified water.
3. Repeat steps 1 and 2 three times for triplicate measurements; when sample measurements have been completed, measure the purified water once more.
4. Calculate the transmissions as F_{sample}/F_w using the F_w measured before and after each sample.
5. Determine the absorption for each transmission using Eq (4.6) and (4.5) by minimizing Eq. (4.8) after the pure water absorption has been corrected for the specific temperature and sample salinity, where

$a_A = a_w(t_{sample}, S_{sample}) + a_{sample}$,

$a_B = a_w(t_w)$,

$T_{AB} = F_{sample}/F_w$,

r_0=0.040 m, (example for a 90 mm diameter cavity),

r=0.045 m, (example for a 90 mm diameter cavity),

and a_{sample} is the unknown absorption to be fitted.

4.4 Corrections for Chlorophyll Fluorescence Inside the PSICAM

As the light inside the PSICAM and the detector spectral responses are not monochromatic, some chlorophyll fluorescence is induced and emitted at about 660–710 nm (max 675–685 nm). This extra light leads to an underestimation of the absorption coefficient (e.g., by up to 15% at 675 nm). To correct for this artifact, the fluorescence intensity, F_{fluor}, is determined by measuring it when a short-pass filter (SPF; blocking light at > 650 nm) is placed in front of the light source and when the cavity is filled with the sample and the reference. This results in light intensities measurements named F_{sample}^{SPF} and F_w^{SPF}, respectively. The obtained fluorescence intensity at wavelengths between 660 and 710 nm is corrected for 1) fluorescence re-absorption, due to light absorption in the sample at 660–710 nm; and 2) reduction in excitation intensity by placement of the short-pass filter, as

$$F_{fluor}(\lambda) = \begin{cases} R_F\left[F_{sample}^{SPF}(\lambda) - F_w^{SPF}(\lambda)\, T_{AB}(\lambda)\right] & : \quad 660\, nm \leq \lambda \leq 710\, nm \\ 0 & : \qquad\qquad else \end{cases} \tag{4.9}$$

where R_F is the ratio of absolute absorption of the light inside the cavity by the sample with and without the short-pass filter integrated over all wavelengths, as

$$R_F = \sum_\lambda \left(F_w(\lambda) - F_{sample}(\lambda)\right) \bigg/ \sum_\lambda \left(F_w^{SPF}(\lambda) - F_{sample}^{SPF}(\lambda)\right) + 0.1. \tag{4.10}$$

The ratio R_F compensates for the fact that fluorescence is a function of absorbed light by the pigments not simply irradiated light and that the number of photons absorbed is reduced by the short pass filter at all wavelengths especially at > 650 nm. The additional "0.1" was obtained empirically (comparing spectrally PSICAM and filter pad measurements) and compensates for the fact that only absorption by pigments not by all absorbing material leads to chlorophyll fluorescence such that R_F is underestimated as only total absorption was taken into account.

Finally, the correct "transmission", T_{AB}^c, is calculated as

$$T_{AB}^c = \left(F_{sample} - F_{fluor}\right)/F_w \tag{4.11}$$

The remaining deviations at 675 nm between PSICAM and filter pad measurements (correctly adjusted for pathlength amplification) are in the range of a few percent only.

4.5 Temperature and Salinity Correction of the Pure Water Absorption in the PSICAM

The absorption of pure water, a_w, is dependent on temperature and salinity. Any difference in temperature and salinity between the sample or the reference to that of the theoretical pure water absorption (i.e. 20 °C and 0 PSU) has to be corrected using instrument-specific temperature and salinity correction coefficients, Ψ_t^i and Ψ_S^i as

$$a_w(t, \lambda) = a_w(t_o, \lambda) + (t - t_0)\Psi_t^i(\lambda) \tag{4.12}$$

and

$$a_w(S, \lambda) = a_w(S_o, \lambda) + (S - S_0)\Psi_S^i(\lambda), \tag{4.13}$$

where t is the specific temperature, S the specific salinity, and t_0 and S_0 the values at which the pure water absorption had been measured, i.e., 20 °C and 0 PSU. Values for Ψ_t^i and Ψ_S^i can be determined for each instrument setup. Ψ_S^i is determined by measuring either a concentrated NaCl solution (100–200 gL^{-1}) or an artificial seawater solution (50–70 gL^{-1}) and dividing the results by the equivalent PSU value of the

solution. Ψ_t^i can be determined by measuring the absorption differences of purified water of e.g., 15 and 40 °C. As the effects of temperature on the refractive index and scattering by pure water are of minor relevance (in opposite to the situation for salinity), published values of Ψ_t for pure water absorption can be used as well (e.g., Röttgers et al. 2014). Besides correction for temperature, salinity, and chlorophyll fluorescence effects, no further corrections are applied. Due to the spectral distribution of the light source, effects of water Raman and CDOM fluorescence are negligible.

4.6 Maintenance and Service of the PSICAM

The PSICAM cavity wall can be cleaned by using pure HPLC-grade ethanol and a lint-free tissue. Touching the wall with unprotected finger should be avoided. Optical influences by organic material attached to the wall can further be removed with bleach using a ca. 0.1% NaOCl solution (500–1000 µl NaOCl in 500 ml purified water). The PSICAM should be filled with purified water 24 hours before the measurement/calibration are done, as water will enter the wall material and changes the reflectance.

4.7 Determination of the Particulate Absorption Coefficient with a PSICAM

The particulate absorption coefficient, a_p, in a water sample is determined by measuring first the absorption coefficient of all water constituents (besides water itself), a_{pg}, defined as the sum of a_p and a_g, the latter here used for the dissolved part (gelbstoff [CDOM]). The sample is then filtered through 0.2 µm and the filtrate's absorption coefficient determined as a_g. Principally a_g can be determined using other optical methods. Finally, a_p is calculated by subtracting a_g from $a_{p,}$ i.e. $a_p = a_{pg} - a_g$ (Fig. 4.3). The filtration through 0.2 µm allows a proper separation of the absorption by particles larger than 0.2 µm and that by all other material (particulate, colloidal, and dissolved) remaining in the filtrate. When using glass-fiber filter for the determination of a_p, it is possible that particulate material is going through the glass fiber filter but retains on the 0.2-µm filter, its absorption is, hence, not part of a_p nor a_g.

As pigment bleaching in suspension cannot be handled yet satisfactorily, the absorption coefficient of pigments (phytoplankton), a_{ph}, has to be determined by combining PSICAM and filter pad measurements, the latter includes the determination of the non-pigmented part of the particulate absorption coefficient after pigment extraction.
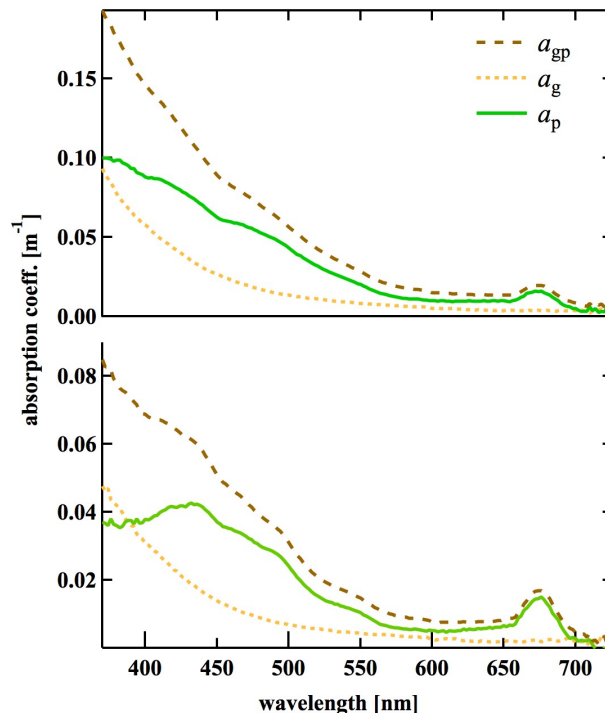
Figure 4.3. Examples of PSICAM measurements from the New Caledonia Lagoon, showing a_{pg}, a_p, and a_g.

REFERENCES

Kirk, J.T.O., 1995: Modeling the performance of an integrating-cavity absorption meter. Theory and calculations for a spherical cavity. *Appl. Opt.*, **34**: 4397–4408.

Kirk, J.T.O., 1997: Point-source integrating-cavity absorption meter: theoretical principles and numerical modeling. *Appl. Opt.*, **36**: 6123–6128.

Leathers, R.A., T.V. Downes, and C.O. Davis, 2000: Analysis of a point-source integrating-cavity absorption meter. *Appl. Opt.*, **39**: 6118–6127.

Lerebourg, C.J.-Y., D. A. Pilgrim, G.D. Ludbrook, and R. Neal, 2002: Development of a point source integrating cavity absorption meter. *J. Opt. A: Pure Appl. Opt.*, **4**: S56–S65.

Pope, R.M. and E.S. Fry, 1997: Absorption spectrum (380–700 nm) of pure water: II. Integrating cavity measurements. *Appl. Opt.*, **36**: 8710–8723.

Röttgers, R., R. Doerffer, 2007: Measurements of optical absorption by chromophoric dissolved organic matter using a point-source integrating-cavity absorption meter. *Limnol. Oceanogr. Methods*, **5**: 126–135.

Röttgers, R., C. Häse, and R. Doerffer, 2007: Determination of the particulate absorption of microalgae using a point-source integrating-cavity absorption meter: verification with a photometric technique, improvements for pigment bleaching and correction for chlorophyll fluorescence. *Limnol. Oceanogr. Methods*, **5**: 1–12.

Röttgers, R., W. Schönfeld, P.-R. Kipp, and R. Doerffer, 2005: Practical test of a point-source integrating cavity absorption meter: the performance of different collector assemblies. *Appl. Opt.*, **44**: 5549–5560.

Röttgers, R, D. McKee, and C. Utschig, 2014: Temperature and salinity correction coefficients for light absorption by water in the visible to infrared spectral region. *Opt. Express*, **22**: 25093–25108.

Chapter 5: Spectrophotometric Measurements of Particulate Absorption Using Filter Pads

Collin Roesler[1], Dariusz Stramski[2], Eurico J. D'Sa[3], Rüdiger Röttgers[4], and Rick A. Reynolds[2]

[1]*Bowdoin College, Brunswick, ME, USA*
[2]*Scripps Institution of Oceanography, University of California San Diego, La Jolla, CA, USA*
[3]*Louisiana State University, Baton Rouge, LA, USA*
[4]*Helmholtz-Zentrum Geesthacht, Centre for Materials and Coastal Research, Germany*

5.1 General Considerations

Prior to the quantitative filter pad approach, particulate absorption was measured in cuvettes to assess absorption spectrophotometrically. These measurements clearly demonstrated the impact of scattering by the suspended particles on the estimation of absorption because scattered photons are generally not collected by the detector and their contribution is assigned to absorption. In the extreme, the derived coefficient more resembled beam attenuation rather than absorption. An additional consequence of particle scattering is that it redirects photons through the suspension of absorbing particles, increasing the absolute pathlength of those photons over that which would have been observed in a non-scattering environment, thereby increasing the probability of absorption, and hence the magnitude of the derived absorption coefficient. This latter effect is termed pathlength amplification, the ratio of the mean optical pathlength to the geometric pathlength (Butler 1962); it leads to overestimated absorption coefficients and, in the extreme, to flatted absorption peaks (Duysens 1956). Modeling suggests that pathlength amplification is minimized by maintaining dilute suspensions where only single scattering occurs over the geometric path (van de Hulst 1981). In most natural samples, however, the suspended particles are sufficiently dilute as to require long geometric path cuvettes, which are more susceptible to scattering losses. Filtering particles onto glass fiber filters solved a number of technical issues inherent in the suspension approach but yielded others.

Advantages: Filtering large sample volumes onto glass fiber filters (e.g., Whatman® glass microfiber filters, grade GF/F with nominal pore size 0.7 μm) solved the issue of the dilute medium and low signal-to-noise ratios by concentrating particles. This yielded a higher optical density in the spectrophotometer by increasing the geometric pathlength. Additionally, the filtration removed the solute from the measurement resulting in separation of the particulate from dissolved fractions of the total absorption. Finally, the extraction of pigments from the filter leaving the non-extractable cellular material and inorganic particles provided a means for estimating the contribution to absorption by the phytoplankton pigments as they were *in vivo*, i.e. as they were packaged (Kishino et al. 1985; Sosik and Mitchell 1991).

Disadvantages: Glass fiber filters are highly scattering. Depending upon the configuration of the spectrophotometer, this yielded significant losses of the incident light from the detector and if not corrected lead to an estimate of particle absorption that included significant scattering by the filter pad. Additionally, the highly scattering nature of the filter fibers increased the optical pathlength of the photons significantly over the geometric pathlength, increasing the likelihood of absorption. As was true for suspensions that do not satisfy the measurement criteria of a single-scattering regime, the pathlength amplification factor on filters is even more significant and leads to a non-negligible overestimation of the absorption coefficient. Finally, the filter pads have their own optical properties that vary slightly from filter to filter. Because the optical properties of the filter pad are typically much larger than those of the natural particles, variations between filters that are not removed by blank filter subtraction provide additional non-negligible contributions to the computed sample absorption coefficient and lead to an increase of the uncertainty in the derived values.

Prior to the implementation of integrating spheres for filter pads (Section 5.7), particulate absorption was assessed on filter pads configured in the transmittance mode (alternatively referred to as transmission mode) on the spectrophotometer (Fig. 5.1a). Note that the use of the term "transmittance mode" in this context of filter pad measurement configuration is not to be confused with the transmittance output of the spectrophotometer. Actually, the filter pad measurements are typically made using an absorbance output of the spectrophotometer, rather than transmittance output (see Section 5.3.1 below). In this configuration

the transmittance through the filter pad with particles is measured relative to the transmittance through a blank filter (Kiefer and SooHoo 1982).

In the transmittance mode, a large portion of the incident light is not detected; and although this is mostly corrected for by the reference through a blank filter, the difference in scattered loss for a blank filter is not the same as for a filter with embedded particles. This error in uncorrected scattering loss is generally lumped into the pathlength amplification factor, β, the so-called "beta correction factor", which theoretically should only correct for the increases in the optical pathlength compared to the geometric pathlength through the absorbing particles (Roesler 1998).

Consensus: As spectrophotometric technology has improved, including the implementation of integrating spheres, the disadvantages of the filter pad approach are declining and the uncertainty in filter pad absorption approaches are improving. In the following sections, the three basic configurations for determining particulate absorption from filter pads are described and configuration-specific protocols are outlined (Fig. 5.1). It is now recognized that the internally-mounted integrating sphere approach (IS-mode) is superior to either the transmittance mode (T-mode) or the transmittance-reflectance mode (T-R-mode) in terms of accuracy, precision, labor, and sample handling. If the filter pad technique is used as a stand-alone method of measurement, then the use of IS-mode is recommended whenever feasible. However, the vast historical data sets were primarily collected using the T-mode and not every research group has access to the more expensive integrating sphere accessories. Thus, it is critical to continue providing protocols that maximize the quality of data collected while providing clear methods for identifying the sources of errors and quantifying the uncertainties that do exist. For example, it has long been recognized that the uncertainties associated with the pathlength amplification in the filter pad technique are somewhat dependent on the sample type or composition of particulate assemblage. Thus, one possible avenue for reducing these uncertainties in the filter pad measurements, regardless of which mode of measurement is used (T, T-R, or IS), is to address the pathlength amplification and potential scattering offsets (the latter being particularly important for the T-mode) on a sample by sample basis. Recent work by Lefering et al. (2016) compared the concurrent measurements with the filter pad technique and point-source integrating cavity absorption meter (PSICAM), which were made essentially on the same samples. This study showed that such an approach applied on a sample by sample basis may lead to improved corrections for pathlength amplification and scattering offsets in filter-pad absorption measurements, including the inferior T-mode that is particularly sensitive to scattering artifacts and related errors.

(a)   (b)   (c)   (d)
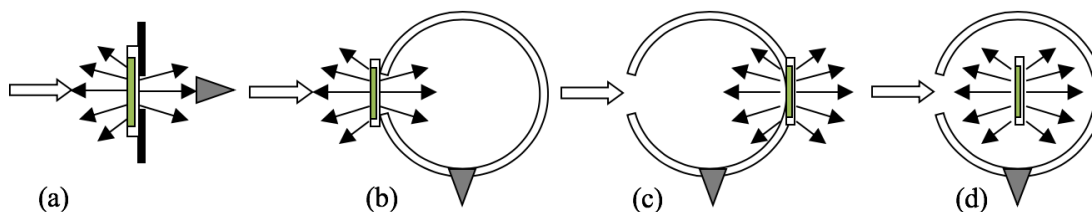
Figure 5.1. Spectrophotometric configurations for determining filter pad optical density: (a) transmittance mode (T-mode), (b and c) transmittance and reflectance mode measured with an integrating sphere with externally mounted samples (T-R-mode); (d) internally mounted sample in integrating sphere (IS-mode). Open arrow indicates incident beam, black arrows indicate beams scattered from filter, grey cone indicates detector for the generalized model.

5.2 Sample Collection and Handling

Water samples are collected using clean Niskin bottles (with non-reactive internal tubing). One large and uncorrectable source of error in the measurement is the preferential settling of particles with time as subsamples are collected from the Niskin bottles. Thus, each bottle should be transferred in its entirety to a large volume carboy protected from light and heat during subsampling. Particles are to be kept in suspension while subsampling by careful but vigorous swirling of the carboy. Swirling three times clockwise, followed by three times counter clockwise, followed by three times clockwise effectively resuspends sinking particles. The reversal of swirling direction is critical as it provides the chaotic mixing motion that is necessary to avoid a non-uniform distribution of particles due to centrifugal forces that results from uniform swirling. This resuspension method is also necessary in the sample bottle prior to measuring out the filtration volume. Sample bottles should never be shaken.

Place a set of filters into the filtration manifold. A sample volume sufficient to obtain an optical density value of 0.1 to 0.4 within the wavelength range of interest is required, for example 400 to 700 nm,

recognizing that there are regions of minimal absorption that may have optical density values <0.1 when peak absorption is within the range. This may require two or more filters to be prepared for a single sample in order to maintain the optical density range for both the UV and visible portions of the spectrum. Until experience provides the intuition for filter pad loading, multiple filter volumes should be prepared. Vacuum pressure should not exceed 5 mmHg or 0.1 psi in order to minimize cell breakage. As the final volume of water goes through the filter, the valve should be turned off to prevent air from being drawn through the filter, leading to cell breakage.

Prepare three to five blank filters along with sample filters, filtering a similar volume of pure water (such as MilliQ®) or 0.2-μm-filtered seawater (FSW) through each. Filter fibers compress as more water is filtered through them, thus they will have different scattering properties with a 50-ml filter volume versus 1000 ml (Roesler 1998). If samples are to be stored from a cruise, collect at least five blank filters from each batch used and keep track of which samples and blanks are from each lot to ensure that analyses are processed within a single lot number.

Filters should be removed from filter cups for immediate spectrophotometric scanning or immediate freezing and storage (Sosik 1999). Notch the edge of each filter to provide a means for identifying the orientation in the spectrophotometer, which is especially important for replicate scans of the sample filter in different orientations as well for repositioning the sample filter in the same orientations for scans after the methanol extraction treatment (see below). If filters are going to be scanned immediately, place them in a petri dish that has been prepared with a bed of very moist Kimwipes® (or like tissues that don't shed particles; use a compatible water, filtered seawater or purified water, to moisten tissue while maintaining sample isotonic balance). Put the lid on the petri dish to maintain moisture and wrap in foil to prevent exposure to light. Filters change their optical properties as they dry (Roesler 1998), likely due to enhanced scattering by air pockets (Fig. 5.2). Additional changes may occur to some samples containing phytoplankton species that are susceptible to pigment degradation on filters over short temporal scales during a spectral scan (Stramski 1990). When making replicate scans on a filter, it is essential to remoisten between the scans.
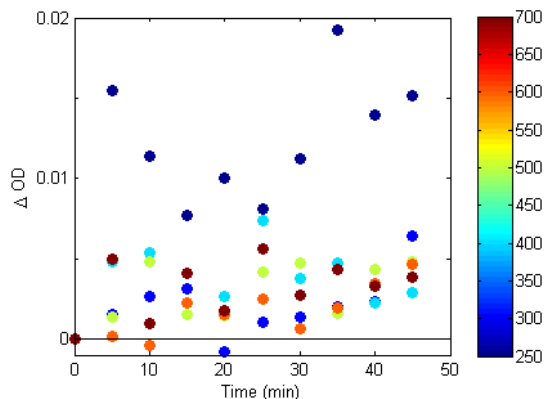
Figure 5.2. Increase in optical density of a blank filter as a function of time for 250 nm, 300 nm, 400 nm, 500 nm, 600 nm and 700 nm (colorbar). The filter was left in spectrophotometer and scanned every five minutes as it dried. Measurements were corrected for initial values.

If filters are going to be stored for later analysis they should be flash frozen with liquid nitrogen either by placing them unfolded in individual labeled Tissue-Teks® (such as the plastic disposable capsules manufactured by Sakura Finetek; Fig. 5.3) and placing them directly into a liquid nitrogen dewar, or by freezing them on a spatula that has been sitting in liquid nitrogen. Once flash frozen, the filters can be quickly placed in a -80 °C freezer until analysis. The flash freezing prevents the differential freezing of particulate and dissolved molecules and best preserves the optical properties of the particles.

Figure 5.3. Example of plastic capsules for storing individual sample filters in liquid nitrogen.

Immediately before measurement, frozen filters (which have lost their original water content but maintained the original salts) are remoistened by placing filter on top of a drop of MilliQ® or other pure water or filtered seawater on a glass slide or in a petri dish. In this case, the MilliQ® water plus the original salts will create isotonic balance. The filter should absorb most but not all of the water within a matter of seconds. Scan immediately.

The first scan of the particles provides the measurement for computing the particulate absorption coefficient, $a_p(\lambda)$. Non-algal particle absorption coefficient, $a_{NAP}(\lambda)$, is computed from the measurement on the same sample filters following pigment extraction. This is done by returning each sample filter to the filtration manifold and gently extracting with a small volume (e.g., 10 ml) of methanol (this is the reason to carefully notch the filter so that it does not impact the filtering portion). In order to minimally impact the particles on the filter, the methanol is slowly sprayed down the side of the filter cup with a squirt bottle. Gently filter the methanol through the filter pad, taking care not to draw air through. Add another small volume of methanol and let sit for approximately 15 minutes to fully extract remaining pigments. Gently rinse the filter with 15 ml of filtered seawater (or MilliQ® for freshwater samples), applied in the same fashion, and filter through. This treatment is also performed on a set of blank filters, which are then used in the baseline—zero and blank scans for the extracted sample filters. This method involving the methanol treatment of filter pads was originally proposed by Kishino et al. (1985) and it is recommended here for routine use. Note, however, that other approaches for experimentally partitioning the total particulate absorption into phytoplankton and non-algal components have been also proposed, for example treatment of sample with a highly oxidizing agent such as sodium hypochlorite NaOCl (Ferrari and Tassan 1999). Both partitioning methods have advantages and disadvantages. Methanol extraction does not remove water-soluble phycobilipigments and occasionally results in incomplete extraction (e.g., residual red peak absorption). It should be noted that, unlike the methanol extraction method, the bleaching method does not remove the pigments from the sample. The pigments are oxidized, remaining with the particulate matter on the filter, and their absorption shifts to the short-wavelength portion of the visible spectrum into UV, making assessment in these spectral regions inaccurate. In addition, the bleach itself absorbs in the UV and washing it out completely can be difficult, which may introduce additional artifacts. However, in the visible spectral region (wavelengths longer than about 450 nm) or for samples with a high proportion of non-algal matter, the performance of the bleaching method is similar to that of the methanol extraction. Bleaching is conducted by placing the sample filter onto a few drops of 1:10 (v:v) diluted bleach (NaOCl, 1% active Cl) in a petri slide until the filter becomes colorless (usually after a few minutes). However, the sample filters from turbid waters may often retain the brownish color after bleaching due to high concentrations of non-algal matter. The bleaching treatment should not take more than 30 minutes to avoid oxidation of molecules other than phytoplankton pigments. The sample filter is then rinsed with filtered seawater to remove the bleach after placing it back onto a filtration unit. Blank filters are handled in the same way.

5.3 Computing Absorption from Absorbance

5.3.1 Absorbance

Commercially available spectrophotometers typically allow selection of output in either absorbance or transmittance. The output of absorbance is referred to by the community of optical oceanographers as optical density, OD (c.f., although the International Union of Pure and Applied Chemistry (IUPAC) recommended against this term in the Compendium of Chemical Terminology). The relationship between

these two outputs is such that $OD = \log_{10}(1/T)$, where T is transmittance. It is important to emphasize that transmittance T in this definition may have different interpretations depending on the geometry of measurement. In particular, if only the radiant power that is directly transmitted through the sample, Φ_t, is measured at the detector, then $T = \Phi_t/\Phi_o$ where Φ_o is the power of collimated beam incident on the sample. Such geometry of measurement is required by an *ideal beam attenuation meter*. In contrast, if both Φ_t and total scattered power in all directions, Φ_B, are measured at the detector, then $T = (\Phi_t + \Phi_B)/\Phi_o$. Such geometry of measurement would yield an *ideal absorption meter* (see Chapter 2).

In practice, it is challenging to perfectly satisfy the geometrical requirement of an ideal absorption meter because it is difficult to ensure that the total scattered power Φ_B is measured at the detector. When a certain portion of scattered power is not detected, the absorption coefficient is overestimated owing to the so-called scattering error (see Eq. 2.6 and related text in Section 2.2). For the spectrophotometric filter-pad technique, the issue of imperfect geometry and associated scattering error is most pronounced in the T-mode configuration (Fig. 5.1a). In contrast, the IS-mode with sample mounted inside an integrating sphere (Fig. 5.1d) approaches an ideal geometry of absorption measurement.

The absorption coefficient is defined as $a = -(1/L) \ln[(\Phi_t + \Phi_B)/\Phi_o]$ (see Section 2.1), while the optical density output from the spectrophotometer is provided as $OD = \log_{10}[\Phi_o/(\Phi_t + \Phi_B)]$. This gives rise to the relationship between spectral optical density measurements and the spectral absorption coefficients, $a(\lambda)$ in units of m^{-1}:

$$a(\lambda) = \ln(10)\, OD(\lambda)/L$$

(5.1)

where $\ln(10)$ converts the common base 10 logarithm ($\log_{10}$) to the natural logarithm that has the number e as its base ($\ln \equiv \log_e$) and L is the geometric pathlength of the sample expressed in meters.

5.3.2 The geometric pathlength

Geometric pathlengths for cuvette measurements are given by the width of the cuvette, equivalent to the geometric path through the sample. For filter pad measurements the geometric pathlength, L, is computed from the volume filtered, V (m^3), and the effective area of the filter, A (m^2), measured as the area over which particles are collected onto the filter:

$$L = (V/A)$$

(5.2)

which yields the height of a column of the sample projected onto the filter pad. In practice, V is typically measured in units of cm^3 (or mL) and A in cm^2 or mm^2, so conversions to m^3 and m^2 are required, respectively.

5.3.3 Optical pathlength and pathlength amplification

The assumption in the expression for absorption (Eqs. 5.1 and 5.2) is that the geometric pathlength (i.e., V/A) is equal to the optical pathlength (the actual average distance that a photon travels through the sample). However, comparisons between particulate samples measured on particle suspension in cuvette placed inside an integrating sphere (which is close to an ideal absorption measurement) and those measured on filter pads indicates that there is an amplification of the mean photon path through the filter compared to geometric path caused by the highly scattering nature of the filter pad. The increased optical pathlength relative to the geometric pathlength allows for increased probability for absorption by particles collected on the filter and therefore overestimation of the absorption coefficient. The correction factor for pathlength amplification is the so-called beta correction, β. Recent routine implementation of the center-mounted integrating sphere configuration for both filter pads and particle suspensions in a cuvette, as well as similar comparisons with PSICAM measurements of suspensions, has highlighted the lack of consensus in published β correction factors. Inconsistencies in β determination are attributable to errors in the measurements used to derive these correction factors, e.g., measurements of the suspended particles made without an integrating sphere and some sample related variability (e.g., Röttgers and Gehnke 2012, Stramski et al. 2015; Lefering et al. 2016).

The consensus for obtaining the absorption coefficient of particles $a_p(\lambda)$ or non-algal component of particulate absorption $a_{NAP}(\lambda)$ from filter pad measurements, when corrected for pathlength amplification, implements the following relationships:

$$a_x(\lambda) = \ln(10)\, OD_s(\lambda)\, /(V/A) \qquad (5.3)$$

where units for the volume filtered V are (m^3) and the effective area of the filter A (m^2), and subscript x represents either the p or NAP components. The optical density $OD_s(\lambda)$ represents the absorbance by particles, which is corrected for pathlength amplification factor β. In other words, $OD_s(\lambda)$ can be interpreted as the optical density of the same particles as collected on the filter pad, which would be measured in suspension over the pathlength V/A under single-scattering regime *without* the effect of pathlength amplification. The $OD_s(\lambda)$ values are calculated from a predetermined relationship involving the optical density of particles measured on the filter, $OD_f(\lambda)$:

$$OD_s = \mathbf{f}(OD_f) \qquad (5.4)$$

where the function $\mathbf{f}$ essentially quantifies the pathlength amplification factor β. Note that β can be calculated from Eq. (5.4) as a ratio OD_f / OD_s. Generally, this ratio can vary as a function of OD_f (particle load on the filter) as the function $\mathbf{f}$ can be nonlinear. In practice, however, in routine processing of filter pad measurements there is no need to calculate β or use explicit values of β because the right-hand side of Eq. (5.4) is simply substituted for OD_s in Eq. (5.3). The OD_f values in Eq. (5.4) represent the optical density of particles on the filter after all necessary corrections for baselines were made (i.e., blank filter baseline and instrument baseline or drift). Note also that the light wavelength argument, λ, is omitted from Eq. (5.4) because this relationship is typically determined by combining data covering a broad spectral range, usually the entire visible part of the spectrum. Therefore, Eq. (5.4) is applicable to any wavelength within the spectral range for which the relationship was determined.

The determination of Eq. (5.4) requires special laboratory experiments, and many such dedicated experiments have been conducted in the past. As a result of these experiments different functional forms were proposed, for example a second-order polynomial or power function. Recently, Stramski et al. (2015) examined the pathlength amplification relationships, $OD_s = \mathbf{f}(OD_f)$, with diverse samples for all configurations of filter pad spectrophotometry (transmittance T, transmittance-reflectance T-R, and inside-sphere IS), and compared their derived relationships to previously published results, with a few showing close agreement. Importantly, in these experiments the OD_s was measured on particle suspensions within the integrating sphere to provide a very close estimate of the true reference absorption coefficient. The methodology of measurements of particle suspensions placed inside the integrating sphere is described elsewhere (Babin and Stramski 2002, 2004; Stramski et al. 2007). As a result of the study by Stramski et al. (2015) we recommend the following relationships to correct for the pathlength amplification of the filter pad technique:

T-mode: $\qquad\qquad\qquad OD_s = 0.679\,(OD_f)^{1.2804} \qquad\qquad\qquad (5.5)$

T-R-mode: $\qquad\qquad\qquad OD_s = 0.719\,(OD_f)^{1.2287} \qquad\qquad\qquad (5.6)$

IS-mode: $\qquad\qquad\qquad OD_s = 0.323\,(OD_f)^{1.0867} \qquad\qquad\qquad (5.7)$

The right-hand side of these equations should be substituted for OD_s in Eq. (5.3) in final calculations of $a_p(\lambda)$ or $a_{NAP}(\lambda)$.

The pathlength amplification correction is generally considered as one of the major sources of uncertainty of the filter pad technique (e.g., Bricaud and Stramski 1990; Roesler 1998; Lohrenz 2000; Röttgers and Gehnke 2012). It is therefore important to recognize some limitations associated with the use of single "average" relationships for pathlength amplification correction, such as those expressed by Eqs. (5.5)–(5.7), for arbitrary samples of aquatic particles. A number of previous studies have shown that the relationships describing the pathlength amplification correction can vary from sample to sample, indicating that this correction is somewhat dependent on the composition and properties of particulate matter retained on the filter. As described in Stramski et al. (2015), the "average" relationships (5.5)–(5.7) were determined as the best-fit regression functions to experimental data obtained with a relatively small number of samples but characterized by a wide range of particle composition with no specific type of composition having a

dominant statistical weight in establishing the relationships. Specifically, the relationships (5.5) and (5.6) for T and T-R-modes were determined from measurements taken on ten different samples using multiple filtration volumes for each sample. These samples included mineral-dominated particle assemblages, organic detritus-dominated assemblages, cultures of phytoplankton, and a few particle assemblages from coastal environments. The relationship (5.7) for the IS-mode was determined from measurements on six different samples, also using multiple filtration volumes. These six samples also encompassed a broad range of particle composition, including nearshore mineral-dominated and red tide samples, a mixture of four phytoplankton species, and a few additional coastal and offshore particle assemblages. These samples were also characterized in terms of ancillary parameters including the spectra of light-scattering and single-scattering albedo, particle size distribution, particulate organic carbon (POC) and dry mass concentration of suspended particulate matter (SPM). For example, the ratio of POC/SPM, which is indicative of relative proportions of organic and inorganic particles, varied from 0.04 (highly mineral-dominated) to 0.44 (highly organic-dominated). Such ancillary information is important in these types of experiments because it provides an understanding of the types of particle assemblages for which the formulated pathlength amplification correction is representative. We also note that for these six samples, a median error of 7.1% was observed for predicted values of OD_s using the relationship (5.7) for the IS-mode in the visible spectral region.

The relationships (5.5)–(5.7) established in the study of Stramski et al. (2015) were compared with previously established relationships for pathlength amplification correction. More than ten historical relationships are available for the T-mode and most of them were obtained from measurements of phytoplankton cultures. These historical data show large variability corresponding to as much as about 3-fold variation in the pathlength amplification factor β at some OD_f values. The relationship (5.5) is located near the middle of the historical set of relationships. The availability of literature data of pathlength amplification for the T-R and IS-modes is more limited compared with the T-mode. Importantly, however, for the T-R-mode the relationship (5.6) is consistent with previous results of Tassan and Ferrari (1995). Similarly, for the IS-mode there is good agreement between the relationship (5.7) and previous results of Röttgers and Gehnke (2012), which were based on data from several marine environments. Notwithstanding this consistency, the use of single relationships for pathlength amplification correction in a diverse suite of samples from various natural water bodies will involve some degree of uncertainty. To better constrain the pathlength amplification correction on a sample-by-sample basis, Röttgers and Gehnke (2012) and Lefering et al. (2016) proposed to use the filter pad technique in parallel with absorption measurements with PSICAM (see Chapter 4) on the same samples. Assuming that the PSICAM measurement provides a "true" reference value of the particulate absorption for a given sample, the pathlength amplification correction for the filter pad measurement taken on the same sample can be determined. Although the concurrent use of multiple absorption techniques can be useful for this or other reasons, it must be recognized that such an approach entails a higher demand on required resources and effort, which may be a limiting factor in many field campaigns or experiments. Further studies dedicated to the assessment of various sources of uncertainty in absorption measurements are needed to provide guidance to improving the experimental approaches and reducing uncertainty in absorption estimates obtained from different methods including the spectrophotometric filter pad technique.

5.3.4 Quantifying Uncertainty in the Filter Pad Absorption Coefficients

A full model for filter pad absorption uncertainty is achieved by arithmetically propagating the uncertainty quantified for each methodological step (JCGM 2008). In general, an experimental measurement equation for the quantity to be determined or measured, y (referred to as the measurand), can be written as

$$y = \mathbf{f}\,(x_1, x_2, \ldots x_n) \tag{5.8}$$

where the function $\mathbf{f}$ is defined by the physics of the measurement problem and $x_1, x_2, \ldots x_n$ are the experimentally determined input variables to which the measurand y is related. The variables $x_1, x_2, \ldots x_n$ have uncertainties associated with them, which give rise to an uncertainty in the estimate of measurand y. In addition, the variables $x_1, x_2, \ldots x_n$ may themselves have measurement equations representing separate determinations.

In our case of determinations of the particulate absorption coefficient from the filter pad technique the measurand at any light wavelength λ is a_p or a_{NAP} (in what follows in this section we omit the argument λ and use the symbol a for a_p or a_{NAP} for brevity). By combining Eq. (5.3) with one of Eqs. (5.5), (5.6), or

(5.7) which characterizes the pathlength amplification correction for one of the filter pad modes (i.e., T, T-R, or IS-mode), we obtain the experimental measurement equation for a:

$$a = \ln(10)\ \alpha\ (OD_f\ )^\gamma\ \frac{A}{V} \tag{5.9}$$

This equation has five input variables x_i which are OD_f, α, γ, A, and V. Note that although the fixed values of α and γ are used for each filter pad mode in the calculations of the measurand a, these quantities should be considered as variables in the context of uncertainty analysis because the assumed fixed values of α and γ just represent the statistical estimates established as the best option in a statistical sense for pathlength amplification correction. In addition, note that the variable OD_f can be written in terms of experimental measurement equation:

$$OD_f = (OD_{fs} - OD_{infs}) - (OD_{fb} - OD_{infb}) \tag{5.10}$$

where the input variables are: OD_{fs} is the best estimate of optical density measured on the sample filter, OD_{fb} is the best estimate of optical density measured for the blank filter, and OD_{infs} and OD_{infb} are the best estimates of optical density representing the instrument baselines (typically the air vs. air measurements in dual beam spectrophotometer), which are applicable to the sample filter and blank filter scans, respectively. OD_{infs} and OD_{infb} may or may not be the same depending on the sequence of specific measurements during the period of measurements. The best estimate of OD_{fs} can be obtained by repeating the scans on the sample filter, for example for different filter orientations (Fig. 5.4a), as well as by taking measurements on replicate sample filters (Fig. 5.4b), if available. Arithmetic propagation in a best-case scenario yields small uncertainties (Fig. 5.4c). However, some experiments with replicate sample filters showed substantial variability in OD_{fs} which can, for example, be associated with heterogeneous distribution of particles on the filters. The best estimate of OD_{fb} can be obtained by averaging measurements taken on multiple blank filters (Fig. 5.5), including repetitive scans for a given filter or, if allowed by the design of experiment, by making measurements of OD_{fb} for a given blank filter that is subsequently used to collect a sample for the OD_{fb} measurements. The magnitude of variability in OD_{fb} is highly dependent upon spectrophotometric configuration.
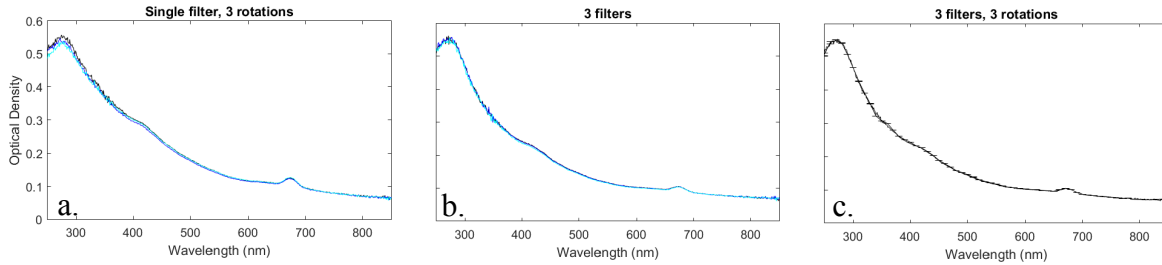
Figure 5.4. Example of best case scenario for sample uncertainty as quantified by (a) three replicate scans of a single filter with three rotations within the beam, (b) scans of three replicate sample filters, and (c) arithmetically propagated uncertainty shown by error bars (every 10 nm for clarity).
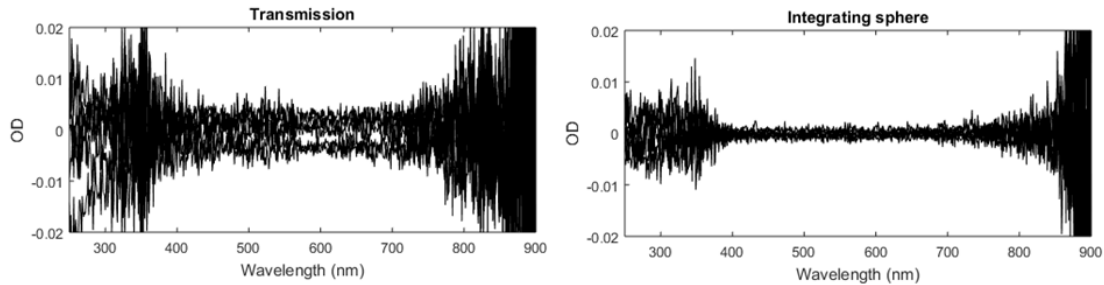
Figure 5.5. Spectrophotometric scans (optical density spectra) for a set of five blank filter pads that have been baseline corrected (a single or average blank filter pad signature removed) as measured in transmittance mode (*left*) or center-mounted integrating sphere mode (*right*).

The equation for the combined (total) standard uncertainty, $u_c(a)$, in the absorption coefficient, a, can be expressed as:

$$u_c(a) = \sqrt{\sum_{i=1}^{n} \left(\frac{\partial a}{\partial x_i}\right)^2 u^2(x_i)} =$$

$$\sqrt{\left(\frac{\partial a}{\partial OD_f}\right)^2 u^2(OD_f) + \left(\frac{\partial a}{\partial \alpha}\right)^2 u^2(\alpha) + \left(\frac{\partial a}{\partial \gamma}\right)^2 u^2(\gamma) + \left(\frac{\partial a}{\partial A}\right)^2 u^2(A) + \left(\frac{\partial a}{\partial V}\right)^2 u^2(V)} \qquad (5.11)$$

where the partial derivatives are referred to as sensitivity coefficients which relate the change in the measurand a with respect to the input variable x_i, and the quantities $u(x_i)$ are the uncertainties assigned to individual variables x_i that are used to calculate a. As explained in relation to Eq. (5.9) the variables x_i are OD_f, α, γ, A, and V, so in this case $n = 5$. Note that the uncertainty associated with the pathlength amplification is represented by the two terms that are associated with α and γ. Equation (5.11) is applicable when there are no correlations between variables x_i which is a reasonable assumption for our experimental problem.

This equation indicates that in order to estimate the total standard uncertainty $u_c(a)$, it is necessary to determine both the sensitivity coefficients with respect to each individual variable x_i and the uncertainty of each variable x_i. Note also that the variable OD_f involved in Eq. (5.11) is itself described by the experimental measurement Eq. (5.10). Therefore, this variable has its own combined standard uncertainty, $u_c(OD_f)$, which can be expressed by an uncertainty equation that is analogous to Eq. (5.11) in which the variables x_i are OD_{fs}, OD_{fb}, OD_{infs}, and OD_{infb}. These variables are also subject to uncertainties that need to, and can, be quantified. For example, the uncertainties in the instrument baselines are associated with the inherent random noise of the instrument for the air vs. air scan, and possibly also a temporal drift in these baselines during the period of measurements. These uncertainties will necessarily vary from instrument to instrument and should be determined and reported. The uncertainties in OD_{fs} and OD_{fb} can be estimated from repetitive scans for a given sample or blank filter and measurements taken on multiple sample or blank filters.

Rigorous quantification of total uncertainty $u_c(a)$ for the experimental problem at hand is very difficult, if not impossible, because of the lack of complete information required to rigorously evaluate each term involved in Eq. (5.11). In general, the uncertainties $u(x_i)$ of individual variables x_i could be estimated from the experimental standard deviation $s(x_i)$, determined from a series of N measurements of variable x_i according to:

$$u(x_i) = \sqrt{s^2(\overline{x}_i)} = \sqrt{\frac{s^2(x_i)}{N}} \qquad (5.12)$$

where $\overline{x}_i$ is the estimated average value of x_i and $s^2(\overline{x}_i)$ is the experimental variance of the mean. Whereas such estimation appears relatively straightforward for some x_i variables, such as A and V (e.g., Fig. 5.6), this task is more difficult and would require special, generally highly laborious, experiments for other variables, OD_f, α, and γ, involved in Eq. (5.11). The additional complexity in the evaluation of $u_c(a)$ from Eq. (5.11) results from the fact that the sensitivity coefficients, $\partial a / \partial x_i$, with respect to any specific input variable x_i depend on the magnitude of other input variables used in Eq. (5.9). It thus appears that a simpler, more pragmatic approach for estimating the total uncertainty $u_c(a)$ for the filter pad technique is to conduct dedicated experiments on many diverse samples, in which the measurand a obtained from the filter pad measurements is simply compared with reference measurements taken on the same samples in suspension with a technique that provides the measurand a in the closest possible agreement with the true particulate absorption coefficient (for example, PSICAM method or particle suspension inside the integrating sphere of the spectrophotometer). Under the assumption that the reference measurements are subject to much smaller uncertainty than the filter pad measurements, the differences between the two measurements are largely attributable to the uncertainty of the filter pad measurements. The drawbacks of this approach involve the uncertainty of the reference measurements (which, however, may be easier to quantify than for filter pad technique) and the inability to resolve the influences of individual input variables x_i on the total uncertainty $u_c(a)$ of the filter pad technique. Some experiments aimed at addressing these uncertainty issues have been recently undertaken by NASA's PACE Science Team but more work in this area will be required

to rigorously quantify both the total uncertainty $u_c(a)$ and the individual terms of Eq. (5.11) for the filter pad technique.

For illustrative purposes of the conceptual framework of the uncertainty analysis based upon Eq. (5.11), the contribution of a single variable, x_i to $u_c(a)$, assuming that other input variables do not contribute to $u_c(a)$, can be considered for V, filtration volume as x_i. Eq. (5.11) simplifies to (assuming that the uncertainty terms associated with OD_f, α, γ, and A are all null):

$$u_c(a) \ = \ u_V(a) \ = \ \frac{\partial a}{\partial V} \ u(V)$$

where

$$\frac{\partial a}{\partial V} \ = \ -\ln(10) \ \alpha \ (OD_f)^\gamma A \ V^{-2} \tag{5.13}$$

which indicates that the sensitivity coefficient is inversely proportional to the squared volume. The uncertainty of volume, $u(V)$, from Eq. (5.12) is obtained by assuming a reasonable value for the standard deviation in V, $s(V)$. This is determined by the graduated cylinder used and each person's ability to measure volume accurately. The former is determined by the graduated cylinder (resolution to one half the distance between marked intervals) and uncertainty is reduced by selecting a graduated cylinder with a volume closest to but larger than the filter volume. The latter is difficult to quantify but effort should be made to assess the user's random uncertainty under standard measuring conditions (obviously greater on a ship in rough seas compared to in the laboratory) by calculating the standard deviation for a reasonable number of measurements, N. To see the impact of filter volume uncertainty, the sensitivity coefficient $\partial a/\partial V$ is calculated by assuming reasonable values used in the filter pad measurements for all components (Fig. 5.6). For example, two samples with equal filter volumes but different measured optical density spectra, within the recommended 0.1 to 0.4 range, will have the same uncertainty spectrum associated with $u(V)$, but it will represent a larger proportional uncertainty for the low optical density sample (Fig. 5.6A, black and blue curves, respectively). Similarly, two identical optical density spectra will have very different absolute uncertainties if one results from filtering 100 mL sample and the other from 500 mL sample (Fig. 5.6B, black and green curves, respectively), even though the proportional uncertainty is the same.
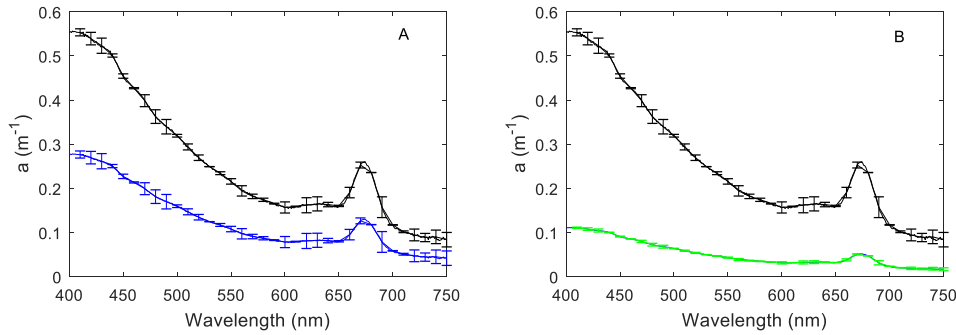
Figure 5.6. Absorption spectra with propagated uncertainty spectra are expressed as error bars for: (A) two particulate optical density spectra for which the optical density magnitudes vary but the filter volumes are the same: and (B) for two identical optical density spectra for which only the filter volumes vary (100 mL and 500 mL).

In practice, some of the uncertainty terms can be determined for a given laboratory setting with robust protocol standards. Some may be easier to analyze (like V and A), while others like α and γ (which both contribute to the uncertainty associated with pathlength amplification) may be harder to quantify because the assumptions underlying their uncertainty are still somewhat speculative in the absence of focused experimentation. Whereas a substantial level of uncertainty ($>\pm15\%$) has been suggested to be associated with sample-to-sample variability in pathlength amplification correction (Röttgers and Gehnke 2012, Lefering et al. 2016) such estimates should be viewed with caution because these results were obtained in the presence of all other sources of uncertainty which were not separately quantified. Further work to assess the level of uncertainty in as many of the variables as possible, quantifying the contribution of each, is needed to provide guidance to improve measurement practices and protocols and reduce uncertainty in spectrophotometric filter pad technique.

5.3.5 Partitioning Particulate Absorption into Contributions by Phytoplankton and Non-Algal Particulates

Once the optical density spectra for particulate and non-algal particulate contributions have been converted to their respective absorption values using Eqs. (5.3), and (5.5), (5.6), or (5.7) depending on the measurement configuration (T-mode, TR-mode, or IS-mode, respectively) the spectral absorption coefficients for phytoplankton, $a_{ph}(\lambda)$, are calculated by difference:

$$a_{ph}(\lambda) = a_p(\lambda) - a_{NAP}(\lambda) \qquad (5.14)$$

The partitioning of the particulate absorption into phytoplankton and non-algal particles is understood to be an operational definition based upon pigment extraction (Fig. 5.7). The phytoplankton component is better described as the "absorption by methanol-extractable phytoplankton pigments *in vivo*". It necessarily does not include other phytoplankton cellular material such as cell walls, membranes, etc., which instead are included in the "non-algal particle" fraction. Note that this operational definition of non-algal
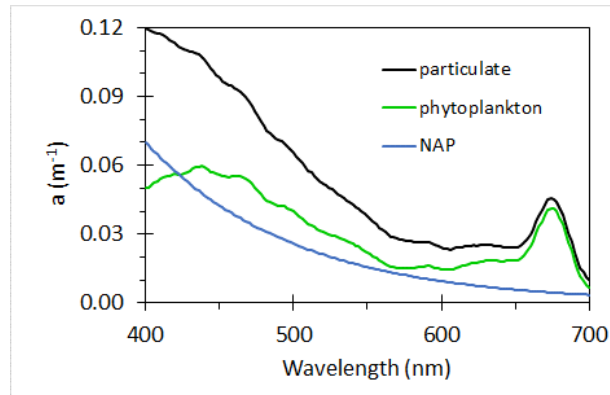
Figure 5.7 Example of particulate absorption spectrum measured on a filter pad (black), the absorption by non-algal particulates (NAP) measured after methanol extraction (blue), and the phytoplankton absorption determined by difference (green).

particulate component includes all kinds of non-algal particles such as organic detritus, mineral particles, mixed organic-inorganic particles, and heterotrophic organisms.

5.4 Measurement of Filter Pad Absorption in Transmittance Mode

While likely the least accurate of the spectrophotometric modes for determining particulate absorption on filter pads, the transmittance mode (T-mode) has the longest legacy. That it does not require expensive accessories such as integrating spheres suggests it may continue to be the most utilized configuration mode. For these reasons, it is critical to understand the uncertainties encountered in this approach and strategies for both minimizing uncertainties and correcting for those that remain. Presently the largest uncertainties are those due to scattering losses to the detector that are not accounted for by blank filter correction and scattering impacts on pathlength amplification. By employing paired analyses with an internally-mounted integrating sphere (IS-mode), both uncertainties can be quantified.

5.4.1 Spectrophotometer configuration in T-Mode

The baseline, blank and sample filter pads will all be placed against the detector side of the sample chamber. The moisture of the filter pad will provide the cohesive properties necessary to hold the filter in place. To protect the spectrophotometer from filter moisture, it is recommended that a thin Plexiglas slide, with a central opening that exceeds the size and shape of opening of the spectrophotometer aperture, be secured to the spectrophotometer for placement of the filters (Fig. 5.8).
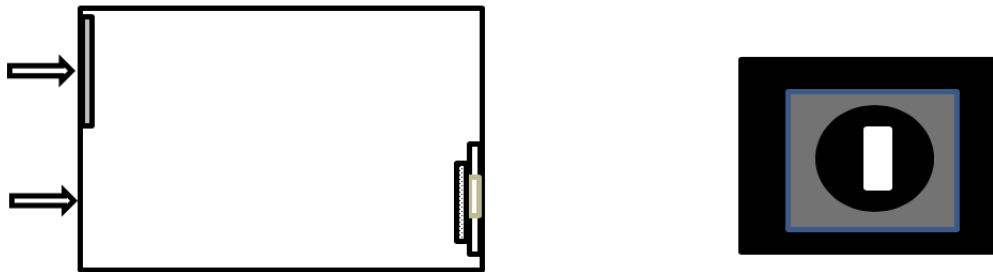
Figure 5.8. *Left diagram* Top view of sampling chamber in dual beam spectrophotometer. Arrows indicate incoming beams for reference (top) and sample (bottom). Neutral density filter (grey) placed on entrance of reference beam. Filter holder with aperture (white) and glass fiber filter (dotted) on exit port of sample beam. *Right diagram* Front view of exit port (white) of sample beam showing spectrophotometer wall (black), glass or Plexiglas filter holder with round aperture (grey). The filter holder aperture is larger than the exit port but smaller than the glass fiber filters.

The spectral optical density, *OD*, of a blank filter pad in transmittance mode is between 2.2 ($T = 0.6\%$) and 2.5 ($T = 0.3\%$) from 350 nm to 850 nm, and increases exponentially into the UV to a value of approximately 4.1 ($T = 0.008\%$) at 200 nm when corrected for air baseline (Fig. 5.9). These values are meant to be illustrative, the specific values will vary slightly between instruments. Thus, in the visible waveband, blank glass fiber filters transmit less than 0.6% of the incident beam to the detector, making for a very low signal-to-noise ratio. The situation can be vastly improved by balancing the amount of light energy that passes through the sample and reference beams. This is achieved by placing a quartz neutral density (ND) filter against the reference port entering the sample compartment (Fig. 5.8, left diagram). Quartz is preferred over glass because of its superior transmittance in the UV portion of the spectrum and the reduced likelihood of being scratched. In this configuration, there is a comparable amount of light energy passing to the detector from both the sample and reference beam, which minimizes the instrumental noise (and in many models, allows the gain to be increased). Fig. 5.9 shows the optical density scan for blank filters relative to air, 0.5 and 2.0 neutral density filters. The 2.0 ND is optimal; the resulting blank filter optical density ranges from 0.3 to 0.4 in the visible, which is equivalent to 50% and 40% transmittance, respectively, a vast improvement in signal to noise. Again, the exact choice of the ND filter may vary between instruments depending upon geometry and how the T-mode is configured.
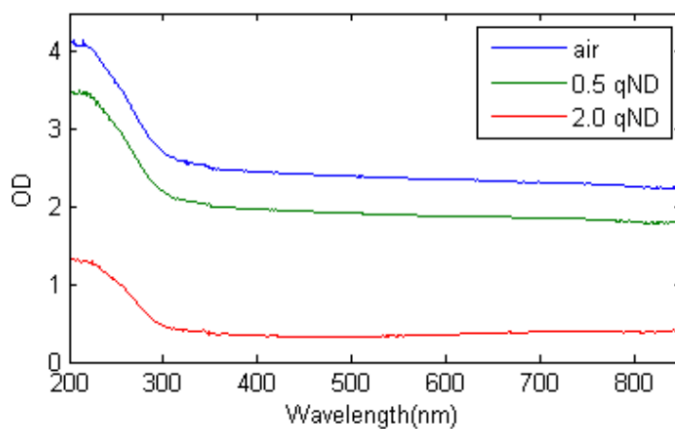
Figure 5.9. Optical density spectra for blank filter pad with air baseline correction applied (blue). Placing a neutral density filter of optical density 0.5 (green) and 2.0 (red) on the entrance port of the reference beam reduces the overall optical density signal of the blank filter pad in dual beam mode by balancing the energy in the sample and reference beams, thereby increasing signal to noise.

5.4.2 Dual-beam versus single-beam spectrophotometry in T-Mode

Dual-beam spectrophotometers are preferred to single beam spectrophotometers because the dual beam automatically corrects for short-term variations in lamp energy that occur both within a single scan and between scans.
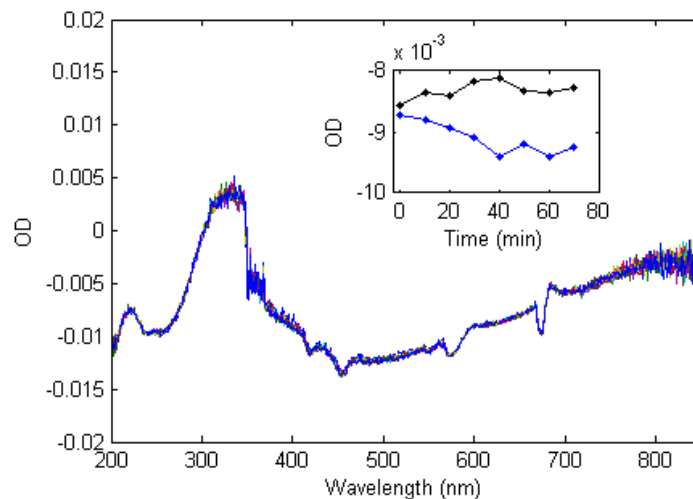
Figure 5.10. Example of time series of spectrophotometric air scans collected over approximately 70 minutes every 10 minutes after instrument is turned on. The inset shows the time series of air OD measured at 275 nm (black) and 400 nm (blue) representing the two lamps, deuterium, and tungsten, respectively.

Instruments should be allowed to warm up for at least 60 minutes as the spectrum of lamp energy changes during warm up. The warm up time can be assessed by running air scans every ten minutes from the time the instrument is turned on until subsequent scans approach differences in optical density < 0.0005 (the target noise value; Fig. 5.10). Establish the warm up time for your instrument; note that it may change as the lamps age.

5.4.3 Instrument performance, instrument settings and spectrophotometric noise in T-Mode

Instrument performance tests should be performed prior to every measurement session. These tests include wavelength accuracy, absorbance calibration and instrument noise. Maintaining a record of these tests allows the user to identify misalignment, lamp degradation, and detector failures.

The recommended wavelength range for filter pad measurements is 250–850 nm. The lower (UV) end of the spectrum will be noisy because of strong absorption by the glass fiber filters and the relatively weak light-energy of the instrument; the upper, red end of the spectrum will be noisy because of the generally weak light and detector sensitivity and strong scattering by the filter. The crossover wavelength between the deuterium and tungsten lamps is between 300 nm and 350 nm and should be consistently maintained. The wavelength resolution, scan speed, and integration times are recommended to be: 1 nm; 120 to 300 nm per minute; 0.1 to 0.2 s, respectively. A slit bandwidth (SBW) of 2 nm is recommended. Smaller SBW lead to reduced light energy and lower signal-to-noise while larger SBWs reduce the resolution of spectral variations associated with distinct pigments.

Spectrophotometric noise varies between manufacturers, between instruments, and over time. This is best assessed by collecting multiple air scans and computing the standard deviation spectrum over the entire wavelength range. The target value is approximately 0.0005 optical density units and is the lowest level of uncertainty.

5.4.4 Baseline, zero and blank scans in T-Mode

Baseline scans are necessary to remove the instrument signal which encompasses the variations due to lamp energy spectrum, spectral sensitivity of the detector and the optical signature of the glass fiber filter. There are two approaches to performing baseline scans: air baselines and filter pad baselines. The end product particulate absorption will be the same but the differences are in what appears on the screen as samples are processed.

The air baseline approach involves collecting a single air scan as a baseline which is automatically removed from subsequent blank and sample scans. The average spectrum of a set of three to five blank filter pads scans are then subtracted from each sample scan to remove the optical signature of the filter

pad. The standard deviation spectrum of the blank scans is used to compute absorption uncertainty using Eq. (5.6). What appears on the screen during measurement is a spectrum that is the sum of the filter pad and the sample optical properties. To maintain the proper sample loading on the filter (optical density between 0.1 and 0.4), the contribution by the blank filter has to be mentally removed. Thus, if the optical density of the blank filter is 0.25 in the UV (as is typical for T-mode) and the sample filter optical density is 0.6, the sample optical density is 0.35, still less than the maximal 0.4 optical density target (Fig. 5.11).
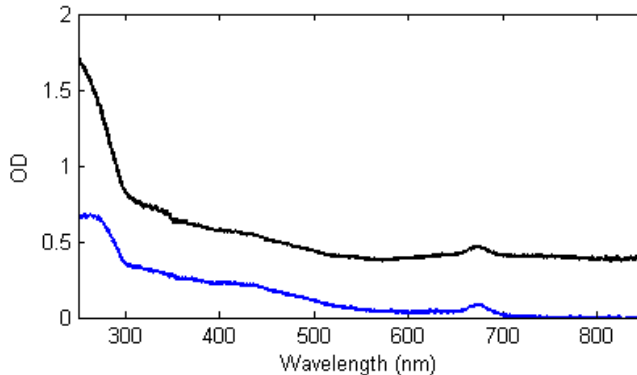
Figure 5.11. Example of a particulate optical density scan run in T-mode with air as a baseline (black) or with a blank filter as a baseline (blue). Note the sample optical density range is between 0.1 and 0.4 (the target range) for the visible portion of the spectrum but begins to exceed this optimal range in the UV portion of the spectrum.

The filter pad baseline approach involves collecting a single scan of a prepared blank filter pad as the baseline which is automatically removed from subsequent blank and sample filter scans. The average spectrum of the blank filter scans should be spectrally flat about zero (Fig. 5.4). The advantage of this approach is that the scans that appear on the screen show the optical density of the sample material and instantly allow the user to determine if the proper loading has been achieved throughout the spectral range. It also provides an instant assessment of the blank filter spectral variations.

5.4.5 Sample analysis for T-Mode

The sequence of sample scans includes the assessment of a baseline, a series of blank filter pads, and the initial scan of the set of sample filter pads. The initial scan of each sample provides the assessment of particulate optical density. After pigment extraction (Section 5.2), the sample filters are scanned again to provide assessment of the non-extractable particulate contribution to optical density, also known as non-algal particles (Fig. 5.12).
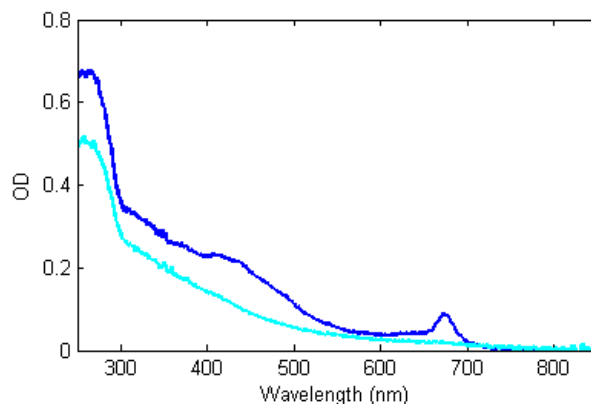
Figure 5.12. Example of a particulate (blue) and extracted non-algal particle (cyan) optical density scans measured in T-mode with a blank filter as a baseline. Note the magnitude and shape of the optical density spectra in the near IR (~700nm -850 nm) is zero and spectrally flat within the uncertainty of T-mode blank filter readings.

The operating protocol of the spectrophotometer with regards to spectral bandwidth, spectral sampling, and scan rates are the same as described earlier in this section. The recommendations regarding

maintaining filter hydration between measurements should also be followed. A typical sequence of making measurements is as follows:

1. The baseline scan is initiated with the quartz neutral density filter placed securely to the light source side of the reference port and a moist blank filter placed securely to the detector side of the sample port (Fig. 5.8). This is the baseline scan. For most instruments, this scan is stored internally and automatically subtracted from subsequent sample scans.

2. Without opening the sample compartment, a second scan is immediately collected. This scan will have the baseline scan automatically removed. Because no changes have been made this scan should be spectrally flat about zero; this is the zero scan. If there is some spectral dependence to this scan or if the noise level exceeds 0.001, the blank filter pad should be replaced with a different moist pad and the baseline and zero scan repeated.

3. A series of three to five blank filters scans are collected relative to the baseline scan; these are the blank scans. They should likewise exhibit no spectral dependence and with signals of order 0.001 throughout the spectrum. The largest variations are likely found in the UV and far-red portions of the spectra (Fig. 5.6). If all the blank filter scans are similar to each other but very different from zero, the baseline filter pad is anomalous and one of the blank pads should be rerun in baseline mode. Repeat the zero and blank scans as above.

4. Sample filters are scanned similarly, relative to the baseline scan. A notch at the edge of the filter is used to align the position of the filter on the holder. This provides a mechanism for placing the filter in the same orientation after pigment extraction. Within sample variability is measured by remoistening and rotating the filter by 90 degrees and performing a second scan. These measurements provide the optical density signature for computing the spectral particulate absorption coefficients $a_p(\lambda)$, via Eqs. (5.3) and (5.5).

5. After pigment extraction (Section 5.2), each sample filter is rescanned to assess the optical density signature of the non-algal particles for computing absorption properties $a_{NAP}(\lambda)$, via Eqs. (5.3) and (5.5).

6. Blank filters are scanned throughout the measurement period to assess any drift in the instrument relative to the initial baseline. If the blank filter spectra vary relative to their initial scans in spectral shape (flat) and magnitude (+/- 0.001 maximally), a new series of baseline, zero, and blank scans should be run.

5.4.6 Data processing for T-Mode

General processing of data and calculation of the absorption coefficient is similar to the general guidelines described in Section 5.3. An important variation unique to the T-mode is that the so-called "null point" correction, in which subtraction of a spectrally-constant value from the NIR spectral region is used to account for large scattering losses. Experience with healthy phytoplankton cultures suggests that there is negligible absorption in the NIR, thus when non-negligible absorption is measured in the NIR using the filter pad technique in T-mode, it is assumed that it is due to scattering losses by the filter pad. The assumption is that these scattering losses are spectrally invariant due to the large size of the scattering fibers of the filter relative to the wavelength of light (and confirmed by their white scattering appearance). Thus, the average absorption value computed in the NIR region is subtracted from the entire spectrum, resulting in a shift down (in the case of positive NIR signal) or shift up (in the case of a negative NIR signal). Problems arise when the sample is composed of particulates other than healthy phytoplankton. In this case the NIR null point correction likely removes some contribution to absorption by these non-algal particles and leads to a larger measurement uncertainty. However, in the absence of other supporting measurements, the null point correction provides the lowest error estimate for T-mode absorption measurements. The data processing procedure is as follows:

1. Instrument drift is quantified from the blank filter pad measurements made at different times throughout the measurement period. If required, all filter baselines and sample spectra are corrected for any observed drift.

2. The average and standard deviation optical density spectra from all blank filter pad scans are computed. If the air baseline approach is used, the average is subtracted from each measured spectrum.

If the blank filter baseline approach is used, no additional subtraction is necessary (as the average of the blank filters relative to a blank filter baseline should be zero within 0.001 optical density units).

3. Replicate measurements of baseline-corrected sample filter optical density, $OD_f(\lambda)$, obtained on the same sample filter are averaged.

4. The null point correction should be applied to $OD_f(\lambda)$ by subtracting the respective average optical density values in the NIR (e.g. over the range 800 nm–850 nm) from the sample spectrum.

5. The blank-corrected, null-corrected and averaged $OD_f(\lambda)$ of the sample can be smoothed, for example with a moving average. The choice of smoothing window width and number of iterations determined based on characteristics of the sample spectra (i.e., presence or absence of sharp peaks, behavior of instrument noise).

6. The particle absorption coefficient, $a_p(\lambda)$ or non-algal particle absorption coefficient, $a_{NAP}(\lambda)$ for each sample are calculated from $OD_f(\lambda)$ using the known filtration volume (V in m^3) and the measured interception area of filtration (A in m^2) as:

$$a_x(\lambda) = \ln(10)\, 0.679\, [OD_f(\lambda)]^{1.2804} / (V/A) \qquad (5.15)$$

which utilizes a beta-correction modeled as a power function for the relationship between OD_s and OD_f (Eqs. 5.3 and 5.5).

7. The phytoplankton absorption spectrum, $a_{ph}(\lambda)$, is computed from the particulate and non-algal particle absorption spectra by difference using Eq. (5.14).

The largest uncertainty in the T-mode approach is associated with the unknown level of absorption in the NIR which cannot be quantified because of the unknown quantity of scattered loss by the filter with embedded particles compared to the blank filter. The IS-mode provides quantitation of the NIR absorption, and, in the presence of any particulate material other than healthy phytoplankton cultures, there is measurable NIR absorption coefficients, which clearly violates the assumption for the null point correction in step 6. It also provides evidence that the scattering corrections approaches for reflecting tube absorption meters that require the null point correction at red wavelengths are also in error (Chapter 2).

5.5 Measurement of Filter Pad Absorption in Transmittance Mode Using Fiber Optics

5.5.1 General Considerations for Fiber Optic T-Mode

Particulate absorption measurements using the filter pad method have been assessed on a single beam fiber-optic based spectrophotometer (Belz et al. 2006; Miller et al. 2011; Naik and D'Sa 2012). The portable fiber-optic based system consists of a single beam optical path with a light source, a filter holder and a fiber-optic spectrometer all connected serially using optical fibers (Fig. 5.13a), The filter holder consists of a filter fixture for a 25 mm GF/F filter and a holder (Fig. 5.13b; QFT1-89575, WPI). In its basic configuration, the output of a high intensity light source (Fig. 5.13c; e.g., D$_2$H consisting of a deuterium and halogen lamp; WPI Inc.) is coupled via an optical fiber with a core diameter of 600 μm to the filter holder. A combination of 600 μm input fiber and a fused silica lens collimates the input light into an approximately parallel beam of 5 mm diameter (Belz et al. 2006). The collimated light beam incident perpendicular to GF/F filter (blank, particulate or extracted) is transmitted or scattered through the filter and is collected by a second collimating lens behind the filter and coupled into an exit 600 μm fiber that is then connected to a photodiode array spectrometer (Fig. 5.13d; e.g., Tidas, J&M Analytische Messung Regeltechnik GmbH) that is optimized for the spectral range of 195–722 nm. The Tidas spectrometer connects via a RS-232 to USB adapter to a Windows based computer with vendor supplied software (e.g., Spectralys) that is used to acquire, display and analyze the spectral data.
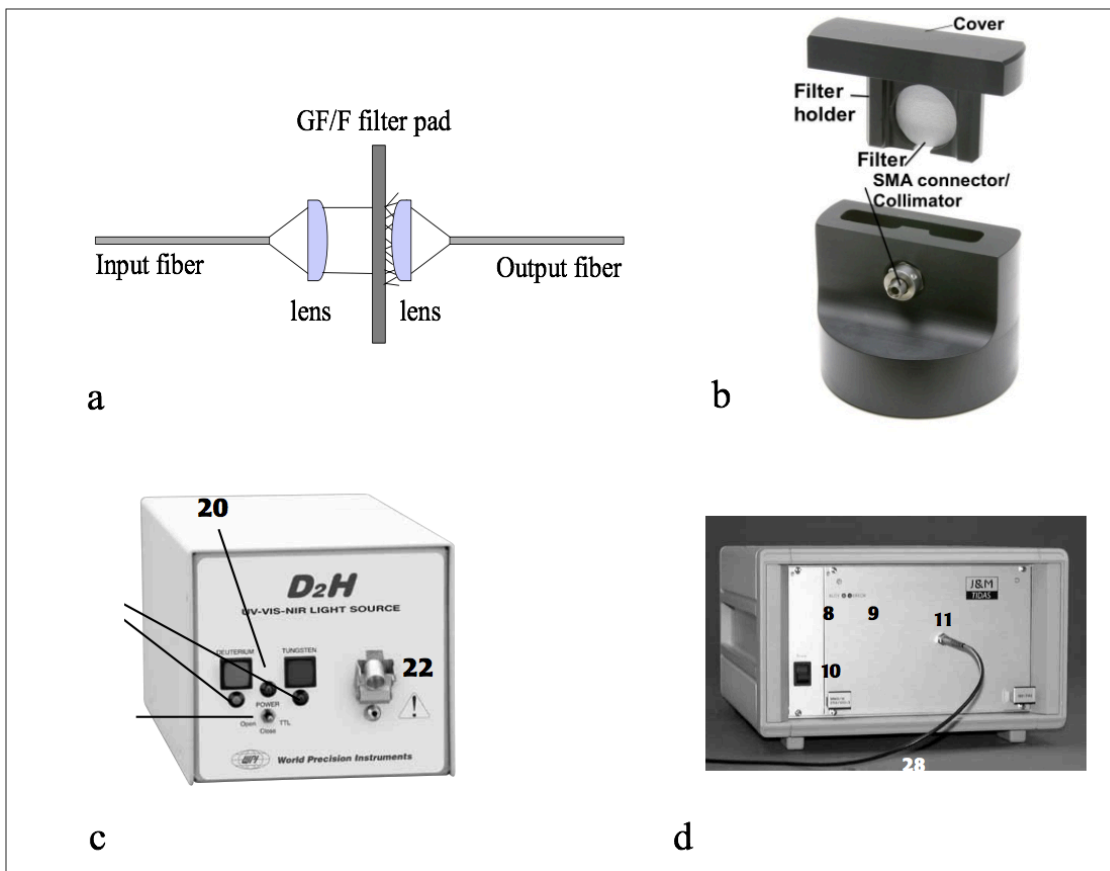
Figure 5.13. (a) Schematic of a portable fiber-optic based filter holder for measuring particle absorption using the filter pad technique. (b) The filter holder (WPI) with the GF/F filter fixture that is inserted into the holder. The input fiber connects to the light source (e.g., D₂H; c) while the output fiber connects to the spectrometer (e.g., Tidas; d).

The fiber-optic-based spectrophotometer for filter pad measurements is small and portable and relatively inexpensive in comparison to the laboratory-based spectrophotometers (e.g., Perkin-Elmer Lambda-850). It can be easily setup on a ship during field campaigns and absorption measurements of suspended particles obtained following seawater sampling onboard the ship. The use of a photodiode array-based spectrometer also allows for greater sensitivity in the absorbance measurements by increasing the integration time of the detector. However, results of a comparison study of particle absorption on a filter indicated small differences (~5%) in $OD_f(\lambda)$ between the fiber-optic-based system and a high performance spectrophotometer (e.g., Perkin Elmer Lambda 850; Miller et al. 2011; Naik and D'Sa 2012).

5.5.2 Sample analysis for Fiber Optic T-Mode

The recommendations regarding maintaining filter hydration between measurements should be followed. A typical sequence of making measurements is as follows:

1. The spectrophotometer (lamps and the spectrometer) should be allowed to warm for about one hour before running the samples. However, as noted in Section 5.4.2, an appropriate warm up time can be assessed for the instrument as it may change as the lamp ages.

2. The Spectralys software is started.

3. The steps for blank and sample filter preparation (Section 5.2) should be followed.

4. A hydrated blank filter is placed on the filter fixture that is then inserted in fiber optic filter holder.

5. Integration time is adjusted on the spectrometer to optimize the light transmission through the blank hydrated filter to obtain peak intensity of ~70% and then select absorbance mode.

6. A "dark spectrum" is obtained with the shutter closed.

7. The shutter switch is moved to "open" mode and "reference spectrum" is obtained. This is the baseline or reference scan and is automatically subtracted from subsequent sample filter scans.

8. The blank filter is replaced with a sample or extracted sample filter.

9. A "sample spectrum" is obtained and repeated after rotating the filter 90 degrees. Additional sample filters can be scanned similarly using the same blank reference, making sure to monitor for any drifts in the spectra.

10. The blank corrected spectra $OD_f(\lambda)$ are then exported and saved as ascii files.

5.5.3 Data processing for Fiber Optic T-Mode

General processing of data and calculation of the absorption coefficient is similar to the general guidelines described in Section 5.3. The data processing procedure is as follows:

1. A null correction should be applied by subtracting the average of spectrally flat region between 712–722 nm.

2. $OD_f(\lambda)$ for representative culture samples measured on the fiber optic based system and the Lambda 850 showed overall very good agreement with strong linear relationship observed between $OD_f(\lambda)$ at chlorophyll absorption peaks (443 and 676 nm) and also over the entire visible domain from 400 to 700 nm (Fig. 5.14). These results suggested that the beta correction factor derived for the Perkin Elmer Lambda 850 with an integrating sphere could be applied to the fiber-optic–based system for filter pad measurements.
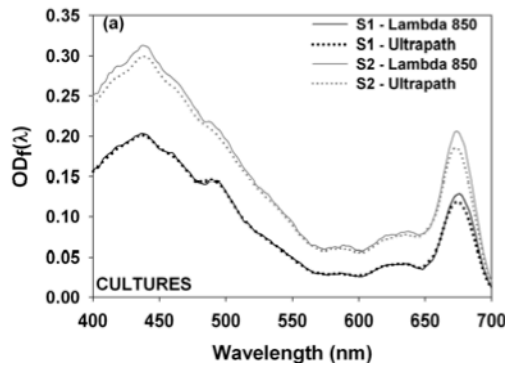
Figure 5.14. Comparison of spectral shape of optical density ($OD_f(\lambda)$) of particles on GF/F filter measured with the fiber-optic based system and a Perkin-Elmer Lambda 850 spectrophotometer with an integrating sphere (Naik and D'Sa 2012).

The equation for beta correction for pathlength amplification effect caused by multiple scattering in the glass-fiber filter applicable to the fiber-optic based absorbance measurements is given as (Naik and D'Sa 2012):

$$OD_s(\lambda) = 0.405[OD_f(\lambda)] + 0.475[OD_f(\lambda)]^2 \tag{5.16}$$

where $OD_s(\lambda)$ is the corrected optical density of particulate matter. The absorption coefficient of the particulate matter, $a_p(\lambda)$ or $a_{NAP}(\lambda)$, is then calculated from Eq. (5.3) using $OD_s(\lambda)$ values from Eq. (5.16). The phytoplankton absorption coefficient, $a_{ph}(\lambda)$, is calculated from Eq. (5.14).

5.6 Measurement of Filter Pad Absorption in Transmittance and Reflectance Mode

5.6.1 General Considerations for T-R-Mode

Tassan and Ferrari (1995) described a modification of the light-transmittance method that corrects for differences in backscattering between the sample and reference filter and, thus, accounts for backscatter differences between different sample filters. This technique combines light-transmittance (T) and light-reflectance (R) measurements carried out using an integrating sphere attached to a dual-beam

spectrophotometer. In contrast to T-mode, the transmittance and reflectance mode (T-R-mode) enables a measurement of a large fraction of both forward-scattered light (T-mode) and backward-scattered light (R-mode), which largely circumvents (or minimizes) the issues associated with scattering error (owing to undetected portion of scattered power for T-mode alone) and null-point correction. The T-R data analysis is performed by a theoretical model that eliminates the effect of differences in light backscattering by the particles and different filters. Modifications of the T-R experimental routine (Tassan and Ferrari 1998; Ferrari and Tassan 1999) yielded a significant reduction of the experimental error. Absolute errors are typically lower for the T-R method than for the T method (Tassan and Ferrari 2002, Röttgers and Gehnke 2012). Tassan and Ferrari (1995) reported that for Case 1 waters that have negligible inorganic particle load, the amplification factor for GF/F filters determined with the T-R method is similar to that determined by Mitchell (1990). Similar results were obtained for Case 2 waters (Tassan et al. 2000). The T-R method is particularly suited for applications to samples containing highly scattering mineral particles that are commonly found in Case 2 waters. When sample measurements of T and R are made with a good spectrophotometer and integrating sphere, the scattering errors are greatly reduced, usually to the point that a null-point correction becomes unnecessary (Tassan and Ferrari 2003, Röttgers and Gehnke 2012). The method should be considered when a good spectrophotometer equipped with an integrating sphere is available, but the sphere does not allow placing a sample inside it and using a superior IS-mode of measurement (see Section 5.7).

The most recent procedure that includes some modifications of the Tassan and Ferrari (1995) routine is described by Tassan and Ferrari (2002). Here, the method is described in a simplified way.

5.6.2 Sample analysis for T-R-Mode

Common procedures for sample preparation, handling, and spectrophotometric measurements as described above should be followed. Some minor differences may be related to the necessity for the use of the integrating sphere in the T-R mode. The properties of the integrating sphere are of lower importance, but usually a sphere with a larger diameter provides better performance. A sphere operating with a double-beam spectrophotometer has typically four ports, two entrance ports and two exit ports, one set for the sample beam and the other set for the reference beam. The exit ports are normally closed with white reflective plates (typically calibrated reflectance standards), and black light traps are usually placed behind these plates. Alignment of the two light beams should be checked with respect to the beam position being in the center of these reflective plates. The baseline is recorded with both entrance ports void and both exit ports closed with reflectance standards.

All spectral measurements can be done using the OD output of spectrophotometer and the following procedure is based on OD measurements. A hydrated blank filter is measured as a reference. When using 25 mm GF/F filters, these, when wet, can be placed directly onto the integrating sphere ports. Some extra support for the filters can be arranged to avoid salt water coming in direct contact with the outside of the integrating sphere. Using glass plates behind the filter as a support is not recommended. Each filter is first measured when placed at the sample beam entrance port, when the reference beam entrance port is void and the exit ports are closed with the reflectance standards. This results in the respective OD of the transmittance mode for the sample filter and the reference filter, OD_{fs}^T and OD_{fr}^T, respectively. Secondly, the same filter is measured (after another hydration if necessary) in reflectance mode when placed (sample side facing the light beam) at the sample beam exit port. The reflectance standard at this port is removed and the space behind the filter serves as a black light trap (otherwise support the filter with a black material). These measurements result in the respective OD of the reflectance mode for the sample filter and the reference filter, OD_{fs}^R and OD_{fr}^R, respectively

5.6.3 Data processing for T-R-Mode

According to the equations provided by Tassan and Ferrari (2002) and omitting the wavelength argument λ for brevity, the OD values are converted to specific transmittances and reflectances using $OD^T = log_{10}(1/T)$ and $OD^R = log_{10}(1/R)$. This results in absolute transmittances and reflectances of the sample and reference filter, T_{fs}, T_{fr}, R_{fs} , and R_{fr}. The ratios of the two transmittance and two reflectance measurements gives the T and R spectra of the sample, i.e., $T_f = T_{fs}/T_{fr}$ and $R_f = R_{fs}/R_{fr}$, respectively. T_f is used to calculate OD_{fs}^T, the optical density of the sample in the transmittance mode. The full set of T and R measurements is used to calculate the absorptance of the sample as

$$A_f = \frac{1 - T_f + R_{fr}(T_f - R_f)}{1 + R_{fr}T_f\tau} \tag{5.17}$$

where τ compensates for the fact that the reflected light inside the filter is diffuse and is no longer a collimated beam. Its effect on A_f is low (<3%). This factor was determined empirically and can be calculated for each sample filter as:

$$\tau(\lambda) = 1.15 - 0.17\, OD_{fs}^{T\,*}(\lambda) \tag{5.18}$$

where

$$OD_{fs}^{T\,*}(\lambda) = OD_{fs}^{T}(\lambda) - 0.5\, OD_{fs}^{T}(750) \tag{5.19}$$

The formulation for τ is valid for $0.02 < OD_{fs}^{T\,*} < 0.7$.

The absorptance of the sample is defined as the fraction of incident power that is lost from the beam owing to absorption (Mobley, 1994), so in this case we have $A_f = \Phi_a/\Phi_o$ where Φ_a is the absorbed power. In addition, by virtue of energy conservation $\Phi_o = \Phi_a + \Phi_t + \Phi_B$, we obtain $1 - A_f = (\Phi_t + \Phi_B)/\Phi_o$. As a result, the final values of the optical density of the sample measured in T-R-mode can be calculated from A_f as (see Section 5.3.1):

$$OD_f = \log_{10}[1/(1 - A_f)] \tag{5.20}$$

The particle absorption coefficient, $a_p(\lambda)$, or non-algal particle absorption coefficient, $a_{NAP}(\lambda)$, are calculated from $OD_f(\lambda)$ using the known filtration volume (V in m^3) and the measured interception area of filtration (A in m^2) as:

$$a_x(\lambda) = \ln(10)\, 0.719\, [OD_f(\lambda)]^{1.2287} / (V/A) \tag{5.21}$$

which utilizes a beta-correction modeled as a power function for the relationship between OD_s and OD_f (Eqs. 5.3 and 5.6). The phytoplankton absorption coefficient, $a_{ph}(\lambda)$, is calculated from Eq. (5.14).

5.7 Measurement of Filter Pad Absorption Inside an Integrating Sphere

5.7.1 General considerations for IS-Mode

Historically, the most common implementation of the filter pad technique involves measuring the transmittance (T) of a sample filter relative to a blank reference filter (Mitchell et al. 2003). This method suffers from a poor geometry as a large fraction of light scattered by the filter is not detected by the spectrophotometer, resulting in unknown errors in the spectral determination of filter optical density, $OD_f(\lambda)$, and ultimately in the particulate absorption coefficient, $a_p(\lambda)$. An alternative approach, referred to as the transmittance-reflectance (T-R) method, employs multiple scans of the sample and reference filters placed at the entrance (transmittance) and exit (reflectance) ports of an integrating sphere (Tassan and Ferrari 1995, 1998). The underlying assumptions of the T-R method are based on the law of energy conversation, but uncertainties arise as these assumptions are not necessarily fully satisfied with the actual measurement configuration. The need for multiple scans at different filter positions also increases uncertainties and makes the method more laborious to implement.

To circumvent these limitations, we recommend an improved refinement of the filter pad technique in which the sample or reference filter is placed inside an integrating sphere during measurement. This inside sphere (IS-mode) technique ensures the detection of nearly all photons scattered by the sample, resulting in improved accuracy and precision of absorption measurements (Maske and Haardt 1987; Babin and Stramski 2002, 2004; Stramski et al. 2004, 2007; Röttgers and Gehnke 2012; Stramski et al. 2015). Because this method does not require multiple scans of the same filter in different optical configurations, the effort is no more laborious than the traditional T-mode.

5.7.2 Sample preparation for IS-Mode

Sample collection and filtering follow the same guidelines recommended for the general filter pad technique (Section 5.2). Filter volumes are adjusted to target an optical density of the sample filter between

0.1 and 0.4 (after corrections for instrument baseline and blank filter baseline, see below). For some spectral regions, especially the UV, multiple filtrations of the sample with different volumes may be needed to satisfy these criteria.

5.7.3 Spectrophotometer configuration for IS-Mode

A suitable dual-beam spectrophotometer equipped with an integrating sphere (e.g., 15 cm diameter sphere) is required to implement the IS method. The instrument performance with regards to wavelength accuracy and absorbance calibration should be verified as described in Section 5.4.3.

Some integrating sphere manufacturers provide a fixture for mounting of samples within the beam inside the sphere, which can be adapted to positioning of sample filters. Alternatively, a custom mounting system can be fabricated. The mounting system should center the sample filter perpendicular to the illumination beam and be secured in a way that ensures reproducible positioning of a filter at the same location. Ideally, the mounting mechanism should be constructed such that only the filter itself interacts with the beam (i.e., no filter supporting structure within the illuminated portion). All materials within the sphere should be made of Spectralon or coated with a similar highly reflective material.

Through the use of various apertures placed with the light path between the source and entrance port of the integrating sphere, the size and shape of the sample beam is adjusted to provide a beam illuminating the center of the filtered area. Beam size should be sufficiently large to cover a representative portion of the filter (e.g., 3 mm wide x 6 mm high). The size of the reference beam is adjusted accordingly to provide a similar amount of light energy associated with the sample and reference beams propagating in air.

5.7.4 Sample analysis for IS-Mode

The operating protocol of the spectrophotometer with regards to spectral bandwidth, spectral sampling, and scan rates are the same as described earlier in Section 5.4.3. The recommendations regarding maintaining sample filter hydration between measurements should also be followed. A typical sequence of making measurements is as follows:

1. After a suitable warm-up period, the spectrophotometer is initially autozeroed by scanning air-vs-air with the empty mounting mechanism placed within the sphere; for most instruments, this scan is automatically stored in memory and subtracted from subsequent scans. The scan is then repeated and the data saved to a data file to provide an actual measure of instrument baseline. This air-vs-air instrument baseline should be performed and saved at regular intervals to check for instrument drift throughout the course of sample measurements.

2. Hydrated blank filters (minimum of three to five) drawn from the same batch as the sample filters are positioned on the mounting mechanism and placed within the center of the integrating sphere for measurement. These blank filters are scanned (relative to air in the reference beam) and these spectra of optical density (absorbance values) are saved to data files for determination of the average blank-filter baseline. These can be run initially before beginning analysis of samples or spaced intermittently between sample filters. This protocol assumes a typical scenario when it is impractical to measure individual blank filter baselines for each specific sample filter, such as when sample filters are collected and frozen on the ship for post-cruise analysis in the lab. However, in some lab experiments with limited number of samples it is possible to measure the filter baseline and then immediately collect sample on the same filter for subsequent measurement of the sample filter. In this case there is no need for the determination of average filter baseline for the purpose of its application to multiple sample filters.

3. After ensuring an appropriate level of hydration and no excess moisture of the sample filter (frozen filters have to be first remoistened by placing them on a drop of water, see Section 5.2), the sample filter is positioned on the mounting mechanism and placed within the center of the integrating sphere for measurement. It is useful to notch or mark an edge of the filter before initial measurement to ensure reproducible positioning of the filter for subsequent scans (e.g., for replicate scans and after pigment extraction).

4. The sample filter is scanned (relative to air in the reference beam) and the measured optical density values (absorbance values) are saved to a data file. Following the initial measurement, the filter is repositioned in a different orientation (e.g., 90-degree rotation) and measured a second time to

check reproducibility and homogeneity of sample distribution on the filter. The replicate scans of sample filter provide the optical density data that are used to calculate the particulate absorption coefficient, $a_p(\lambda)$.

5. Following measurement, sample filters can be extracted in solvent to remove phytoplankton pigments (Section 5.2 and 5.3.5) and re-measured in the spectrophotometer to estimate the non-algal particulate absorption coefficient, $a_{NAP}(\lambda)$.

5.7.5 Data processing for IS-Mode

General processing of data and calculation of the absorption coefficient is similar to the guidelines described in Section 5.3. In contrast to T-mode, the so-called "null point" correction, in which subtraction of a spectrally constant value of particulate absorption from the NIR spectral region is used to account for scattering losses, is not applied. Experience suggests that scattering losses with the IS technique are small enough to be considered negligible, and the application of a null point correction can mask true particulate absorption in the NIR.

The general sequence of data processing is:

1. Instrument drift is checked from the air-vs-air measurements (i.e., instrument baselines) made at different times throughout the measurement period. If needed, all blank filter baselines and sample spectra are corrected for any observed drift of the instrument using appropriate instrument baselines.

2. Measurements from all blank filters are averaged to create the final values of optical density for the filter baseline (relative to air). Importantly, the *OD* values of blank filters mounted inside the integrating sphere as measured relative to air in the reference beam are close to zero (typically within ±0.04 in the spectral region between 300 and 850 nm).

3. The spectrum of the final filter baseline is subtracted from each spectrum of sample filter optical density.

4. Replicate measurements of baseline-corrected sample filter optical density, $OD_f(\lambda)$, obtained on the same sample filter are averaged.

5. The blank-corrected and averaged $OD_f(\lambda)$ of the sample can be smoothed, for example with a moving average. The choice of smoothing window width and number of iterations is determined based on characteristics of the sample spectra (i.e., presence or absence of sharp peaks, behavior of instrument noise).

6. The particle absorption coefficient, $a_p(\lambda)$, or non-algal component, $a_{NAP}(\lambda)$, of each sample is calculated from $OD_f(\lambda)$ using the known filtration volume (V in m^3) and the measured interception area of filtration (A in m^2) as:

$$a_x(\lambda) = \ln(10)\ 0.323\ [OD_f(\lambda)]^{1.0867} / (V/A) \tag{5.22}$$

which utilizes a beta-correction modeled as a power function for the relationship between OD_s and OD_f (Eqs. 5.3 and 5.7). The phytoplankton absorption coefficient, $a_{ph}(\lambda)$, is calculated from Eq. (5.14).

As mentioned previously, no null-point scattering correction is applied to the calculated $a_p(\lambda)$. If a corresponding absorption spectrum of the particles after pigment extraction (a_{NAP}) is measured, this spectrum is adjusted with an offset in the near-infrared so that the average value of $a_{NAP}(\lambda)$ equals the average value of $a_p(\lambda)$ in the NIR spectral range (e.g., 800–820 nm). When using the IS technique this adjustment of $a_{NAP}(\lambda)$ is usually very small, which supports the common assumption that phytoplankton pigments do not absorb in this spectral region.

REFERENCES

Babin, M. and D. Stramski, 2002: Light absorption by aquatic particles in the near-infrared spectral region. *Limnol. Oceanogr*., **47:** 911–915.

Babin, M. and D. Stramski, 2004: Variations in the mass-specific absorption coefficient of mineral particles suspended in water. *Limnol. Oceanogr*., **49:** 756–767.

Bricaud, A. and D. Stramski, 1990. Spectral absorption coefficients of living phytoplankton and nonalgal biogenous matter: a comparison between the Peru upwelling area and the Sargasso Sea. *Limnol. Oceanogr*., **35**: 562–582.

Belz, M., K. Larsen, and K. Klein, 2006: Fiber optic sample cells for polychromatic detection of dissolved and particulate matter in natural waters, in *Advanced Environmental, Chemical, and Biological Sensing Technologies IV,* (Proceedings of SPIE, Boston, MA, USA).

Butler, W.L., 1962: Absorption of light by turbid materials. *J. Opt. Soc. Am.*, **52(3)**: 292–299.

Duysens, L. N. M., 1956: The flattening of the absorption spectrum of suspensions, as compared to that of solutions. *Biochim. Biophys. Acta*, **19:** 1–11.

Ferrari, G.M. and S. Tassan, 1999: A method using chemical oxidation to remove light absorption by phytoplankton pigments. *J. Phycol.*, **35:** 1090–1098.

JCGM, 2008: Evaluation of measurement data—Guide to the Eexpression of uncertainty in measurement. 134 pp. Working Group 1 of the Joint Committee for Guides in Metrology (JCGM/WG 1). International Organization for Standardization, Geneva, Switzerland.

Kiefer, D.A. and J.B. SooHoo, 1982: Spectral absorption by marine particles in coastal waters of Baja California. *Limnol. Oceanogr., ***27(3)**: 492–499.

Kishino, M., M. Takahashi, N. Okami, and S. Ichimura, 1985: Estimation of the spectral absorption coefficients of phytoplankton in the sea. *Bull. Mar. Sci.*, **37(2)**: 634–642.

Lefering, I., R. Röttgers, R. Weeks, D. Connor, C. Utschig, K. Heymann, and D. McKee, 2016: Improved determination of particulate absorption from combined filter pad and PSICAM measurements. *Opt. Express*, **24**: 24805–24823.

Lohrenz, S. E., 2000. A novel theoretical approach to correct for pathlength amplification and variable sampling loading in measurements of particulate spectral absorption by the quantitative filter technique. *J. Plankton Res.*, **22:** 639–657.

Maske, H. and H. Haardt, 1987: Quantitative in vivo absorption spectra of phytoplankton: detrital absorption and comparison with fluorescence excitation spectra. *Limnol. Oceanogr., ***32:** 620–633.

Miller, R.L., C. Buoassissi, C. Del Castillo, and M. Belz, 2011: A portable fiber optic system for measuring particle absorption using the quantified filter technique (QFT). *Limnol. Oceanogr: Methods*, **9:** 554–564.

Mitchell, B.G., M. Kahru, J. Wieland, and M. Stramska, 2003: Determination of spectral absorption coefficients of particles, dissolved material and phytoplankton for discrete water samples, in *Ocean Optics Protocols for Satellite Ocean Color Sensor Validation, Revision 4, Volume IV: Inherent Optical Properties: Instruments, Characterizations, Field Measurements and Data Analysis Protocols*, NASA/TM-2003-211621/Rev4-Vol. IV, edited by J.L. Mueller, G.S. Fargion, and C.R. McClain, pp. 39–64, NASA Goddard Space Flight Center, Greenbelt, Maryland.

Mobley, C.D., 1994: *Light and Water: Radiative Transfer in Natural Waters*, Academic Press.

Naik, P., and E.J. D'Sa, 2012: Phytoplankton light absorption of cultures and natural samples: comparisons using two spectrophotometers, *Opt. Express*, **20**: 4871–4886.

Roesler, C.S., 1998: Theoretical and experimental approaches to improve the accuracy of particulate absorption coefficients from the Quantitative Filter Technique. *Limnol. Oceanogr*., **43:** 1649–1660.

Röttgers, R. and S. Gehnke, 2012: Measurement of light absorption by aquatic particles: improvement of the quantitative filter technique by use of an integrating sphere approach. *Appl. Opt.,* **51:** 1336–1351.

Sosik, H.M., 1999: Storage of marine particulate samples for light-absorption measurements. *Limnol. Oceanogr.,* **44(4)**: 1139–1141.

Sosik, H.M., and B.G. Mitchell, 1991: Absorption, fluorescence and quantum yield for growth in nitrogen-limited *Dunaliella tertiolecta. Limnol. Oceanogr.,* **36(11):** 910–921.

Stramski, D., 1990: Artifacts in measuring absorption spectra of phytoplankton collected on a filter. *Limnol. Oceanogr.,* **35(8):** 1804–1809.

Stramski, D., M. Babin, and S. B. Woźniak, 2007: Variations in the optical properties of terrigeneous mineral-rich particulate matter suspended in seawater. *Limnol. Oceanogr.,* **52:** 2418–2433.

Stramski, D., R. A. Reynolds, S. Kaczmarek, J. Uitz, and G. Zheng, 2015: Correction of pathlength amplification in the filter-pad technique for measurements of particulate absorption coefficient in the visible spectral region. *Appl. Opt.*, **54**: 6763–6782.

Stramski, D., S. B. Woźniak, and P. J. Flatau, 2004: Optical properties of Asian mineral dust suspended in seawater*, Limnol. Oceanogr.,* **49:** 749–755.

Tassan S. and G. M. Ferrari, 1995: An alternative approach to absorption measurements of aquatic particles retained on filters. *Limnol. Oceanogr.,* **40:** 1358–1368.

Tassan S. and G. M. Ferrari, 1998: Measurement of light absorption by aquatic particles retained on filters: determination of the optical pathlength amplification by the 'transmittance-reflectance' method. *J. Plankton Res.,* **20:** 1699–1709.

Tassan, S., G.M. Ferrari, A. Bricaud, and M. Babin, 2000: Variability of the amplification factor of light absorption by filter-retained aquatic particles in the coastal environment. *J. Plankton Res*., **22:** 659–668.

Tassan, S., and G.M. Ferrari, 2002: A sensitivity analysis of the 'transmittance-reflectance' method for measuring light absorption by aquatic particles. *J. Plankton Res.,* **24:** 757–774.

Tassan, S., and G.M. Ferrari, 2003: Variability of light absorption by aquatic particle in the near-infrared spectral region. *Appl. Opt.,* **42:** 4802–4810.

van de Hulst, H. C. 1981. *Light Scattering by Small Particles*, Dover, New York.

SYMBOL LIST BY CHAPTER

CHAPTER 1

a = Volume absorption coefficient
a_g = Absorption coefficient of dissolved material
a_m = Absorption coefficient of minerals
a_{NAP} = Absorption coefficient of non-algal particles
a_p = Absorption coefficient of particles
a_p^* = Chlorophyll-a–specific absorption coefficient of total particulate matter
a_{pg} = Absorption coefficient of particulate and dissolved material
a_{ph}^* = Chlorophyll-a–specific absorption coefficient of phytoplankton
a_{ph} = Absorption coefficient of pigment-containing phytoplankton
a_w = Pure water absorption
c_g = Attenuation of dissolved material
c_w = Attenuation of water
a_t = Total absorption coefficient
λ_r = Reference wavelength (150 nm)
T = Temperature (degrees Kelvin)
$v = 10^7 \left(\frac{1}{\lambda_r} - \frac{1}{\lambda} \right)$
$Z_c = \left(\frac{v^{11/12}}{\sqrt{T}} \right)^{2/3}$

CHAPTER 2

Sections 2.1–2.4
A = Absorptance
a = Absorption coefficient
a_{corr} = Calibration corrected absorption
a_{wcal} = Water calibration absorption
a_m = Measured absorption coefficient
c = Beam attenuation coefficient
S = electronic noise
$N\,(r_T - r;\ \Psi)$ = Average number of wall reflections required for a ray path to reach the detector following a scattering event
$\rho_g\,(\Psi)$ = Net reflectance of the quartz tube beyond the critical angle
Φ_K = Sum of directly transmitted and scattered fluxes
Φ_i = Incident source flux
Φ_B = Scattered flux
Φ_T = Directly transmitted flux measured by the detector
Φ_o = Flux entering the water at the source window
Ψ_c = Critical angle
Ψ = Scattering angle
r = Pathlength

V_{samp} = Detector reading for water sample
V_{rcal} = Reference reading during water calibration

V_{wcal} = Detector reading during water calibration

V_{fcal} = Detector reading from the factory water calibration, a device file that should be used for all measurements

V_{rfac} = Reference reading from the factory water calibration, a device file that should be used for all measurements

$W(\Psi)$ = Weighting coefficient

Sections 2.5–2.7

a_{wcal} = Absorption of the water calibration

a_m^{TS} = Temperature and salinity corrected measured absorption

a_{corr}^{TS} = Temperature and salinity corrected total absorption

b = Total scattering

b_b = Total backscatter

c_m^{TS} = Temperature and salinity corrected measured attenuation

ε = Scattering error

E_d = Downwelling irradiance

E_u = Upwelling irradiance

E_o = Scalar irradiance

E_{ou} = Upwelling scalar irradiance

E_{od} = Downwelling scalar irradiance

$F = \varepsilon / b$

K_d = Downwelling diffuse attenuation coefficient

$\vec{K}$ = Vertical attenuation coefficient for vector irradiance

S = Salinity (PSU)

T = Temperature (Celsius)

T_r = Reference temperature

$W(\Phi)$ = Weighting function

CHAPTER 3

C_i = Signal normalization constant

C_o = Offset constant

E = Vector irradiance

K_i = Proportionality constant (in)

K_o = Proportionality constant (out)

L = Scalar radiance

n = Refractive index

$\hat{\mathbf{n}}$ = Outward unit vector normal to the surface

P_{abs} = Power that is absorbed (the power entering the cavity minus the power leaving the cavity)

P_{in} = Power entering the sample

P_{out} = Power leaving the sample

r_i = inner radius of ICAM quartz tube

r_o = outer radius of ICAM quartz tube

S_i = Signal voltage (in)
S_o = Signal voltage (out)
S = Ratio of the measured signal voltages
U = Radiant energy density
V = Volume of sample

CHAPTER 4

F_0 = Diffuse reflected irradiance
F_{fluor} = Fluorescence intensity
F_{sample}^{SPF} = Light intensity of sample water using a short pass filter
F_w^{SPF} = Light intensity of pure water using a short pass filter
F_{sample} = Light intensity of sample water
F_w = Light intensity of pure water
$G(a(\lambda))$ = Least square function to solve for $a(\lambda)$
N_c = Number of times a photon is reflected by the wall
P_0 = Probability that a photon, coming from the central light source, reaches the wall directly
P_s = Probability that a photon, which is reflected, will return to the wall
ρ = Reflectivity of the wall
R_F = Ratio of absolute absorption of the light inside tge cavity by the sample with and without the short-pass filter integrated over all wavelengths
r = Inner radius of the cavity
r_s = Radius of the central light source
S_{sample} = Salinity of the sample
T_{AB} = Transmission difference between two samples
t_{sample} = Temperature of sample water
t_w = Temperature of pure water
T_{meas} = Measured transmission
T_{num} = Numerically calculated transmission
Ψ_t^i = Instrument-specific temperature correction coefficients
Ψ_S^i = Instrument-specific salinity correction coefficients

CHAPTER 5

IS-mode = Inside-sphere mode
T-mode = Transmittance mode
T-R = Transmittance-Reflectance

A_f = Absorbance of the sample
A = Effective area of the filter (cm^2)
a_p = Absorption coefficient of particles
a_{NAP} = Absorption coefficient of non-algal particles
a_{ph} = Absorption coefficient of phytoplankton
β = Pathlength amplification or Beta correction factor
L = Geometric pathlength

OD = Optical density

OD_f = Optical density of a filter pad after the baseline and reference filter are subtracted or backscatter corrected optical density of the sample

OD_{NAP} = Optical density of non-algal particles

OD_p = particulate optical density

OD_s = Optical density of the same particles in suspension which is not affected by pathlength amplification

OD_{fs} = the best estimate of optical density measured on a sample filter

OD_{infs} = the best estimate of optical density representing the instrument baseline applicable to the sample filter scans

OD_{fb} = the best estimate of optical density measured on a blank filter

OD_{infb} = the best estimate of optical representing the instrument baseline applicable to the blank filter scans

OD_{fs}^{T} = OD of the transmittance mode for the sample filter

OD_{fr}^{T} = OD of the transmittance mode for the reference filter

OD_{fs}^{R} = OD of the reflectance mode for the sample filter

OD_{fr}^{R} = OD of the reflectance mode for the reference filter

OD^{T} = Specific transmittance

OD^{R} = Specific reflectance

Φ_o = Power of the collimated beam incident on the sample

Φ_t = Power directly transmitted through the sample

R_f = Reflectance spectrum of sample filter

R_{fr} = Absolute reflectance of reference filter

R_{fs} = Absolute reflectance of sample filter

T_{fs} = Absolute transmittance of sample filter

T_{fr} = Absolute transmittance of reference filter

T_f = Transmittance spectrum of sample filter

$u_c(a)$ = Total standard uncertainty

$u(V)$ = Uncertainty of volume

V = Filtration volume

σ_a = uncertainty in absorption

μ_{blank} = Computed mean of blank filter scans

σ_{blank} = Computed standard deviation of blank filter scans

τ = Compensation for reflected light inside the filter that is diffuse

APPENDIX

LIST OF WORKSHOP PARTICIPANTS

11-13 June 2014, NASA Goddard Space Flight Center

NAME	AFFILIATION
Emmanuel Boss	University of Maine, Orono, ME, USA
Annick Bricaud	Laboratoire d'Océanographie de Villefranche, France
Eurico J. D'Sa	Louisiana State University, Baton Rouge, LA, USA
Scott Freeman	NASA Goddard Space Flight Center, MD, USA
B. Greg Mitchell	Scripps Institution of Oceanography, La Jolla, CA, USA
Aimee R. Neeley	NASA Goddard Space Flight Center, MD, USA
Rick A. Reynolds	Scripps Institution of Oceanography, La Jolla, CA, USA
Collin Roesler	Bowdoin College, Brunswick, ME, USA
Rüdiger Röttgers	Helmholtz-Zentrum Geesthacht, Germany
Brian Schieber	Scripps Institution of Oceanography, La Jolla, CA, USA
Dariusz Stramski	Scripps Institution of Oceanography, La Jolla, CA, USA
Mike Twardowski	Harbor Branch Oceanographic Institute, FL, USA